New Jersey Institute of Technology

Digital Commons @ NJIT

Theses

Electronic Theses and Dissertations

Fall 1-31-1995

Measurement of the reaction to stress and meditation using brain wave coherence and heart rate variability

Christopher B. King
New Jersey Institute of Technology

Follow this and additional works at: https://digitalcommons.njit.edu/theses

Part of the Biomedical Engineering and Bioengineering Commons

ABSTRACT

MEASUREMENT OF THE REACTION TO STRESS AND MEDITATION
USING BRAIN WAVE COHERENCE AND HEART RATE VARIABILITY

by
Christopher B. King

Measurement of physiological parameters associated with the stress response and

the relaxation response caused by various forms of meditation can provide valuable

information about the reaction of the body to the mind and to the external environment.

This study used two different techniques to evaluate physiological parameters. The

first part examined the meditation response by recording the EEG and calculating the

coherence between brain waves originating from different parts of the brain. It was found

that high levels of coherence in the alpha portion of the EEG frequency band coincided

with a restful state associated with the relaxation response. In an effort to measure the

autonomic nervous system reaction to relaxation using heart rate variability analysis, it was

found necessary to separate sympathetic from parasympathetic influences. This led to

measuring the stress reaction in order to find the sympathetic contribution.

The stress reaction was measured by acquiring skin temperature data and heart

rate data, and comparing the changes in skin temperature to changes in heart rate

variability calculated using time frequency analysis. Skin temperature was found to react

gradually to sympathetic changes. A strong mental component was found to influence the

stress reaction that was being measured.

MEASUREMENT OF THE REACTION TO STRESS AND MEDITATION USING BRAIN WAVE COHERENCE AND HEART RATE VARIABILITY

by
Christopher B. King

A Thesis
Submitted to the Faculty of
New Jersey Institute of Technology
in Partial Fulfillment of the Requirements for the Degree of
Master of Science in Biomedical Engineering

Biomedical Engineering Committee

January 1995

APPROVAL PAGE

MEASUREMENT OF THE REACTION TO STRESS AND MEDITATION USING BRAIN WAVE COHERENCE AND HEART RATE VARIABILITY

Christopher B. King

Dr. Stanley S. Reisman, Thesis Advisor   Date
Professor of Electrical Engineering and Associate
Chairperson for Graduate studies, NJIT

Dr. David Kristol, Committee Member   Date
Professor of Chemistry and Director of Biomedical
Engineering Program, NJIT

Dr. Thomas W. Findley, Committee Member   Date
Associate Professor of Medicine, UMDNJ
Director of Research, Kessler Institute for
Rehabilitation

BIOGRAPHICAL SKETCH

Author: Christopher B. King

Degree: Master of Science in Biomedical Engineering

Date: January 1995

Undergraduate and Graduate Education:

- Master of Science in Biomedical Engineering
  New Jersey Institute of Technology, Newark, NJ, 1995

- Bachelor of Science in Biomedical Engineering
  Rensselaer Polytechnic Institute, Troy, NY, 1993

Major: Biomedical Engineering

This thesis is dedicated to my parents
Richard and Betty King
for all their support and guidance
through my education.

ACKNOWLEDGMENT

TABLE OF CONTENTS

Chapter **Page**

TABLE OF CONTENTS
(Continued)

TABLE OF CONTENTS
(Continued)

Chapter   **Page**

LIST OF FIGURES

LIST OF FIGURES
(Continued)

LIST OF FIGURES
(Continued)

LIST OF TABLES

CHAPTER 1

INTRODUCTION

1.1 Scope of the Research

Stress has become a prominent feature in the fabric of American life. Almost everyone, from the student cramming for an exam, to the factory worker who was just laid off, to the CEO worried about his company's fourth quarter losses experiences the effects of stress in American society. In 1988, for example, the cost of stress to business alone was estimated at 150 billion dollars. Stress management programs are widely available, but have proven generally ineffective. [9]

By definition, stress is the body's reaction to a perceived mental, emotional, or physical distress. Physiologically, this reaction manifests itself as a mass discharge of the sympathetic portion of the autonomic nervous system. The effects of the mass discharge include faster heartbeat, increased blood pressure, increased blood flow to vital organs such as the brain and skeletal muscles with a corresponding decrease in blood flow to "non-essential" organs such as the skin, kidneys, and gastrointestinal tract, and a mobilization of fat reserves. This response is often called the "fight or flight response," as an animal in this state will decide instantly whether to stand and fight or to run away. [10] In American society, this reaction many times cannot lead to physical activity, so the body creates the stress reaction without an appropriate release. Chronic stress reactions of this nature can therefore lead to physical and mental disorders such as peptic ulcers, heart attacks, and nervous breakdowns.

Recent studies have demonstrated that the practice of meditation has a measurable effect on the body's reaction to stress, and suggests that persons may be deriving both physical and psychological benefits from the practice of meditation. [17] These studies have shown links between the clear relaxed subjective state a person experiences during

meditation and such measurable physiological phenomena as increased coherence of the EEG, changes in heart rate, respiration, and autonomic function, and changes in peripheral circulation and skin conductance, among others. [17] This thesis will show how the autonomic components of stress can be measured noninvasively, how both the central nervous system and the autonomic nervous system react to stress, and how relaxation techniques such as meditation affect the physiological reaction to stress.

1.2 Meditation

1.2.1 Background

Before detailing the physiological effects of meditation, it will be helpful to understand what is meant by the term "meditation" as it is used here and in the literature. The practice of meditation as a method of quiescent, tranquil restfulness has been used for centuries in Vedic, Bhuddist, and Taoist traditions in southern and eastern Asia. Practitioners report experiencing a wakeful state of "samadhi," or "pure consciousness," that is very pleasant and relaxing. [17]

In the late 1950's, Maharishi Mahesh Yogi introduced the technique of Transcendental Meditation (TM). The technique caught on quickly, and by 1973, over 350,000 Americans alone were practicing the technique. Also by 1973, over 6,000 teachers of the technique in the US had been trained through Maharishi International University, which was formed to coordinate training, academic courses, and other programs. [1]

The novelty of TM was that it required no special circumstances for practice, nor any diet or lifestyle changes. It was claimed that any normal individual capable of following simple standardized instructions could become proficient at this technique. The technique utilizes a "mantra", which is simply a sound word, or short phrase (traditionally sanskrit). Meditators will sit quietly in a comfortable chair, close their eyes, and mentally repeat the chosen sound. Most meditators regularly practice TM twice daily, morning and

evening, for 20 minutes. The end result of this technique is a "relaxed, peaceful mental state of heightened awareness." [17] Because of its simplicity and standardized instruction, TM has spread widely across the world, creating a large pool of practitioners that made investigating the practice easier.

Other researchers have generalized the techniques used in TM into what is known as a general "relaxation response". For instance, Benson has created a model of the relaxation response that has been used by other researchers. In this model, Benson argues that the relaxation response consists of four main elements: "a quiet environment, decreased muscle tonus, a passive attitude, and focus of attention on a repetitive, internal stimulus." [16] Essentially these techniques are similar to TM, so in further discussions the term "meditation" will be used to describe TM and related relaxation techniques. Subjects who participated in the meditation portion of the present study practiced a variety of these similar techniques.

1.2.2 Meditation Research

For the past two decades there has been continued interest in the physiology of meditation and its effects on the health of people. Much of the work, especially in the 1970s and early to mid 1980's, dealt with changes in EEG coherence in subjects during different meditation techniques. M. A. West has summarized some of the earlier findings of these researchers as follows: [29]

1. On beginning meditation alpha amplitude increases. In some cases, alpha frequency can decrease 1 to 3 Hz.

2. Bursts of theta activity may occur later in the meditation intermixed with the alpha activity, especially if the person is experienced in meditation.

3. During deep meditation, when subjects report the "clear experience" or "samadhi", high frequency beta bursts can occur, usually between 20 to 30 Hz, but sometimes as high as 40 Hz.

4. Alpha activity sometimes persists after meditation is over, even when the eyes are open.

Studies by Levine have shown a long range spatial ordering in EEG coherence spectra. Coherence is a measure of the linear dependence between a pair of signals, which can be thought of as a correlation coefficient in frequency. [3], [14] Levine measured coherence bilaterally and homolaterally from the frontal and central EEG electrode positions. He found long range coherence during meditation that was not apparent during eyes closed rest. Much of the coherence was concentrated in the alpha and theta bands. [19] Levine's methods for calculating and presenting EEG coherence have been used in the current study, so a detailed explanation appears later in this chapter.

Other studies have reported a facilitated paired H-reflex (an electrically evoked measure of motoneuron activity) in advanced meditators [27] as well as correlations with flexible performance on concept learning tasks. [7] Invasive measurements of blood norepinepherine showed reduced norepinepherine blood level after stress in subjects who regularly meditate, indicating reduced sympathetic nervous system activity. [15]

Perhaps most striking of all, however, is research seeming to indicate a field effect in EEG coherence. For example, statistical studies have shown that in cities where 1% of the population practice TM, crime rate decreased after controlling for demographic variables that influence the crime rate. [26] Some meditators indicate that subjectively, they feel that their meditations are deeper and their experiences clearer when they meditate in a group than when they meditate alone. In one study, intersubject EEG coherence was measured in three individuals in Farfield, Iowa, while at the same time a group of 2,500 individuals were meditating in Amherst, Massachusetts. It was found that, although the intersubject coherence was low, it was significantly higher on the experimental days (the days when the Amherst group was meditating) than on the control days. [21] Another study showed the effects of an advanced meditator on a test subject performing a concept learning task in a separate room. The study found that changes in

the meditators 5.7-8.5 Hz coherence led to parallel changes in the test subject's coherence, even though there was no direct interaction between the two. [26] These studies indicate that there may be a field effect between persons, and that this field effect may be amplified through meditation. Tourenne has proposed a model of this field using the dipole moment of the extracellular electric field of the cerebral cortex, which would radiate at frequencies in the microwave range. A more detailed discussion of this theory will follow in the next section, where the physiology of the EEG is discussed. [25]

1.3 Physiology

1.3.1 Cerebral Electrical Activity and the EEG

1.3.1.1 Anatomy of the Brain

The brain is the main structure of the central nervous system, and is the seat of all conscious and most subconscious control of the body. The brain can be divided into three major portions: the brainstem, the cerebellum and the cerebrum. Doing so facilitates discussion of the localization of brain functions with respect to structure. (refer to figure 1.1)

The brainstem is a short extension of the spinal cord at the base of the brain. It is the oldest part of the brain, having changed little with the evolution of vertebrates. It has three main functions:

1. A connecting link between the spinal cord, cerebellum, and cerebrum.

2. An integration center for autonomic functions such as control of heart rate and respiration.

3. An integration center for various motor reflexes.

The brainstem also contains groups of cell bodies that receive sensory information from and send out motor information to the head and neck. It contains as well the reticular formation, which controls sensory information such as pain, temperature, and touch, as well as controlling the patterns of sleep. [4]
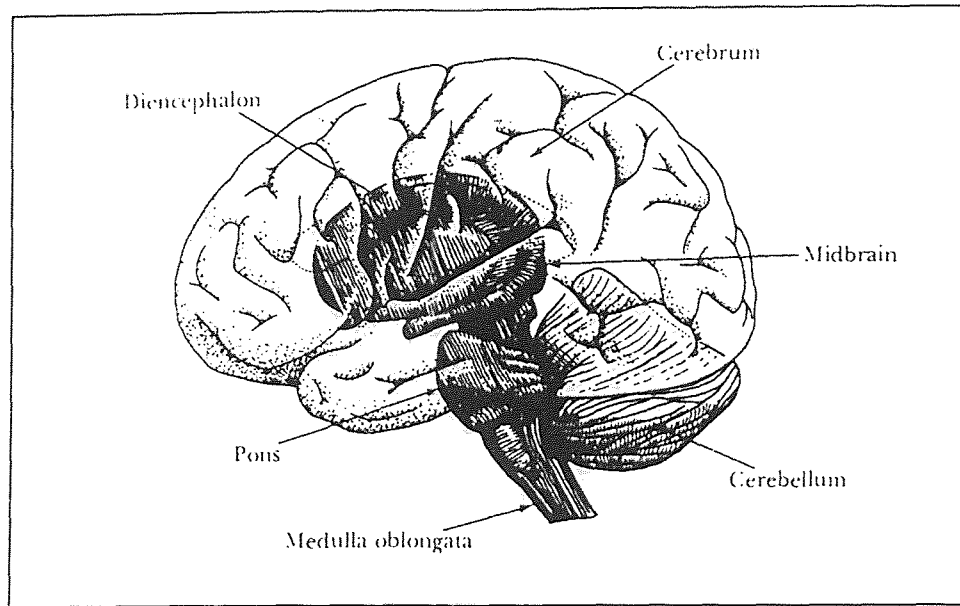
Figure 1.1 Anatomy of the Brain (from Clark, J. W. *Medical Instrumentation,* 1992)

The cerebellum is located inferior to the cerebrum below the occipital lobe and posterior to the brainstem. Its main function is motor coordination of the body. The cerebellum receives information about where the various portions of the body are in space, and compares it to information received from the cerebral cortex about where they should be. The cerebellum then sends out motor signals to the skeletal muscles to correct the discrepancies. [4]

The cerebrum is the most massive portion of the human brain, occupying most of the space in the cranial vault. The uppermost layer of the cerebrum is called the cortex; it is here that sensory information from the entire body are processed and conscious motor activity is initiated. The cortex is also the source of the EEG, which will be discussed in detail shortly. [11]
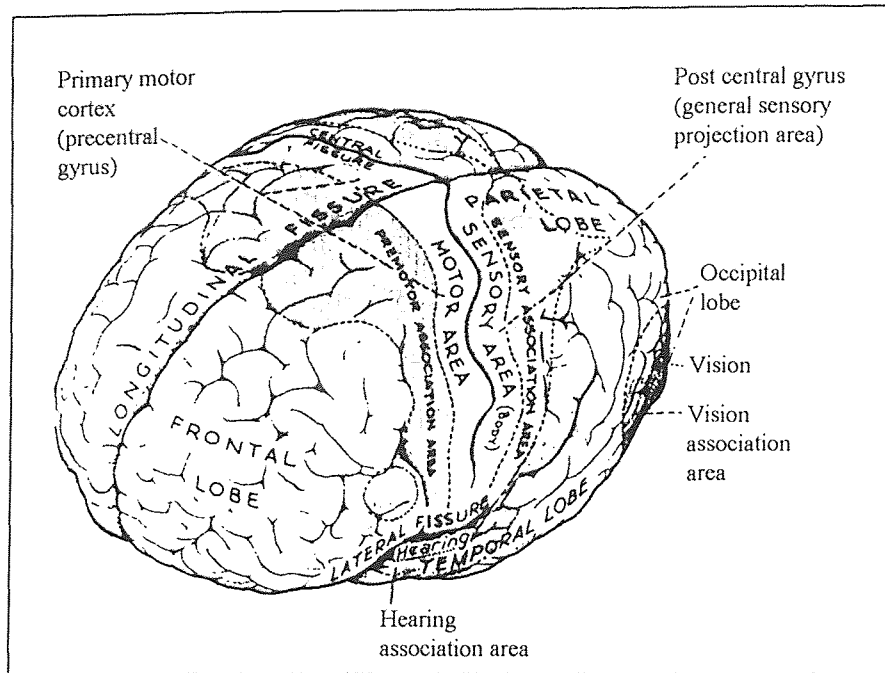
Figure 1.2 The cerebrum, showing the four lobes. (from Clark, J. W. *Medical Instrumentation,* 1992)

The cortex has a very convoluted surface, with three prominent fissures that divide the cortex into convenient anatomical sections, or lobes. (see figure 1.2) The longitudinal fissure runs anterior to posterior through the center of the brain, dividing it into two hemispheres. A second fissure, the central fissure, runs laterally from the longitudinal fissure along the coronal plane, dividing the frontal lobes from the parietal lobes. The lateral fissure runs close to the base of the cerebrum and divides the temporal lobes from the frontal lobes. A fourth pair of lobes, the occipital lobes, is located posterior to the parietal lobes but is not separated by a fissure. [4]

1.3.1.2 Cellular Structure of the Cerebral Cortex

The cerebral cortex is a thin layer (1.5-4.0 mm) on the surface of the cerebrum. The cortex is of two distinct types: the phylogenically older paleocortex, which is located on the base of the brain and within the longitudinal fissure, and the newer neocortex, located

on the superior and lateral surfaces of the brain. The term *cortex* will be used here to refer specifically to the neocortex. [4]
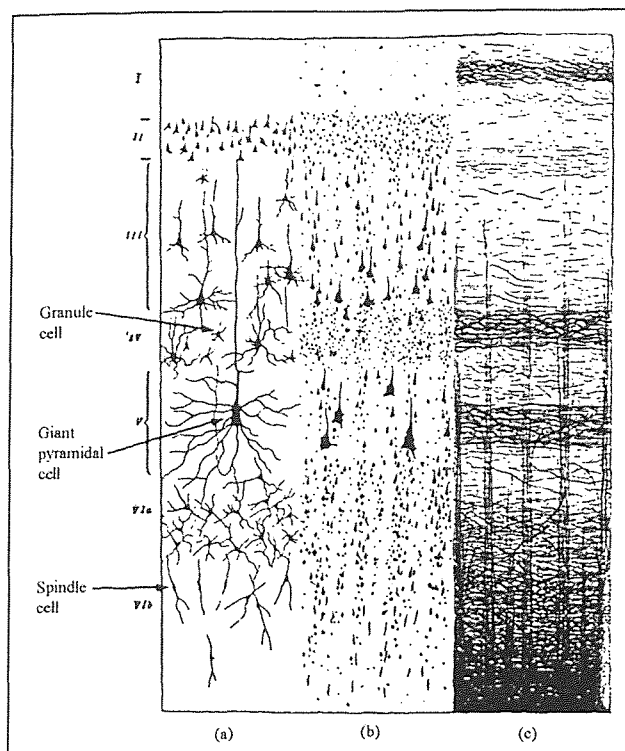
Figure 1.3 Cellular structure of the cerebral cortex: (a) Golgi stain, (b) Nissl cellular stain, and (c) myelin sheath stain. (from Guyton, A. C., *Textbook of Medical Physiology,* 1991)

Figure 1.3 shows the typical structure of the cortex, using three different histological stains. Most cells are of three types: granule (or stellate) cells, pyramidal cells, so called because of their characteristic pyramidal shape, and fusiform cells, sometimes called spindle cells. [4], [11] The granular cells tend to have short axons and function mainly as intracortical interneurons. The pyramidal and fusiform cells, however, are the source of most of the output fibers from the cortex. In particular, the pyramidal cells, which are larger and more numerous than the fusiform cells, give rise to the long

large nerve fibers that extend to the spinal cord. They are also the source of most of the large subcortical association fibers that travel from one part of the brain to another. [11]

1.3.1.3 Origin of Brain Biopotentials

When a scalp EEG is recorded, what is measured is the resultant field potential of a multi-element conducting medium. Because this measure is performed on a gross anatomical scale compared to the size of a typical neuron, the action potential of a single neuron will contribute little to the overall surface record, because it usually fires asynchronously with respect to the large number of axons around it. [4] This is seen in the surface EEG when a subject is under mental stress of some kind, such as performing mental arithmetic. Though the brain is obviously under strong activity, the EEG will be low in amplitude because most of these fibers are firing asynchronously and will tend to cancel each other's effects to the field. Rather, to generate EEG records, many thousands of neurons must fire synchronously. [11]

It has been theorized that the vertically oriented pyramidal cells are the source of the EEG. (see figure 1.4) When the dendrites of the pyramidal cell are excited, this stimulates an action potential down the dendritic tree to the soma of the cell, ultimately returning to the dendritic synapses via the extracellular fluid. The result is that the soma behaves as a current source, and the dendritic tree as a current sink, and a radially oriented dipole is created. When millions of these dipoles are active, variations in their strength and orientation produce wavelike fluctuations in a volume conductor. It is the potential difference between the surface electrode that measures these variations in the conduction field and distant reference electrodes that gives rise to the EEG. [4]
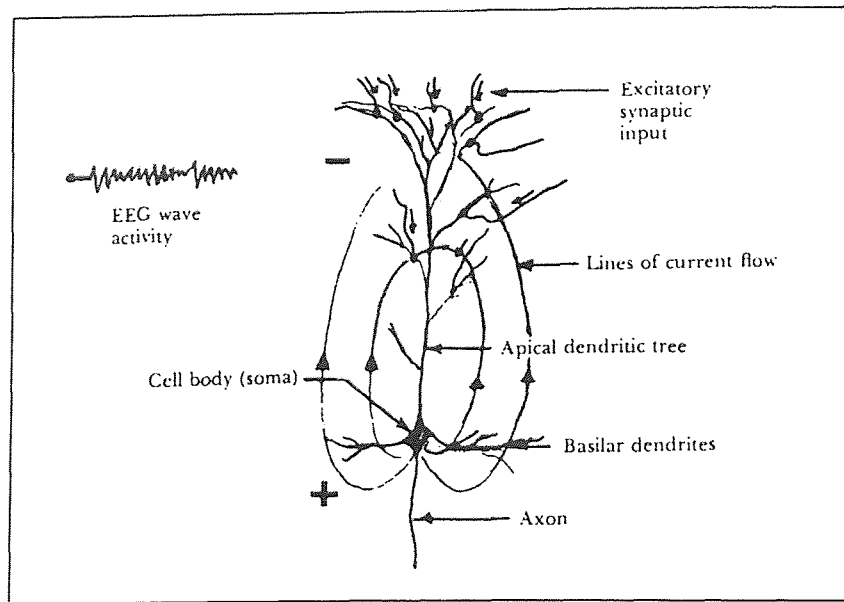
Figure 1.4 Dipole model of a pyramidal cell (from Clark, J. W. *Medical Instrumentation,* 1992)

Tourenne has taken this model one step further and has proposed that the volume conductor model can also radiate at microwave frequencies (1 to 10 GHz), giving rise to the field effect of consciousness mentioned earlier. Briefly, Tourenne calculates the equivalent dipole moment of a single pyramidal cell, and extends that calculation to microwave frequencies. He then calculates the radiative strength of the core conductor model for a distance outside the head. From these calculations based on the model, Tourenne concludes that the model plausibly suggests the existence of an extracranial field that oscillates at microwave frequencies, most probably toward 1 GHz rather than 10 GHz. [25] It is by this mechanism that the field model of EEG coherence is theorized to operate. [21], [26]

1.3.1.4 The Electroencephalogram

As mentioned briefly in the previous section, electrodes placed on the head measure continuing oscillations due to the electrical activity of the brain. These variations in

potential are called brain waves, and when they are recorded, the record is termed an electroencephalogram. The amplitude of these waves when measured through the scalp is about 50-100 µV, and their frequency can vary from 0.5 up to 100 Hz. The character of the brain waves is highly dependent on the degree of activity in the cortex. [4] Much of the time, especially during alert activity, the brain waves are small amplitude and quite asynchronous. However, at other times the brain will exhibit very rhythmic activity that is almost sinusoidal in nature. These patterns have been divided into four different types of waves: alpha, beta, theta, and delta waves. (see figure 1.5) [11]
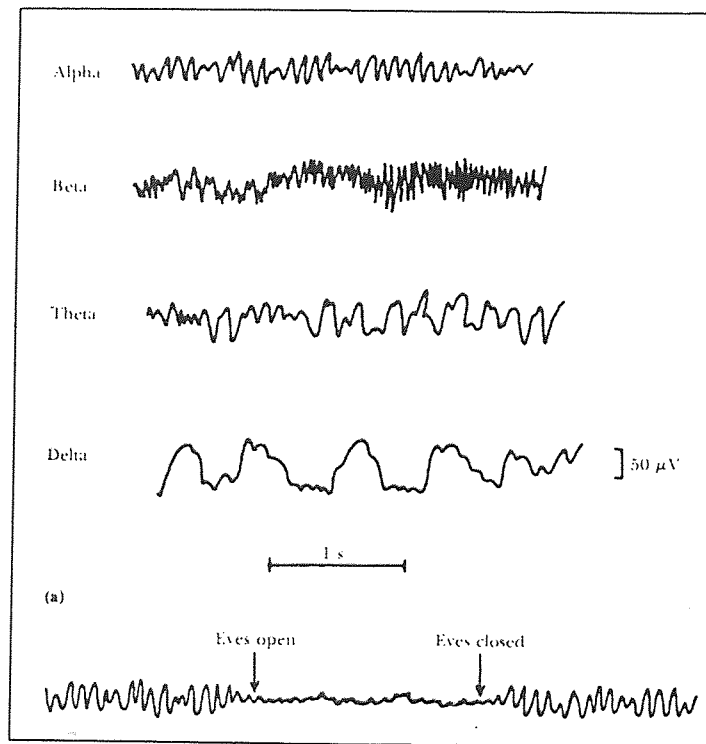
Figure 1.5 Examples of EEG (from Guyton, A. C., *Textbook of Medical Physiology,* 1991)

Alpha waves oscillate at frequencies between 8 and 13 Hz. They occur in almost all adults when they are awake but in a quiet, resting state. Often they appear when the eyes are closed. Alpha waves will disappear during sleep and when an awake person

focuses attention on a specific mental activity. [11] Alpha waves are also prominent during meditation, and tend to decrease in frequency as meditation progresses. In experienced meditators, lower frequency alpha waves sometimes persist even after the person stops meditating. [29] Alpha waves will not occur in the cortex without connections with the thalamus, so it is likely that a general thalamocortical origin of alpha waves exists, producing the periodicity and the ability to activate millions of neurons in the cortex. [11]

Beta waves occur at frequencies above 14 Hz, sometimes as high as 50 Hz. These mostly appear in the parietal and frontal lobes during intense mental activity. [11]

Theta waves oscillate at frequencies between 4 and 7 Hz. These waves occur mainly in the parietal and temporal lobes of children, but they can also appear during emotional stress in adults, especially during disappointment and frustration. [11] Theta waves also appear during deep meditation, especially in experienced meditators. [29]

Delta waves include all frequencies below 4 Hz. These occur in very deep sleep, in infants, and in serious organic brain disease. They also have occurred in animals whose cerebral cortex has been transected from the thalamus, indicating the waves can occur in the cortex independent of other brain areas. [11]

1.3.2 Autonomic Nervous System

The autonomic nervous system is the part of the nervous system that controls the visceral functions of the body. Regulation of internal activities such as blood pressure, heart rate, gastrointestinal motility, and body temperature, among many others, is performed by the autonomic nervous system. Autonomic activity is controlled mainly by centers in the spinal cord, brain stem, and hypothalamus. Table 1.1 below summarizes the effects of the autonomic nervous system on selected organs. [11]

Table 1.1 Autonomic effects on selected organs of the body. (from Guyton, A. C., *Textbook of Medical Physiology*, 1991)

Organ	Effect of Sympathetic Stimulation	Effect of Parasympathetic Stimulation
Heart		
Muscle	Increased rate	Slowed rate
	Increased force of contraction	Decreased force of contraction (especially atria)
Coronaries	Dilated (β_2); constricted (α)	Dilated
Lungs		
Bronchi	Dilated	Constricted
Blood Vessels	Mildly constricted	? Dilated
Systemic Arterioles		
Abdominal Viscera	Constricted	None
Muscle	Constricted (adrenergic α)	None
	Dilated (adrenergic β_2)	
	Dilated (cholinergic)	
Skin	Constricted	None

The autonomic nervous system is divided into two anatomical and functional units with opposite properties. The sympathetic nervous system is responsible for creating an increased level of activity in an organism. Anatomically, sympathetic nerves are composed of two neurons: a preganglionic neuron and a postganglionic neuron. These nerves pass from the spinal cord through the white ramus into one of the sympathetic ganglia before reaching their destination. (see figure 1.6) Most postganglionic sympathetic nerve endings secrete norepinepherine, a neurotransmitter that activates excitatory receptors, but in some cases can inhibit certain organs. The sympathetic nervous system is also responsible for the alarm or fight-or-flight response. This is caused by a mass discharge of all sympathetic nerve endings. [11]

The parasympathetic nervous system, by contrast, generally lowers the activity of an organism, and is associated with a relaxed state. Anatomically, parasympathetic fibers leave the brain through cranial nerves III, V, VII, IX, and X, and the second and third sacral spinal nerves. (see figure 1.7) Cranial nerve X is also called the vagus nerve, and

since the vagus innervates much of the thorax and abdomen, especially the heart, for the parasympathetic nervous system, parasympathetic activity is often called vagal activity. All parasympathetic nerve endings secrete acetylcholine. Although acetylcholine generally has an excitatory effect, it is also known to have inhibitory effects as well, such as the slowing of the heart by the vagus nerve. [11]
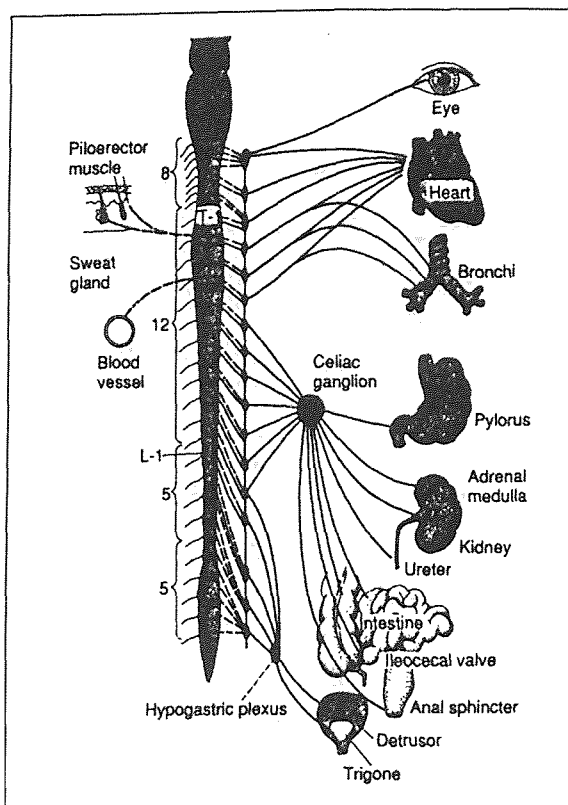
Figure 1.6 The sympathetic nervous system (from Guyton, A. C., *Textbook of Medical Physiology,* 1991)
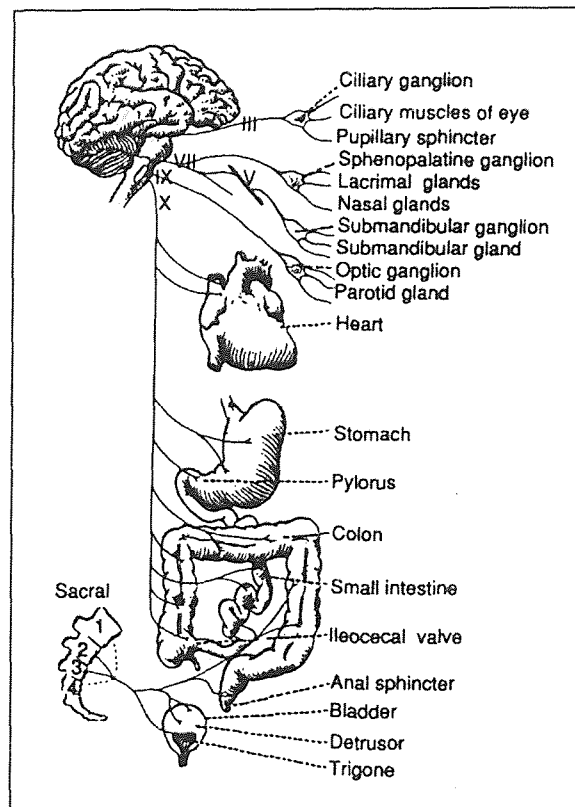
Figure 1.7 The parasympathetic nervous system (from Guyton, A. C., *Textbook of Medical Physiology,* 1991)

Both the sympathetic and parasympathetic nervous systems are continually active. These basal rates of activity are known as sympathetic and parasympathetic tone. The advantage of tone is that is allows a single nervous system to increase or decrease activity in an organ. For instance, normal sympathetic tone keeps the systemic arterioles

constricted to approximately half their maximum diameter. By changing the degree of

sympathetic tone, the diameter of the arterioles can be increased or decreased. Without

tone, the sympathetic nervous system can only cause vasoconstriction, never vasodilation.

[11]

1.3.3 Heart Rate Variability As A Measure of Autonomic Function

The autonomic nervous system plays the greatest role in the regulation of beat to beat

variations in heart rate. Sympathetic nerve fibers terminate at the sinus node pacemaker,

the heart musculature and vasculature. Parasympathetic fibers terminate on the sinoatrial

(SA) and atrioventricular (AV) nodes as well as within the cardiac musculature and

vasculature. Interplay between the two systems will cause the heart to speed up or slow

down, depending on which system is more active. (see figure 1.8) [18]
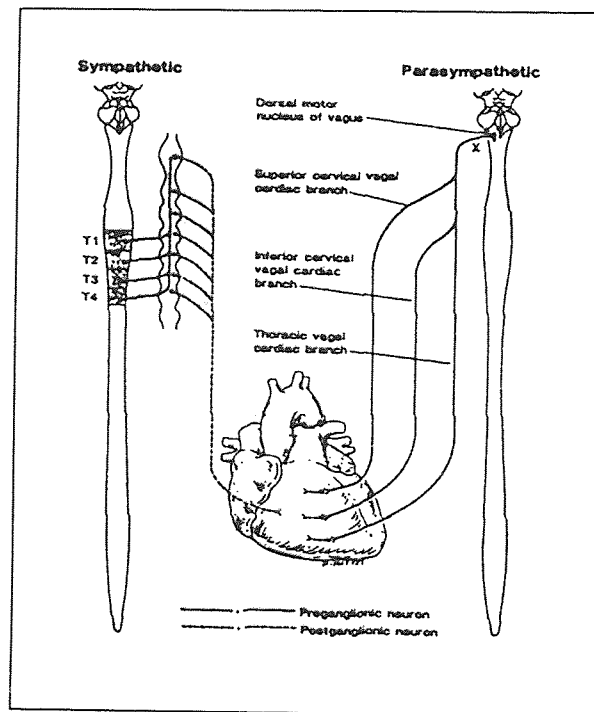
Figure 1.8 Autonomic innervation of the Heart (from
Kamath, M. and E. Fallen, *Power Spectral Analysis
of Heart Rate Variability,* 1993)

Spectral analysis of the interval between R-waves in the ECG (called the interbeat interval or IBI) results in a graph similar to figure 1.9. Three distinct peaks are usually evident. The high frequency peak, which usually falls between 0.15 and 0.4 Hz, is representative of parasympathetic activity or parasympathetic tone. [22] The frequency of this peak is influenced by the frequency of respiration (a phenomenon called respiratory sinus arrhythmia), and spectral analysis of the respiration signal has shown that the high frequency IBI peak and the respiratory peak usually coincide. Changes in the frequency of respiration will cause both peaks to shift together.[18]
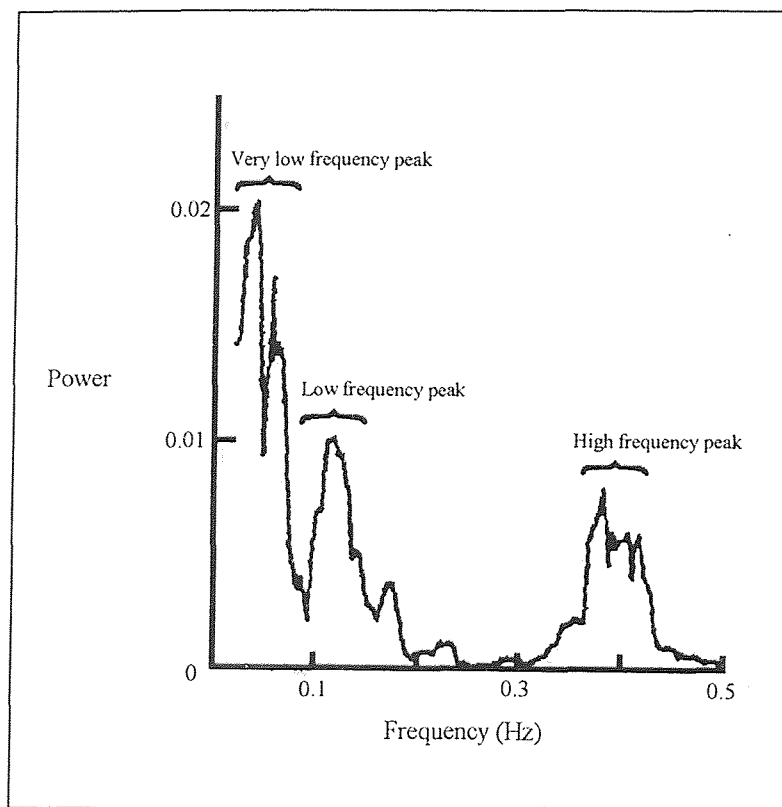
Figure 1.9 Typical Power Spectrum of Heart Rate Variability (from Kamath, M. and E. Fallen, *Power Spectral Analysis of Heart Rate Variability,* 1993)

The low frequency peak, which falls usually between 0.06 and 0.15 Hz, is representative of a mixture of both sympathetic and parasympathetic effects. [22]

Because of this, it is difficult to tell what the sympathetic nervous system is doing independent of the parasympathetic nervous system. In addition, if the respiratory frequency falls below 0.15 Hz, which is 9 breaths per minute, the high frequency peak will appear in the low frequency range, and determination of parasympathetic activity also becomes extremely difficult.

The very low frequency peak has been linked to vasomotor control and/or temperature control. Contributions from the renin-angiotensin system also contribute to this peak. [18] Because so many different events contribute to the low frequency peak, the information was not used for the present study.

1.3.4 Skin Temperature

The temperature of the skin is directly proportional to the amount of blood flowing through the cutaneous tissues. Skin temperature varies due to three different factors:

1. Changes in the core temperature of the body, which is regulated by the hypothalamus.

2. Changes in the environmental temperature, which cause local vasodilation or vasoconstriction. Widespread changes in skin temperature will cause temperature regulatory reactions from the hypothalamus.

3. Changes in sympathetic tone, which vary the amount the peripheral arterioles are constricted. [11]

Studies have shown that vasomotor reflexes are controlled almost entirely by the sympathetic nervous system. [2], [5], [12] A study by Halperin *et. al.* demonstrated decreased fingertip blood flow in subjects under mental stress using venous occlusion plethysmography. Differences in basal sympathetic tone have also been shown to be a cause of the differences in cutaneous blood flow between males and females, [4] and may be a contributing factor to Raynaud's disease. [12]

One aspect of the present study is to use measures of skin temperature as an indicator of changes in sympathetic tone. Skin temperature changes were used together with heart rate variability analysis in an attempt to measure sympathetic response independent of parasympathetic response.

1.4 Signal Processing

1.4.1 Coherence Spectral Array (COSPAR)

The coherence spectral array, or cospar, is a graphical representation of the coherence between two signals. For the EEG, a high coherence (near 1) over time is indicative of long range spatial ordering. This type of ordering increases in physical systems as they relax to lower states of excitation. Therefore, increased spatial ordering in the EEG indicates a lowering of the excitation level of the brain, which is the response obtained from relaxation. The cospar graph makes this order in the EEG much easier to visualize. [19]

Coherence can be viewed as a correlation coefficient in the frequency domain, analogous to the autocorrelation function in the time domain. [3] Coherence is a measure of the linear dependence between a pair of signals, normalized to values between zero and one. The coherence is unity if two signals have the exact same frequency content, in other words if one signal is completely linearly dependent on the other; however for most pairs of real signals coherence is less than unity. [14]

If the autocorrelation function of a random process $X(t)$ is defined as [3]

$$R_X(\tau) = E[X(t+\tau), X(t)] \qquad (1.1)$$

then the power spectrum of that process can be further defined as

$$S_X(j\omega) = \mathcal{F}[R_X(\tau)] = \int_{-\infty}^{\infty} R_X(\tau)e^{-j\omega\tau}\,d\tau \qquad (1.2)$$

Similar expressions can be written for the autocorrelation and power spectral density of a second random process $Y(t)$. The cross correlation of the two signals $X(t)$ and $Y(t)$ can further be defined as

$$R_{XY}(\tau) = E[X(t+\tau), Y(t)] \qquad (1.3)$$

with the corresponding cross spectral density.

$$S_{XY}(j\omega) = \mathcal{F}[R_{XY}(\tau)] = \int_{-\infty}^{\infty} R_{XY}(\tau)e^{-j\omega\tau}\,d\tau \qquad (1.4)$$

The coherence function is then defined as the ratio between the cross spectral density of $X(t)$ and $Y(t)$ to the product of the individual power spectral densities.

$$\gamma_{XY}^{2} = \frac{|S_{XY}(j\omega)|^{2}}{S_X(j\omega)S_Y(j\omega)} \qquad (1.5)$$

Levine developed a method for calculating the coherence spectrum between pairs of EEG signals. In this technique, the two signals were first divided into short epochs of 256 samples, which for Levine's work corresponded to 5.12 seconds of EEG. The power spectra and cross spectrum of each epoch were computed using an ensemble average on overlapping data segments first discussed by Welch. [19]

Welch first outlined this method of power spectrum estimation in 1967. One of its main advantages is that it involves the transformation of data sequences which are much shorter than the whole record, which is an advantage on machines with limited memory

space or for very long records. Welch states that if $x(n)$, $n=0, ..., N-1$ is a stationary second order stochastic process, then the sequence can be divided into K sections of length L, that may overlap. To estimate the power spectrum, the sequence x(n) is multiplied by a window w(n), and then the Fourier transforms of the K sequences are calculated. From the Fourier transforms, K peiodograms (magnitude squared function) are calculated, then averaged to produce the power spectrum estimate. [28]

Once the power and cross spectra are computed, the squared coherence spectrum for each epoch was calculated. A threshholding was applied to the coherence spectrum at a fixed level. Levine used 0.95 as the coherence threshold to reduce the likelihood of spurious coherence, or coherence events not representative of long range spatial ordering. The resulting coherence spectra for all epochs were assembled together in time, resulting in a three-dimensional looking graph of coherence level versus time and frequency. [19]

For the present study, an algorithm based on the methods of Levine was written in MATLAB to compute the squared coherence function of two EEG channels (see Appendix C). The output of the program was a surface mesh plot of coherence above a 0.95 threshold versus time and frequency. Details of the data analysis technique are presented in Chapter 2.

1.4.2 EEG Power Spectrum

A simple technique to measure average spectral power in 1 Hz bands in an epoch of EEG was based on clinical research conducted by Tansey. Tansey worked with children with learning disabilities, and used EEG biofeedback to decrease behavioral problems and increase scores on a standardized intelligence test. [23] The method used was to sample the EEG at 8 kHz, calculate online the spectrum, and display the power averaged over 1 Hz bands around selected frequencies. A tone representing each selected frequency band generated by Tansey's equipment was used as the biofeedback source to the patient during the therapy sessions. [24]

For the current study, an algorithm was written for off-line analysis of EEG to calculate average EEG power in 1 Hz frequency bands in the range from 3 Hz to 28 Hz..

1.4.3 Heart Rate Variability Analysis and ECG Derived Respiration

As described in Section 1.3.3, spectral analysis of the beat to beat variations of heart rate can reveal valuable information about the functioning of the autonomic nervous system. One of the most important aspects of heart rate variability analysis is that it is non-invasive. In other words, there are no external influences used to alter the state of the body, such as the use of drugs to block specific portions of the autonomic nervous system from functioning. The advantage of this is that physiologic parameters can be measured with the body in a more "natural" state. However, difficulties in measuring some desired parameters can arise, which require unique and imaginative solutions.

The analysis of heart rate variability was conducted using programs developed by Shin, Reisman, and colleagues. [22] The programs calculated the distance between successive R-wave peaks, and plotted them versus their time of occurrence. Since this procedure produced interbeat interval samples of unequal length along the time axis, a backward step function interpolation was used to create an equidistant IBI signal. The method assumes no new information about the time series can be obtained until the next beat occurs, Thus, the interpolated values between a beat at time $T(m-1)$ and the next at time $T(m)$ are set equal to the time difference between $T(m)$ and $T(m-1)$. The resulting interpolated interbeat interval (IIBI) was then detrended using a locally weighted robust regression procedure that passed frequencies above 0.00158 Hz. This detrending eliminated artifact from the recording apparatus as well as from subject movement. [22] The spectrum of the detrended signal was then calculated and graphed.

Normally during heart rate variability studies a respiration signal is recorded simultaneously. There are several different ways to accomplish this. One way is to use a spirometer and mask to directly measure the volumes of gas moved into and out of the

lungs. A major problem with this method is that the mask is a minor nuisance that can become a major distraction during relaxation techniques and thus taint the data.

A way to avoid this is to use impedance pneumography to measure respiration., which measures the change of impedance across the chest as its dimensions change with breathing. However, when breathing rates become very slow, as often happens during meditation, the impedance signal tends to fall back toward zero from the previous maximum or minimum, a phenomenon known as DC drift. This phenomenon introduces artifact to the respiration signal that is difficult to remove. Fortunately, there exists an alternative way to measure respiration indirectly from variations in the ECG signal.

A technique for deriving the respiration signal was developed by Zhao using two orthanormal cardiac vectors. [30] Variations in the amplitude and area of the recorded ECG reflect changes in the heart and chest as a volume conductor. Therefore, the movement of the chest wall during breathing is reflected in the recorded ECG. [30]

The technique involved calculating the changes in the mean cardiac electrical axis by calculating the areas under the QRS complexes for ECG leads I and III. The angle between the areas of the two leads was calculated, and the result interpolated to form a smooth curve. [30]

1.4.4 Time Frequency Analysis

One of the drawbacks of the spectral analysis of heart rate variability is that it cannot track rapid changes in heart rate variability over time. The algorithms of Shin *et al.* described in the previous section were usually used on lengths of data on the order of minutes, so an average level of autonomic activity was represented. [22] Often the level of autonomic activity can change in as rapidly as ten to fifteen seconds. [8] Time frequency analysis was performed on the IIBI data using the Wigner distribution to show vagal tone and the sympatho-vagal balance as a function of time.

The Wigner distribution was first introduced by Wigner (1932) and was subsequently incorporated into signal analysis by Ville (1948). The distribution is defined by the following equation.

$$P_w(t,f) = \int_{-\infty}^{\infty} e^{-j2\pi ft} s^*(t - \tfrac{1}{2}\tau)s(t + \tfrac{1}{2}\tau)d\tau \qquad (1.8)$$

The time signal is represented above by $s(t) = A(t)e^{j\varphi(t)}$, where $A(t)$ is the amplitude and $\varphi(t)$ the phase. The Wigner distribution decomposes a signal into time and frequency components, and it has been shown to be a good method for estimating a nonstationary time series. [8]

Programs written by Fernando were used to calculate the Wigner distribution of the IIBI signal, calculate instantaneous frequency, and then find the areas under the distribution for the low frequency and high frequency heart rate variability ranges. [8]

CHAPTER 2

METHODS

2.1 Acquisition of Data

2.1.1 EEG Acquisition

The EEG was recorded using silver electrodes affixed to the scalp with EEG paste, and plugged into Gould universal amplifiers (model 13-4615-58, Gould, Inc., Valley View, OH) with attached isolation amplifiers (model 11-5407-58). The signal from the amplifier was fed into the data acquisition computer, which will be discussed in detail later in this chapter.

The placement of EEG electrodes on the scalp historically has been subject to much debate. In 1958, the International Federation of Societies for Electroencephalography and Clinical Neurophysiology presented the "10-20 electrode system" to standardize the placement of scalp electrodes. (see figure 2.1) As its name implies, electrodes are placed in intervals of 10 or 20% of the distance from the nasion to the inion in the sagittal plane and between the preaurical points in the coronal plane. [10] Because of the need for standardization, many EEG laboratories now make use of the International 10-20 system for electrode placements.

Electrical potentials can only be measured in reference to a second point. Since this is the case, electrode placement is crucial, since the measured signal is the algebraic difference of the potentials measured between the two points. The resulting signal is by definition bipolar. Much of the time in EEG study, a "monopolar" recording is desired so that the activity in one part of the brain can be studied independently of the rest. Monopolar recording (sometimes called common reference recording) assumes the existence of an electrically inactive site for the reference electrode. Strictly speaking, this is not true, since all the cells in the body can conduct electrical potentials. However, the
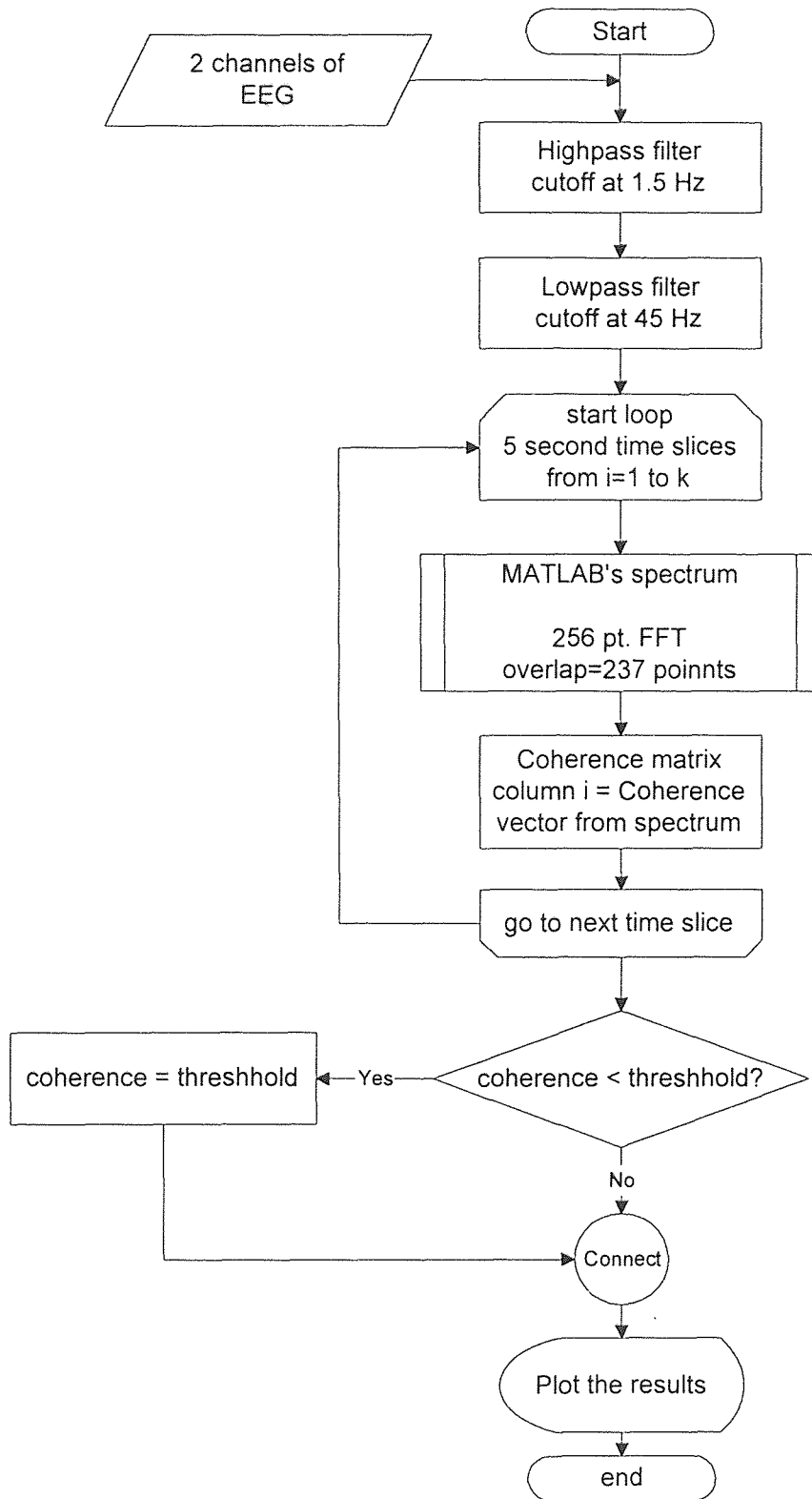
Figure 2.3 Flowchart of cospar.m

The output of the Gould was set at the factory as ±5 volts. The input channels to the A/D board were also set at ±5 volts. EEG signals generally range from around 50 μV to close to 1 mV. The gain of the amplifier was set so that the output EEG signal from the Gould was around 1 V_{p-p}, which would leave plenty of buffer at the A/D board for relatively high voltage artifacts such as blinking or eye movements. The filters on the amplifier were set for a passband of 1 to 30 Hz, which included the alpha (8 to 12 Hz) and theta (4 to 7 Hz) EEG bands. EEG waveforms were monitored with a digitizing oscilloscope (Tektronix model TDS544A, Tektronix, Inc., Beaverton, OR) connected to the BNC outputs on the rear of the amplifier. Shielded cable connected the 37 pin data output connection, also on the rear of the amplifier, to the data acquisition computer.

2.1.2 ECG Acquisition

The ECG was acquired with a Quinton Q4000 Stress Test Monitor (Quinton Instrument Co., Seattle, WA), with electrodes placed in the three bipolar limb lead configuration. Output from the Q4000 was ECG leads I, II, and III, plus a sync pulse, all about 3 V_{p-p}. The sync pulse is a short duration square wave pulse that is synchronized with the QRS wave of the ECG. Two channels, the sync pulse and Lead II outputs, were connected by shielded cable to the data acquisition computer.

The skin of the subject was cleaned with alcohol swabs. Silver-silver chloride ECG electrodes (Medtronic Andover Medical, Haverhill, MA) were placed on the left and right clavicles (right arm and left arm positions), and on the left and right ribs below the pectoral muscles (right leg and left leg positions). These were connected to the Q4000 using its RA, RL, LA, and LL leads.

2.1.3 Skin Temperature Acquisition

Two thermistors (model G22K7MCD10, BetaTherm Corp., Shrewbury, MA) were connected to a small amplifier circuit consisting of a LM324N quad inverting op-amp.

(see Appendix B). The lower left portion of the circuit is the thermistor circuit, consisting of the power supply V_{cc}, resistor R_3, and the thermistor T. As the temperature measured by the thermistor rises, the resistance of the thermistor falls. The output voltage from this circuit was fed into the op-amp circuit at the (+) input, where it was amplified by a gain factor of 10. The output of the amplifier (V_{out}) was then sent by shielded cable to the das-1601 A/D board. A schematic diagram of the circuit and power supply appears in Appendix B. The gain of the amplifier was calculated using the following equation:

$$Gain = 1 - \frac{R_2}{R_1} = \frac{2.2 \times 10^6}{2.0 \times 10^5} = 10 = A_{vi} \qquad (2.1)$$

One thermistor was taped to a small table to the left of the subject on which the amplifier device sat. Its purpose was to monitor the ambient room temperature. It was taped down to reduce artifact resulting from ambient air currents, such as from the ventilation system. The other thermistor was taped to the distal middle finger of the subject's left hand, approximately at the center of the fingerprint. A gauze pad was taped in place over the thermistor and tape to provide thermal insulation.

2.1.4 Data Acquisition Procedure

Data was acquired and recorded with an IBM compatible microcomputer with a 286 CPU, 1 MB ram, and a 230 MB hard disk drive. Each piece of equipment was connected by shielded cables to the das-1601 A/D converter board in the computer (Keithley MetraByte/Asyst, Taunton, MA). Subjects sat in a comfortable chair facing away from the equipment so the displays would not be a source of biofeedback. A diagram of this setup appears in Appendix A.

Once the subject has been connected to the amplifying equipment, the inputs to the A/D board could be monitored using a display program called Primplot (J. F.

Andrews). Any adjustments in gain settings or connection problems could be resolved at this time. When all was in order, data could be collected using Streamer v3.25 (Keithley MetraByte/Asyst), a data collection program included with the das-1601 board. Once collected, the data files were moved to Bernoulli disks (Iomega Corp., Roy, UT) for storage and subsequent analysis. For protocols involving the acquisition of ECG, data was sampled at 200 Hz. Otherwise, data was sampled at 150 Hz.

2.2 Experiment Protocols

2.2.1 Alpha Band Coherence Studies

The coherence studies were conducted in part to reproduce the results of Levine, Dillbeck and Orme-Johnson, and others, and also in conjunction with the analysis of heart rate variability to attempt to determine autonomic function during meditation. These studies were divided into three protocols: two eyes open/eyes closed studies and a meditation study. Before each experiment, subjects were briefed as to the protocol and electrodes were applied as described previously. Subjects were seated in a comfortable chair facing away from the displays of the equipment so the displays would not be a source of biofeedback.

For the first eyes open/eyes closed study, subjects were asked to sit quietly for five minutes with their eyes open, then to close their eyes (but not meditate, if the subject happened to be a meditator) for five minutes. Four channels of EEG were recorded, and each five minute session was saved to a separate file.

For the second eyes open/eyes closed study, ECG and QRS sync from the Quinton Q4000 were also acquired so autonomic function during the experiment might be ascertained. Since changes in autonomic response around the point of eye closure were of interest, one file of 8 minute length was taken.

For the meditation studies, the setup was the same as it was for the eyes open/eyes closed studies. Five experiments were conducted, and the protocols varied based on the

results of the previous trial. The first protocol was a 10 minute session where the subject would vary his mental state at two minutes, four minutes, and eight minutes into the session. Three subjects took part in this protocol.

The second and third protocols were similar, as both involved a length of meditation. The second protocol was a three minute eyes closed baseline followed by ten minutes of a meditation technique. The third protocol involved two minutes of pre-meditation eyes closed rest, six minutes of meditation, and two minutes of post meditation eyes closed rest. Two different subjects took part in these protocols.

2.2.2 Autonomic Studies

The autonomic studies were conducted to determine if there was an experimentally useful relationship between sympathetic nervous system function and skin temperature. The relevant physiology of the autonomic nervous system and its relationship to skin temperature and heart rate were discussed in Section 1.3 of Chapter 1. Two channels of EEG, two thermistor channels, ECG lead II, and QRS sync pulse data were collected. Subjects were seated in a chair with arms so that they do not face the equipment. The subjects placed their left arm comfortably in their lap, making sure that the middle finger was not touching any surface, and held the pace breathing box in their right hand. The paced breathing box is a small box with a vertical column of LEDs that light up and down in sequence. The rate of movement is adjusted by a knob on the front calibrated in breaths per minute. A breath is one complete inhalation and exhalation, and is represented by the box as one complete up-and-down cycle.

Development of the protocol was an iterative process. For the first protocol, the subjects were instructed as to the general organization of the experiment (pacing, then stress), but the details were not revealed. This would cause problems with the results which will be explained in Chapter 3.

The first protocol consisted of paced breathing at 18, 12, 9 and 6 breaths per minute for four minutes each, and stress session. The stress session consisted of an eight minute file during which the subject paced at 12 breaths per minute. The reason for the paced breathing was to keep the high frequency component of the heart rate variability spectrum above 0.15 Hz, so that this peak would represent only parasympathetic tone. During the middle three minutes of the stress file, the subjects were stressed with loud whistles and camera flashes at quasi-random intervals. One important aspect of the type of stress applied to the subject is that it had to be passive, since the subject needed to keep his attention on the paced breathing box. This would exclude such stressors as mental arithmetic, and left distractions such as bright lights in the peripheral vision, obnoxious or loud noise, or pain. Vision and hearing were chosen in this instance because they seemed easiest to implement, and it was felt that they would give the desired results. Five subjects participated in this protocol.

After these four trials, the protocol was changed in three significant ways. First, the subject was allowed to acclimate to the environmental temperature until his skin temperature stabilized. Second, to reduce the effects of mental anticipation on the subject's part, as little information about the protocol as possible was revealed to the subject. Finally, the stressor was changed to a more annoying high frequency audio feedback noise. After testing the protocol on two trial subjects, the protocol took its final form.

Subjects were told that the experiment would involve relaxation and stress, but were not told the details so that they would not anticipate upcoming events in the protocol and bias the results. The subject was allowed to acclimate to the temperature and the equipment until his finger temperature was stable over more than 60 seconds. Once this was achieved, data acquisition began.

Data was collected continuously over the entire time of the protocol. First, the subject merely rested for four minutes. Following that, the subject began paced breathing.

Using the paced breathing box as a guide, subjects paced their breathing rates at 12 and 6 breaths per minute for four minutes each. Then they rested as a washout period before the stress section and allowed their skin temperature to stabilize again. For the stress, the subjects paced at 12 breaths per minute. After allowing the subject's skin temperature to stabilize again, the experimenter disappeared behind the equipment to purposefully elicit an anticipation response. Since the subject knew that something was to happen, it was hoped that the act of preparing to do something would make the subject nervous. Next, still observing the skin temperature, the subject was stressed with three minutes of recorded high frequency audio feedback. Care was taken to ensure the sound was loud enough to cause psychological discomfort without causing pain or physical damage to the ear. Finally the subjects rested for five minutes for a post-experiment recovery.

For one subject who was an experienced meditator, a meditation section consisting of three minutes of eyes open rest, four minutes of eyes closed rest, fifteen minutes of meditation, followed by four minutes eyes closed and three minutes eyes open was performed. EEG data was collected for this portion in addition to the other physiological data.

2.3 Data Analysis

2.3.1 Unpacking Data

Data collected on the data acquisition computer by Streamer is saved to the root directory of the hard drive in a packed binary format, using 2 bytes per sample. The software used for data analysis, MATLAB v4.0 (The Math Works, Inc., Natick, MA) and S-Plus v3.1 (Statistical Sciences, Inc., Seattle, WA), cannot read the data in this format, so the data needs to be converted to an ASCII format which these programs can use. Of the two analysis programs used, MATLAB is more stringent in its format requirements than S-Plus, so data was converted in the format MATLAB required, which S-Plus could also read. A program called Kunpack2 (a modified version of the unpack utility that Keithley

MetraByte/Asyst provided with the das-1601 A/D board) was utilized to unpack the data. Kunpack2 converted the raw data files to an ASCII file where each channel of data was represented as a column in a matrix and spaces separated the columns. The raw data files were moved to Bernoulli disks for storage while the ASCII files were copied onto the C drive of the signal processing workstations for analysis.

2.3.2 Coherence Spectral Array (COSPAR)

Analysis of the data was performed on an IBM-compatible 486/50MHz computer. Unpacked data files were imported into MATLAB, a software package that included engineering design and analysis algorithms and permitted the writing custom MATLAB programs. The version of MATLAB also included a Signal Processing Toolbox, which included many digital signal processing algorithms such as filters, transforms, and windowing algorithms.

A program called cospar.m was written to calculate the cospar using Levine's methods described in Chapter 1. Two channels of EEG data were given as input arguments to the program. For the four channel EEG recordings, the input was arranged as four different pairs: bilateral frontal signals (channels F_3 and F_4), bilateral central signals (channels C_3 and C_4), homolateral left signals (channels F_3 and C_3), and homolateral right signals (channels F_4 and C_4). Output was the mesh and contour plots of coherence above 0.95 vs. time and frequency. A listing of the MATLAB code appears in Appendix C.

The program worked in the following way. Two channels of EEG signal were lowpass filtered using a 9th order Butterworth filter with cutoff frequency at 45 Hz to remove any residual 60 Hz interference. The signals were then highpass filtered with a 7th order elliptical filter with a cutoff frequency at 1.5 Hz, passband ripple of 0.05 dB, and stopband ripple of −50 dB. The elliptical filter provided the steepest cutoff characteristics, which allowed the low frequency trend to be removed while preserving

EEG frequencies above 2 Hz. A zero phase filter algorithm included in MATLAB was employed to eliminate phase distortion.

In order to keep EEG epochs short (thus improving time resolution), Levine specified that a procedure described by Welch be used, where overlapping segments of data are ensembled and averaged. [17] This method was described in Chapter 1. Conveniently, MATLAB also contained an algorithm that computed the power spectrum using Welch's method. Five second epochs of EEG were chosen. For each epoch, the two signals were divided into a number of 256 point sections, each of which overlapped by 19 points. Each section was windowed with a Kaiser window algorithm, a 256 point FFT was taken, and then accumulated with a running sum of the previous sections. The cross spectral density of both signals was also calculated in the same way. Specifically, the program calculated the power spectral density as:

$$P_{xx}(e^{j\omega}) = \sum_{i=1}^{k} \left| X_i(e^{j\omega}) \right|^2 \tag{2.1}$$

and the cross spectral density is:

$$P_{xy}(e^{j\omega}) = \sum_{i=1}^{k} Y_i(e^{j\omega}) X_i^*(e^{j\omega}) \tag{2.2}$$

where:

$$k = \frac{n - overlap}{m - overlap} \tag{2.3}$$

Here, *n* is the sequence length, *m* is the size of the FFT (256 points), and *overlap* is the number of points the next sequence overlapped the previous one (237 points). (see figure 2.2)
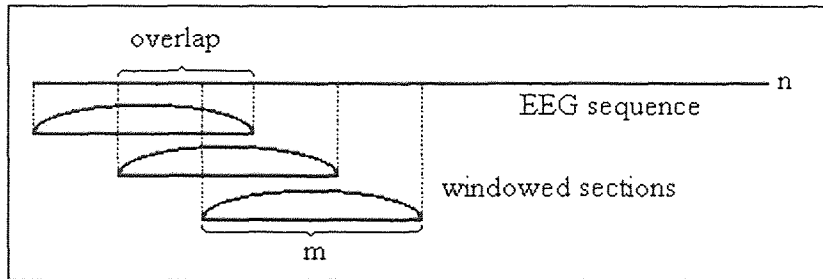
Figure 2.2 Sectioning and Windowing of EEG in MATLAB

With the spectral densities calculated, calculating the coherence for the epoch was a simple matter.

$$C_{xy} = \frac{\left| P_{xy}(e^{j\omega}) \right|^2}{P_{xx}(e^{j\omega}) P_{yy}(e^{j\omega})} \tag{2.4}$$

For each five second epoch, a vector of coherence versus frequency was produced, with the coherence values ranging between 0 and 1. These vectors were assembled as columns in a matrix, then thresholded at the value 0.95, so that any coherence value below 0.95 was discarded and set to 0.95. The resulting matrix was graphed as a surface mesh plot and a contour plot of coherence versus time and frequency. Figure 2.3 shows a flowchart of this process. An example of a cospar plot can be seen in Chapter 3.

2.3.3 EEG Power Spectrum

Two or four channels of EEG were input to a program named powspec.m, which calculated the average power spectrum of each EEG signal in 1 Hz bands based on the

Figure 2.3 Flowchart of cospar.m

methods of Tansey described in Chapter 1. The output was a graph of average power vs. frequency for each EEG channel.

Average power in a large epoch of EEG was calculated as follows. Twenty-six 1 Hz frequency bands were created between 3 Hz and 28 Hz, based on a 2048-point FFT. For a sampling rate of 200 Hz, this gave ten frequency points in each 1 Hz band. The EEG signal was divided into five second segments. For each segment a 2048 point FFT was calculated, and the power i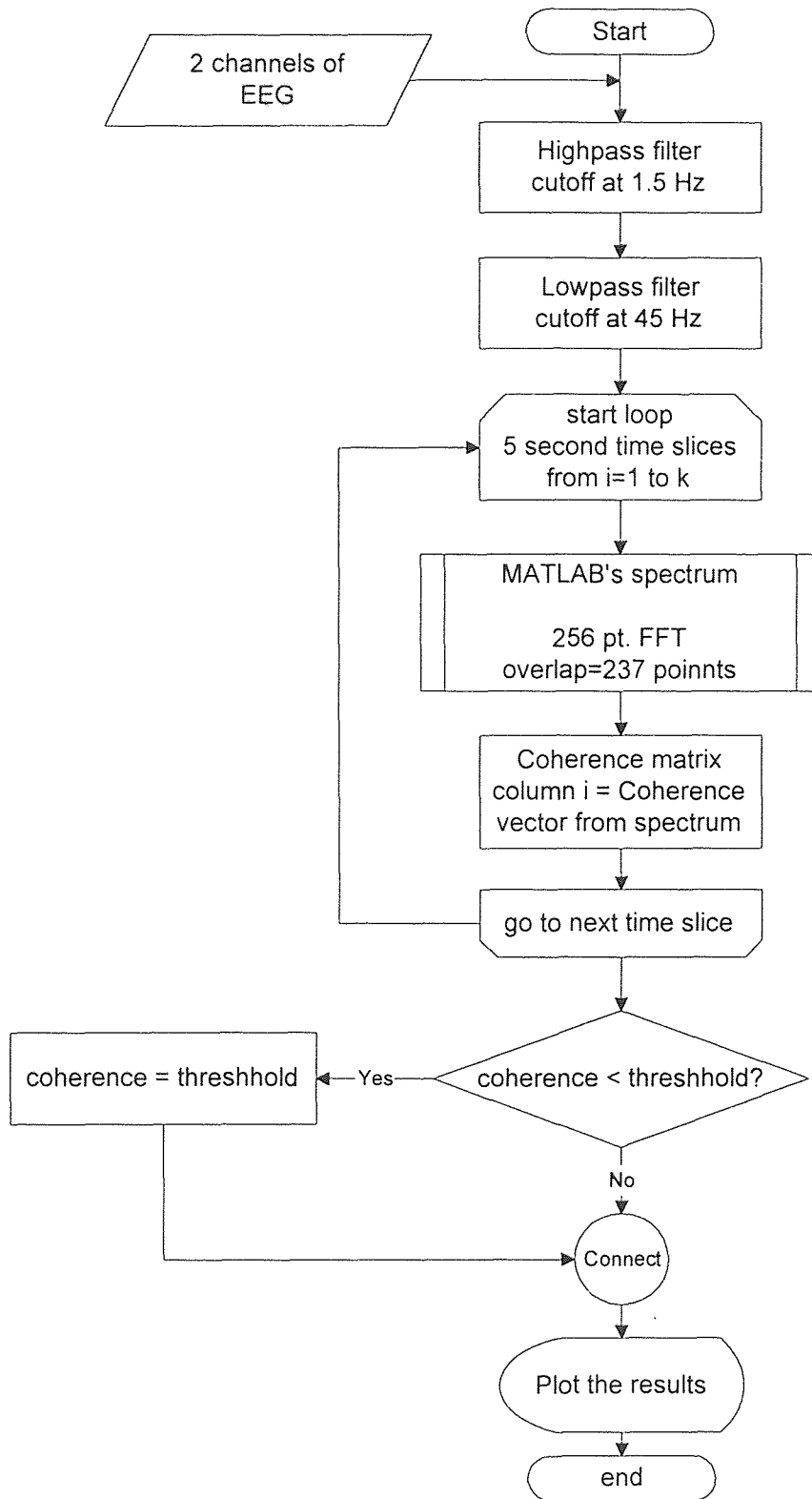n each band was calculated by taking the area under the curve in each frequency band. The area was simply the sum of the FFT magnitude squared values in the band. The average power over the epoch in each band was the mean of the areas in each five second segment. These values were plotted for each EEG channel recorded together with a curve representing a +1 standard deviation to indicate the amount of spreading in each band over the epoch. A listing of the MATLAB code appears in Appendix C.

2.3.4 Heart Rate Variability Spectrum and ECG Derived Respiration Signal

The spectrum of heart rate variability was calculated in S-Plus using previously developed algorithms described in Chapter 1. Briefly, the interbeat interval signal (IBI) was calculated from the ECG sync pulse produced by the Quinton Q4000 Monitor, and represented the distance between two successive R waves. the IBI signal was interpolated to equidistant time samples, with signal amplitude representing the R-R interval. Any outliers, indicating misdetections (either additional beats or skipped beats), were removed by hand. The spectrum was then calculated in a separate routine that calculated the FFT of the detrended IIBI signal.

The respiration signal was derived from the raw ECG signal using the algorithms developed by Zhao that were also described in Chapter 1. The first output graph displayed the interbeat intervals versus beat number, the IIBI signal, and the derived

respiration signal, and the second showed the spectra of the IIBI and the derived respiration.

2.3.5 Time Frequency Analysis

Time frequency analysis of the IIBI signal was conducted using an algorithm implemented in MATLAB by Fernando. The input to the program was the IIBI signal that was calculated in S-Plus, and saved in ASCII format to be imported into MATLAB. The program calculated the Wigner distribution of the IIBI signal. From the Wigner distribution, the areas under the high frequency range and low frequency range versus time were calculated. The area under the high frequency range is known as vagal power, and the area under the low frequency range is known as sympathovagal power because it represents influences of both the sympathetic and parasympathetic nervous systems. (see Section 1.3.3 of Chapter 1) Output consisted of three graphs: the original IIBI and the detrend line, the detrended IIBI, and the calculated instantaneous frequency; the plot of the Wigner distribution of the IIBI; and plots of vagal power, sympathovagal power, and the ratio of sympathovagal power to vagal power.

CHAPTER 3

RESULTS AND DISCUSSIONS

The following chapter details the progression of research in measuring physiological response to relaxation and stress. The design of the study was iterative in fashion, with a series of experiments that led to the final autonomic stress experiment. The preliminary experiments will be presented briefly along with the final results to give a clear picture of the scope of the research. A brief synopsis of each protocol will be given before each experiment description. For a detailed description of the experimental protocols, refer back to Section 2.2.

3.1 Meditation Studies

3.1.1 Eyes Open/Eyes Closed Protocol I

The investigation began by looking at EEG coherence in individuals while their eyes were open and while their eyes were closed. Data were taken on six subjects. The results were graphed in the cospar format. A typical cospar appears in figure 3.1. The upper half of each graph is a three-dimensional mesh plot of coherence versus time and frequency. The lower half is a contour plot of the same information, essentially viewing the upper graph along the coherence axis. Figure 3.1(b) shows typical alpha band coherence at 10 Hz. Coherence that appears in 3.1(a) is due to artifact such as EMG from eye blinks.
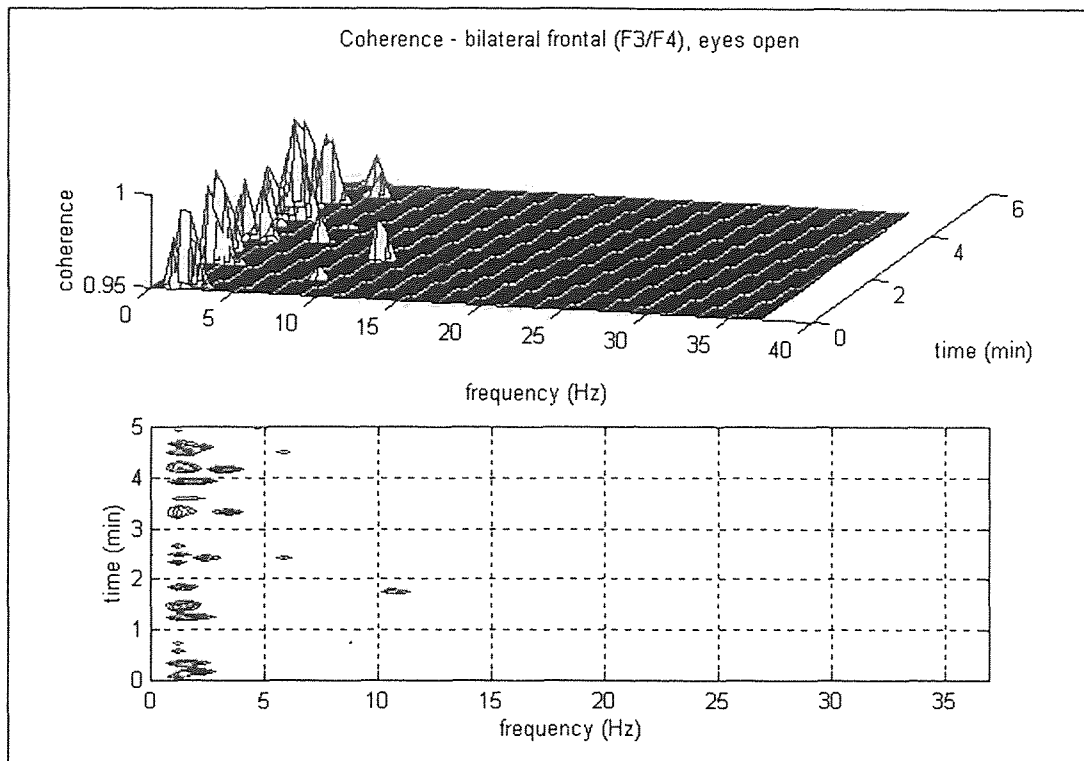
(a)
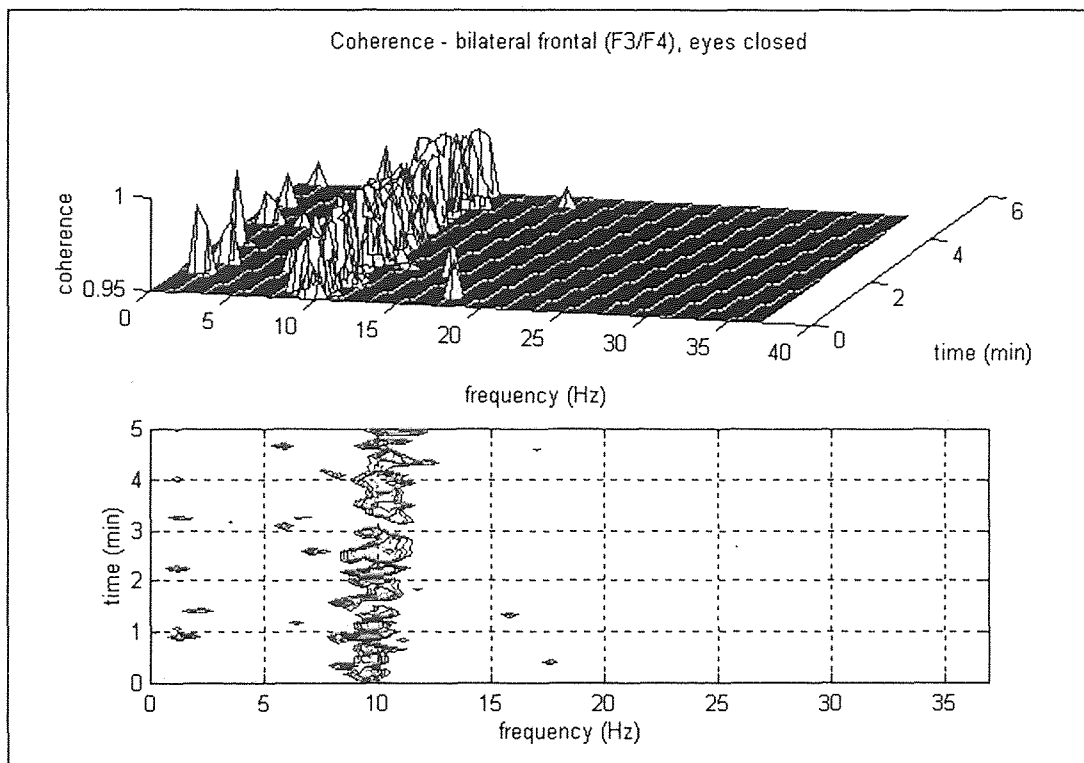
(b)

Figure 3.1 Cospar plots for eyes open/eyes closed protocol I: (a) eyes open, and (b) eyes closed.

All subjects showed alpha band coherence between the frontal electrodes (F3 and F4 in the International 10-20 system; see Section 2.3.2) with their eyes closed, usually in the frequency range of 10 to 11 Hz. Subjects who showed greater amounts of bilateral frontal coherence also showed some bilateral central, homolateral right, and homolateral left coherence, but to a much lesser degree than the frontal coherence. Figure 3.1 shows a graph of bilateral frontal coherence in one subject. Notice the alpha band coherence on the eyes closed graph, in the range of 10 to 11 Hz.

3.1.2 Eyes Open/Eyes Closed Protocol II

The second eyes open/eyes closed protocol was essentially the same as the first save for the addition of recording the ECG. Five subjects were studied using this protocol.

Four channels of EEG were again analyzed using the cospar program, and similar results to the first protocol were obtained. Heart rate variability analysis, however, did not show any significant information. The results of the heart rate variability analysis (figure 3.2) closely resembled baseline resting files that were analyzed for other research projects
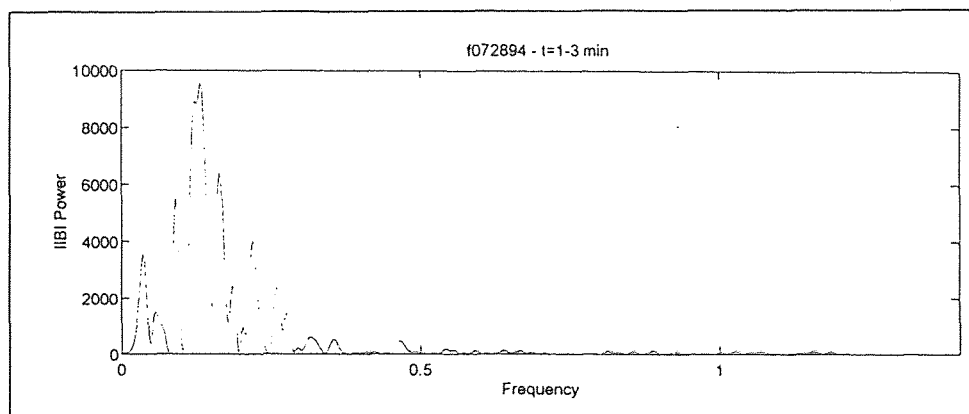

Figure 3.2 Heart Rate Variability Spectrum for Eyes Open/Eyes Closed Protocol II

at Kessler Institute for Rehabilitation. This is not surprising, as the subject merely was sitting quietly for the duration of the experiment, with the only change being the closing of the subject's eyes halfway through the experiment.

At this point it was decided that data should be recorded from subjects while they perform a relaxation technique to try to elicit an autonomic response. It is known that respiration rate decreases during relaxation and meditation techniques (see Chapter 1), so it was hoped that these changes would be reflected in the heart rate variability spectra. It was also decided to begin using the time frequency analysis programs that were recently developed by Fernando [8] to examine any rapid changes in autonomic activity, especially at transition points in the protocol, where the subject would have changed his activity. [8] (see Section 2.3.5)

3.1.3 Meditation Protocol

Three subjects took part in the first meditation protocol, which was a ten minute session during which the subject changed his technique at 2 minutes, 4 minutes, and 8 minutes into the session. This resulted in three short 2 minute techniques and one longer 4 minute technique. Of interest were not only the changes in EEG coherence over the ten minutes, but also changes in heart rate variability. Time frequency analysis was used to measure the rapid changes in variability, especially at the transitional points where the subject's technique was changed.

Figure 3.3(a) shows a typical coherence plot for this meditation protocol for one subject. The subject sat with eyes closed during the first two minutes. For the second two

minutes, the subject sat with eyes open. For the next four minutes, the subject performed

a meditation technique. Finally, the last two minutes consisted of an alternation between

eyes open and eyes closed. Note that the demarcations between restful activity (eyes

closed or meditation) and alert activity (eyes open or combination) can easily be seen.
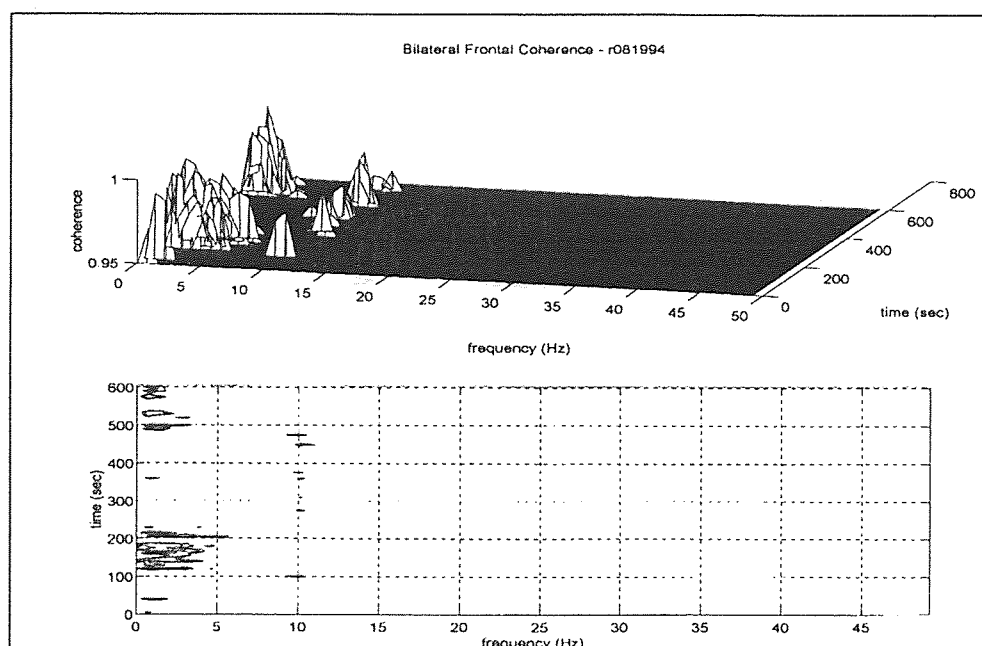
(a)
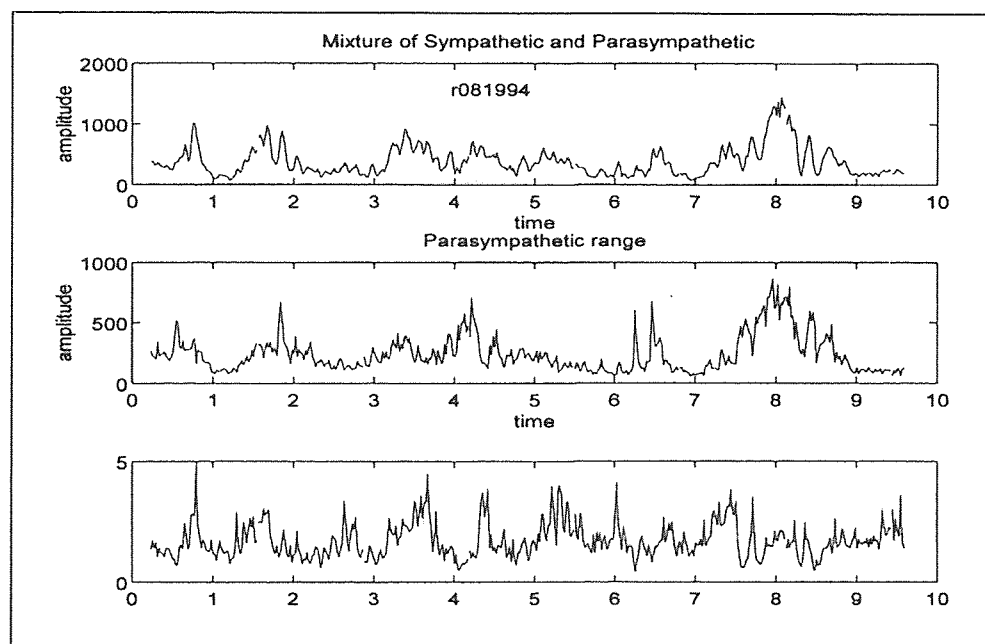
(b)

Figure 3.3 Meditation protocol results. (A) EEG coherence. (b) Time frequency analysis.

Figure 3.3(b) shows the time frequency analysis for the same subject. There seemed to be no correlation between the activity of the autonomic nervous system and the activities of the subject. For example, the upper graph shows a change in the low frequency range at 3 minutes, yet the subject did not change his activity at that point, according to the protocol. However, it is possible that his mental activity may have changed. This prompted further investigation into measuring the autonomic response as well as a refinement of the experimental methods.

A major stumbling block in the interpretation of the time frequency analysis results (and the heart rate variability criteria on which they are based) for relaxation techniques is the position of the respiration peak. Usually, breathing rates during meditation are much slower that 9 breaths per minute, so the high frequency IIBI peak and the respiration peak fall below 0.15 Hz. This means that these peaks appear in the low frequency range, where the heart rate variability peak has both sympathetic and parasympathetic components. (see Section 1.3 in Chapter 1) Since the separate contributions of the sympathetic and parasympathetic nervous systems could not be discerned this way, another method was needed to separate parasympathetic from sympathetic activity.

Skin temperature changes under influences from the sympathetic nervous system almost exclusively, as explained in Section 1.3.4. Sympathetic tone will also change dramatically and quickly when an organism is exposed to a stressful situation. It was theorized that if a subject was exposed to a stressful situation (creating a sympathetic response) while controlling the respiration rate by paced breathing, the changes in skin

temperature could be correlated with changes in the low frequency peak in the heart rate variability and time frequency analyses. Thus the stress protocols were created to test this hypothesis.

3.2 Autonomic Studies

3.2.1 Preliminary Stress Protocol

The preliminary stress protocol represented development of the approach to measuring the skin temperature with the different tasks the subject was required to do. Four subjects were tested using this protocol, though its implementation varied slightly from subject to subject, based on problems encountered with the previous subject. Stress was implemented in all four subjects by quasi-random bright light flashes and loud whistles in order to startle the subject. During this time, the subject paced his breathing at 12 breaths per minute.

Figure 3.4 shows a typical time frequency graph for the preliminary stress protocol. The subject was paced breathing at 12 breaths per minute during the time represented on the graph. The subject was stressed for the time between 2 and 5 minutes. Although the graph would seem to indicate a rise in low frequency activity around t=2 minutes, the graph actually rises around 1 minute 30 seconds, 30 seconds before the onset of stress. Also notice the parasympathetic range rises throughout the experiment. Further investigation was necessary to determine what was happening.

Subjects reported that they did not feel stressed or annoyed by the flashes and noise. One subject stifled a small laugh upon the first flash of the stress procedure. The
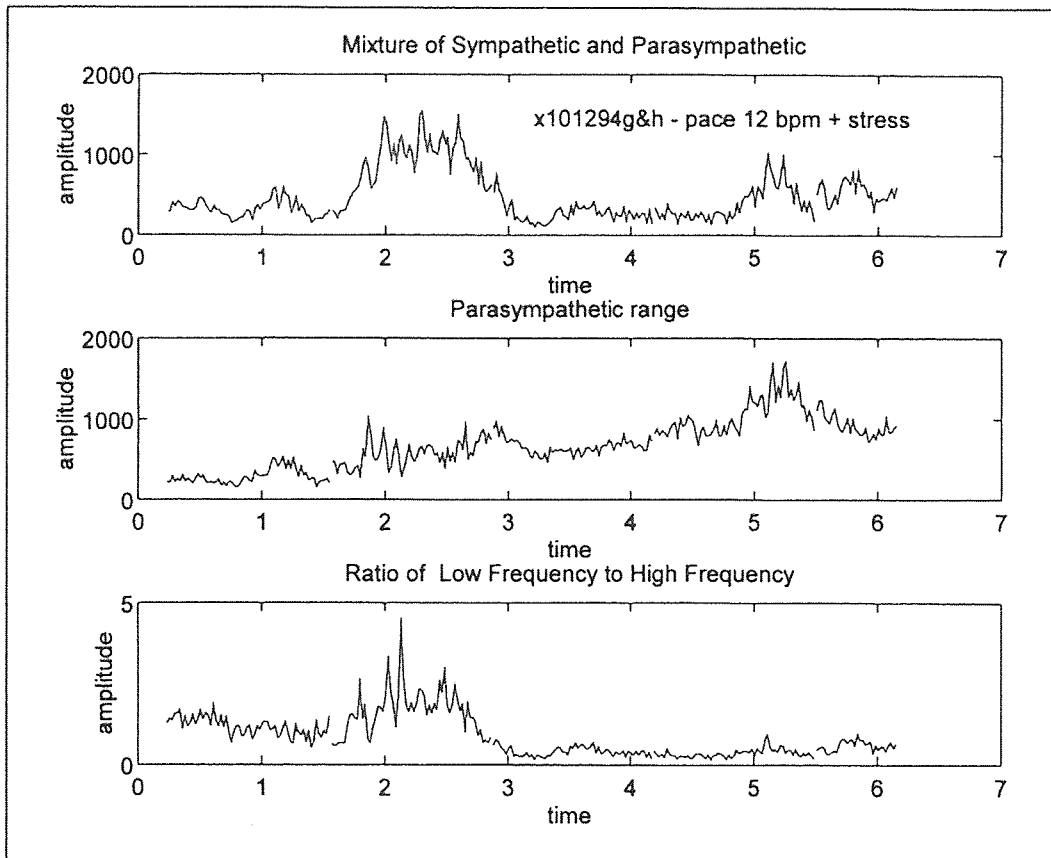
Figure 3.4 Typical time frequency graph for preliminary stress protocol. The Subject was stressed between t=2 and t=5 minutes

idea behind the stress procedure was that once the first startle happened, the subject would be unsure of the time of the next stimulus, and therefore would be anticipating it happening. Since the stimuli were not unpleasant enough, this reaction did not happen. In fact, once the subjects heard the stressors, they were relieved that the stimuli were mild.

Other factors that may have biased the early results could have been mental anticipation before the time of the first stress stimulus. Since subjects knew that they were to be stressed in the later part of the protocol (because they were told so at the beginning of the experiment), they may have been anticipating something unknown happening. When the stress actually happened, its mildness coupled with anticipation of

something worse caused a different reaction than the one intended. There were also problems of acclimation to the environment.

Based on these hypotheses, the protocol was changed to control for these factors, so that they would not be a confounding influence on the results. The two most important changes were a new stressor noise and extra time given to allow the subject to stabilize before the next phase of the experiment began.

3.2.2 Final Stress Protocol

The final form of the stress experiment was implemented on four subjects. Three subjects were male and one was female. One of the male subjects was an experienced meditator, and the other three subjects were non-meditators. All four subjects followed the same stress protocol, with the addition of a meditating portion for the meditator.

The experiment included two large divisions: a paced breathing protocol and a stress protocol. The paced breathing protocol included a baseline rest period, paced breathing at 6 breaths per minute and 12 breaths per minute, and a pre-stress rest period.

The stress protocol contained both the stress portion and the recovery portion of the experiment. During the stress period, the subject paced his breathing at 12 breaths per minute. The subject knew that something unpleasant was to happen, so the experiment was designed so that the subject would mentally anticipate the unpleasant event before it happened. To do this, the experimenter moved from the seat he was occupying up to that point to a position behind the subject (thus out of the subject's field of vision) where the tape recorder was (see Appendix E for a diagram of the equipment setup). There he

waited for some time before playing the tape of audio feedback noise. The obnoxious sound was played, and then the subject continued to pace breathe after the noise stopped for a few minutes. For the recovery period, the subject simply sat at rest. Complete results for two subjects appear in Appendix A. For a complete description of the protocol, refer back to Chapter 2.

3.2.2.1 Skin Temperature Response

In general for the four subjects, the skin temperature accurately reflected when the subject was being stressed. During a restful event, the skin temperature rose to a relatively high level, and when the subject experienced stress, either from anticipation, noise, or at times from an uncomfortable breathing frequency, the skin temperature fell to a relatively low level.

The skin temperature response during the stress portion of the protocol was very similar for the three non meditating subjects. When the temperature had stabilized during paced breathing at 12 breaths per minute, the experimenter disappeared behind the equipment, waited for between 3 to 6 minutes to create the psychological stress of mental anticipation, then played the noise tape for a physical stress of an unpleasant sound. In all three cases skin temperature fell beginning around the time the experimenter moved behind the equipment. Changes ranged from as little as 0.4° C to as much as 3.5° C. Once the stress was removed, the temperature rebounded to about its original level.

Figure 3.5 shows a typical set of skin temperature plots. Figure 3.5a is the skin temperature during the paced breathing portion of the protocol. The subject sat at rest for
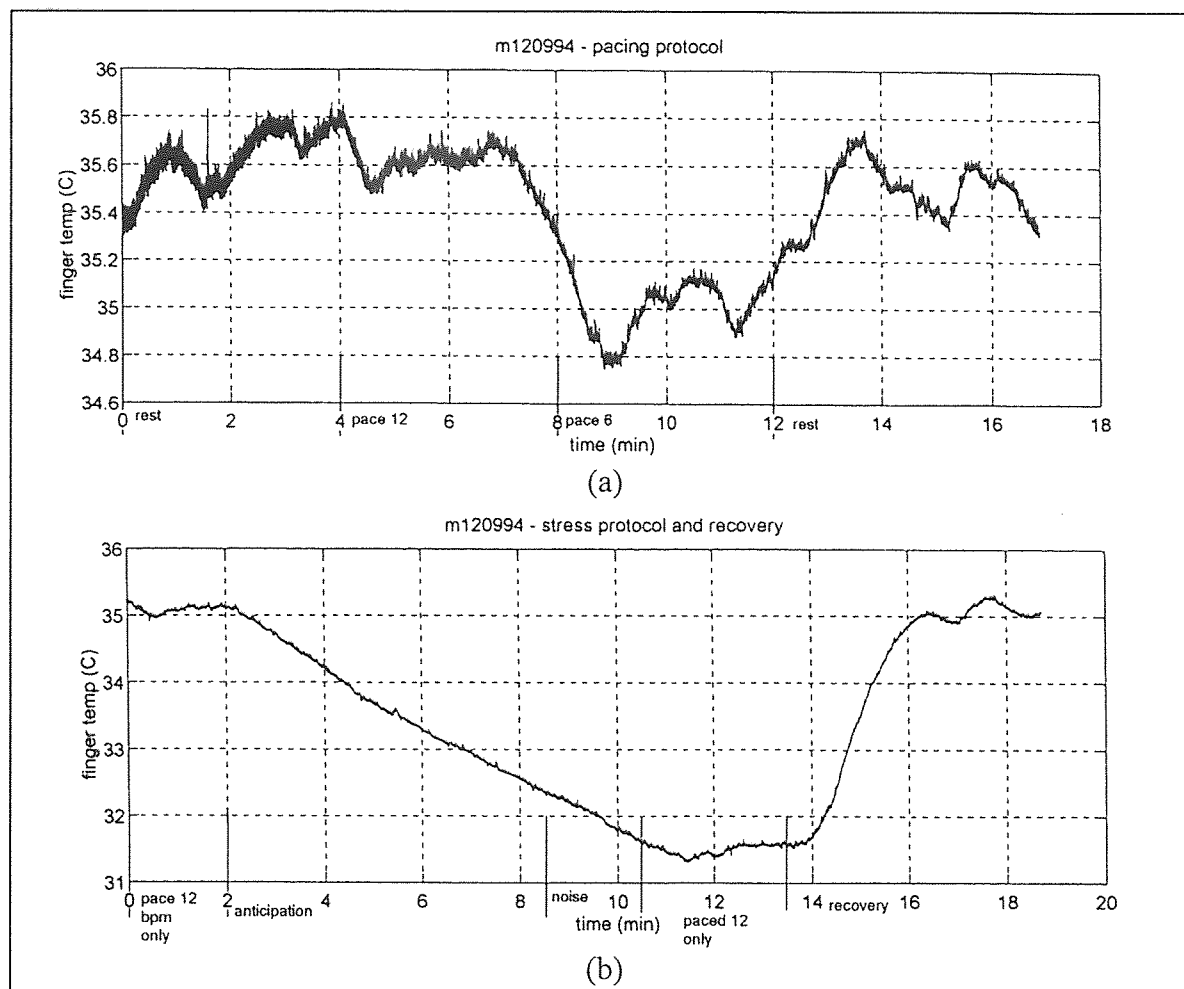
Figure 3.5 Skin Temperature during the stress experiment. (a)Paced breathing protocol (b) Stress protocol

the first for minutes. The subject then paced his breathing at 12 breaths per minute for four minutes, then paced at 6 breaths per minute for four minutes. Finally the subject rested for five minutes. Skin temperature fell during the breathing at six breaths per minute, indicating that this breathing frequency may have been uncomfortable for this subject.

Figure 3.5b shows the skin temperature during the stress portion of the protocol. The subject breathed at 12 breaths per minute from t=0 to t=12 minutes. At two minutes,

the experimenter went behind the equipment, and the subject began to get anxious, mentally anticipating what may happen next. The noise started at t=8.5 minutes, and lasted for two minutes. Temperature fell though the anticipation and the noise, and stayed somewhat steady in the time from t=10.5 minutes to t=13.5 minutes, when the subject was paced breathing only. At 13.5 minutes, the subject stopped pacing and the experimenter reappeared from behind the equipment, the subject relaxed, and the skin temperature rose rapidly to pre-stress levels. Notice that there is also a time delay of about a minute between the change in the protocol and the reaction of the skin temperature. This is because of the thermal inertiance of the skin, and will be explained in detail later in this chapter.

From this data, it is clear that however the stress was caused, there was a definite sympathetic response, which is represented by the drop in skin temperature caused by the constricting of the cutaneous blood vessels. Since these vessels are controlled by the sympathetic nervous system only, changes in skin temperature correspond to changes in sympathetic tone.

3.2.2.2 Autonomic Response

Measuring the autonomic response to stress and relaxation has proved to be complicated. There are many reasons why the interpretation of the results is difficult. These fall into four main categories. One is the thermal inertiance of the skin to changes in blood flow, which is a physiological difficulty. Second is the sensitivity of the Wigner distribution to low amplitude spectral components and the appearance of cross terms in the calculation

of the Wigner distribution, which is a signal processing difficulty. Third, there is intersubject variability; subjects reacted differently to both the paced breathing and the method of stress. This is both a physiological and a psychological difficulty. Finally, when a subject breathes below 0.15 Hz (9 breaths per minute), the heart rate variability peak at the respiration frequency which is normally in the high frequency range, appears in the low frequency range, where it contains information about both the sympathetic and parasympathetic nervous system and not just the parasympathetic. Two subjects in this study had resting respiration rates below 9 breaths per minute. This difficulty was detailed in section 3.1.3.

Figure 3.6 details the recovery portion of figure 3.5b, where the skin temperature rose rapidly as the subject relaxed. The origin (t=0) on figure 3.6 corresponds to t=13.5 minutes on figure 3.5b. There is a delay of approximately 30 seconds to one minute from the time an event is initiated to the time the skin temperature begins to change. Almost a full three minutes is required for the temperature to rise and stabilize at its new level. This delay results from the fact that heat from the increased volume of blood in the finger
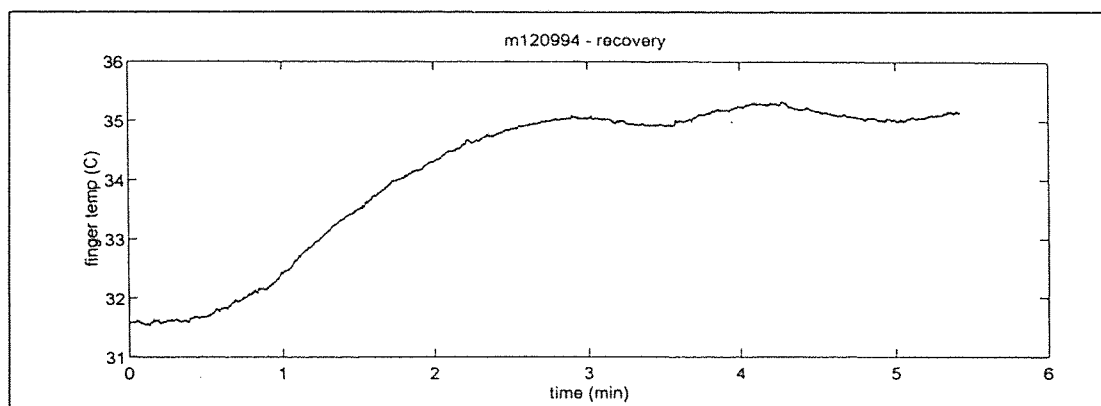

Figure 3.6 Illustration of the time delay in the skin temperature response. Time zero here is time 13.5 minutes on figure 3.5b.
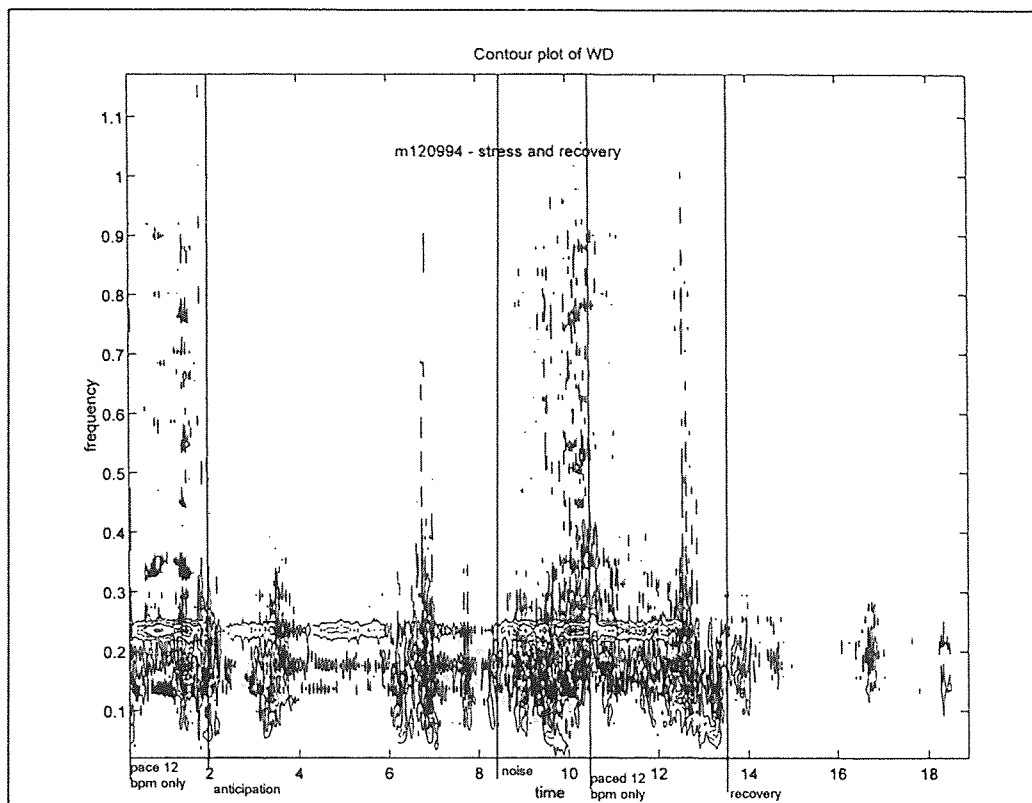
Figure 3.7 Contour graph of the Wigner distribution during the stress protocol. Dark areas indicate areas of highest power.

capillaries must travel through some layers of tissue before it can be transferred from the skin to the environment.

A contour graph of the Wigner distribution for the stress protocol and recovery on one subject is shown in figure 3.7. This is a graph of the heart rate variability spectrum versus time and frequency. The dark areas on the graph indicate points of higher power, and the open shapes indicate areas of lower power. The prominent horizontal band at about 0.23 Hz contains several concentric contours, which represent increasing power moving toward the center of the contours. Areas with more contours within this band have higher power than areas with fewer contours.

The horizontal band that occurs at about 0.23 Hz represents the subject pacing his breathing at around 12 breaths per minute. The peaks that appear below the high frequency or respiration peak in the low frequency range (at around 0.13 Hz) are a low frequency peak. However, the graph also includes other low amplitude artifacts which appear as the vertical bands, or cross terms, which appear in several places, including a band between the low and high frequency peaks. It can be seen that the desired information is present in the data, but extracting useful information from the Wigner distribution has proven to be difficult. General trends and large scale changes can be seen, and these trends have revealed the third complexity arising from the stress experiments.

Two subjects' data for the paced breathing part of the experiment are shown in figures 3.8 and 3.9. Figures 3.8a and 3.9a show the interbeat interval for each subject, 3.8b and 3.9b show the area under the low frequency peak using time frequency analysis, and 3.8c and 3.9c show the areas under the high frequency peak. The protocol for this portion of the experiment was four minutes of rest, four minutes of paced breathing at 12 breaths per minute, four minutes of paced breathing at 6 breaths per minute, and four minutes of rest.

The subject for figure 3.8 was a 27 year old athletic male who exercised on a fairly regular basis. There are 11 cycles in the variability shown in the first two minutes of graph (a), which shows that this subject's resting respiration rate was between 5 and 6 breaths per minute. When the subject was forced to breathe at 12 breaths per minute, the variability in the heart rate decreased dramatically. This is clearly shown in (b) and (c), where between 4 and 8 minutes, the variability spectrum drops to near zero for both the

Figure 3.8 Time frequency analysis of a 27 year old male subject. (a) Interpolated interbeat interval. (b) Area under the low frequency range versus time. (c) Area under the high frequency range versus time.
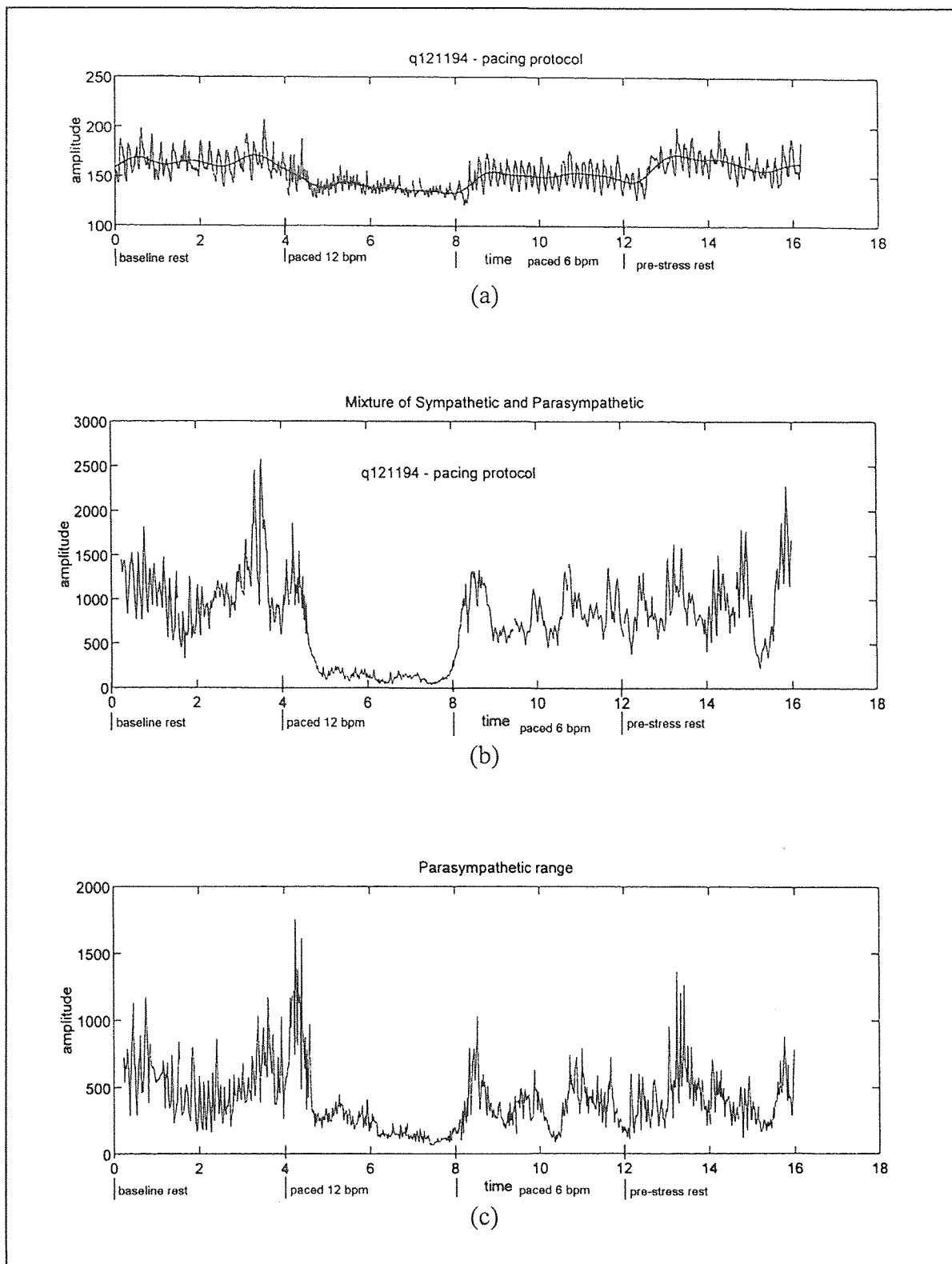
Figure 3.9 Time frequency analysis of a 24 year old female subject. (a) Interpolated interbeat interval. (b) Area under the low frequency range versus time. (c) Area under the high frequency range versus time.
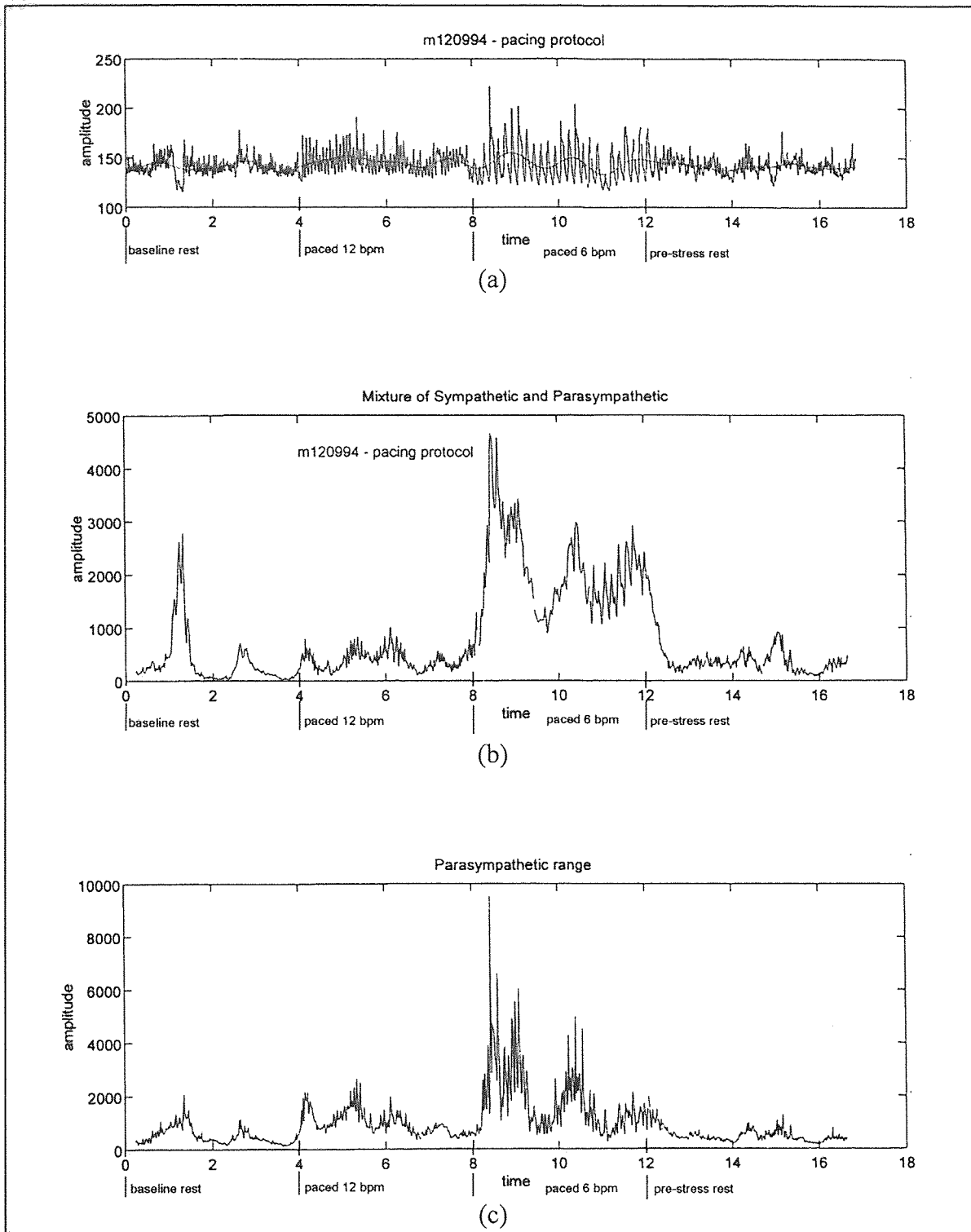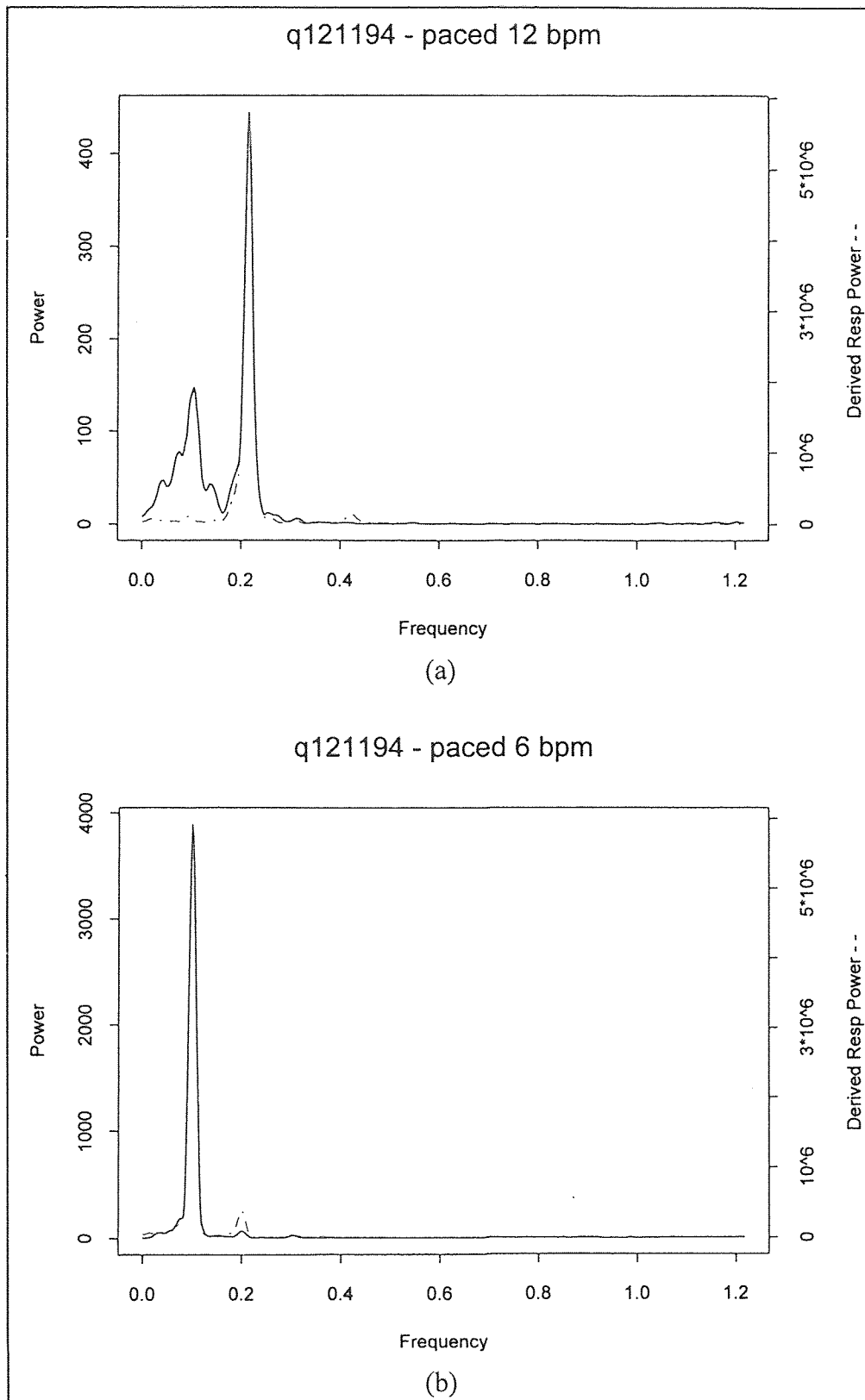
Figure 3.10 Heart rate variability spectra for the subject shown in figure 3.8. (a) paced breathing at 12 breaths per minute (b) Paced breathing at 6 breaths per minute

low and high frequency ranges. When the subject started pacing at 6 breaths per minute at 8 minutes into the test, the variability rose again to resting levels. The transition between pacing at 6 breaths per minute and resting at 12 minutes into the test is impossible to see, since the subject's resting breathing rate is close to 6 breaths per minute. It is interesting to note that with the increase in breathing rate to 12 breaths per minute, the respiration peak should have moved above the 0.15 Hz threshold. Figure 3.10 shows the heart rate variability spectra corresponding to the paced 12 and paced 6 parts of figure 3.8 (t=4 to 12 minutes). Close examination of the heart rate variability spectra shown in figure 3.10a clearly shows the respiration peak around 0.2 Hz. It also shows that its relative amplitude was ten times lower than the respiration peak during pacing at 6 breaths per minute (figure 3.10b). This indicated that the subject was quite uncomfortable pacing at 12 breaths per minute, a fact confirmed by post-experiment questioning of the subject.

The subject in figure 3.9 was a 24 year old sedentary female of about the same age as the previous subject. In contrast to 3.8a, counting the cycles in the first 2 minutes of 3.9a shows that she has a much higher resting breathing rate of around 14 breaths per minute. When this subject began to breathe at 12 breaths per minute, the high frequency peak increased, and was much higher in amplitude that the first subject. When the subject began to breathe at 6 breaths per minute, there was a dramatic jump in the low frequency area. There was also a jump in the high frequency area, but the ratio of the low to high frequency area also rose, indicating that the rise in low frequency area was much higher than the rise in high frequency area. This is expected to happen, as breathing at 6 breaths per minute will force the respiratory peak below 0.15 Hz. When pacing stopped, the

subject's breathing returned to its resting level and the respiration peak was again above 0.15 Hz. The results from these three subjects do not indicate whether the differences in heart rate variability responses are due to physical training or gender differences. Indeed there may be contributions from both causes. However, exercise studies by Fernando on a group of male subjects has shown differences between subjects who regularly exercise and those that do not. [8] Comparison of these three subjects dramatically illustrates that interpretation of the results of experiments of this kind depends greatly on the physiology of the subject.

The above effects of individual physiology on the autonomic response during paced breathing was also evident during the stress portion of the experiment. For the two male subjects especially, since pacing at 12 breaths per minute was uncomfortable and unnatural, the heart rate variability data was skewed in the direction of a stressful event before the anticipation or noise stresses began. Data from the 27 year old male appear in Appendix A. Both the high frequency and low frequency graphs were attenuated in a similar manner to figure 3.8 (b) and (c), which was described earlier. However, the skin temperature responded very similarly to the 24 year old female which was shown in figure 3.3, indicating a sympathetic nervous system response to the stress.

3.2.2.3 Meditation

One of the tested subjects was an experienced meditator, so he was asked to perform his meditation technique in addition to the stress protocol. EEG was recorded along with ECG and skin temperature for this subject. The meditation protocol consisted of the
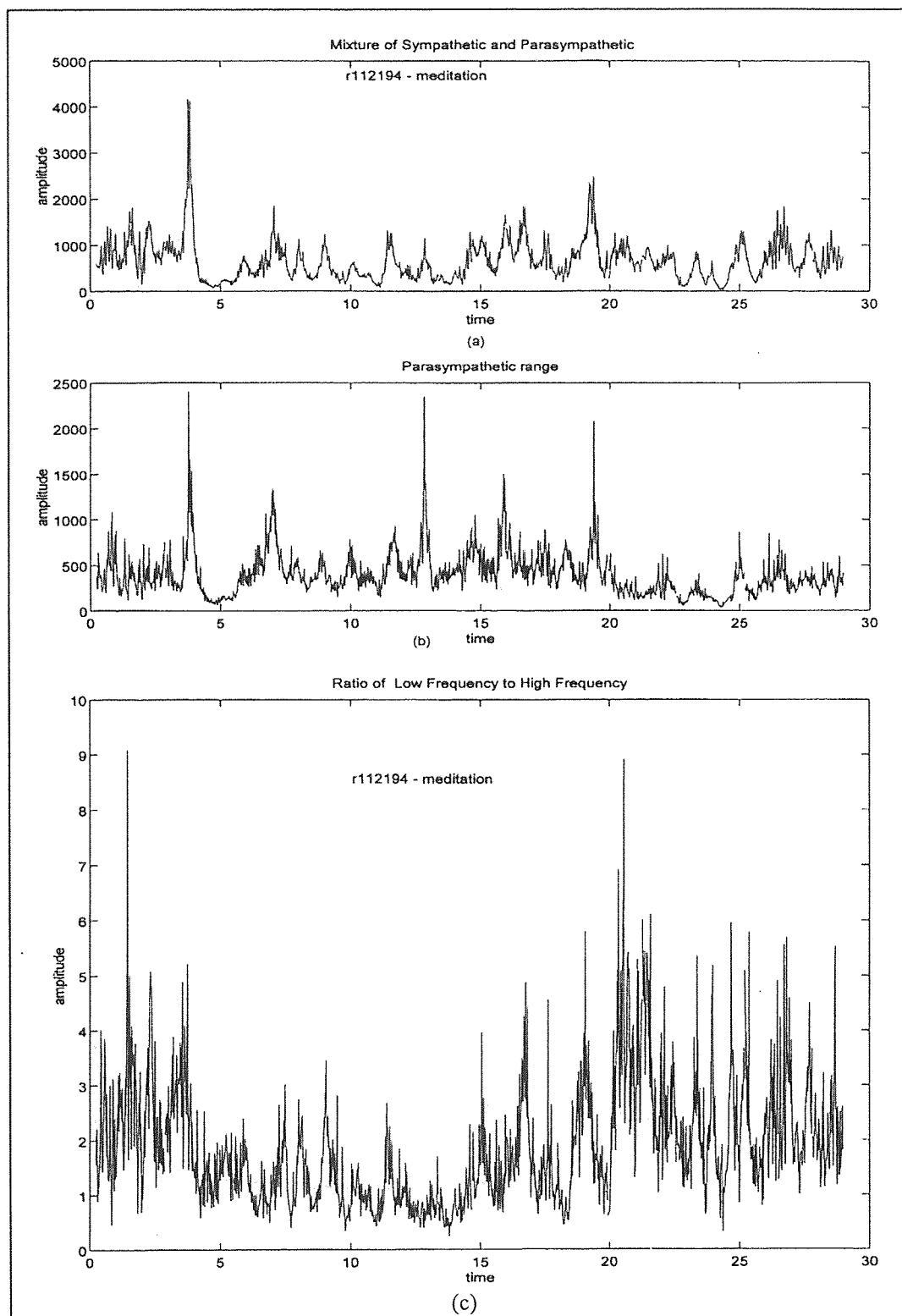
Figure 3.11 Time frequency analysis of meditation. (a) Area under low frequency range. (b) Area under high frequency range. (c) Ratio of low frequency to high frequency area.

subject sitting quietly with eyes open for 4 minutes, sitting with eyes closed for three minutes, meditating for fifteen minutes, then eyes closed for three minutes and eyes open for four minutes.

Analysis of EEG coherence indicated alpha coherence in the 9 to 10 Hz band during the eyes closed and meditation portions of the protocol. Figure 3.11 shows the time frequency analysis of heart rate variability. Figure a shows the low frequency area versus time, figure b shows the high frequency area versus time, and figure c shows the ratio of the low frequency to high frequency area. There still was a very slight rise in the high frequency or parasympathetic range (shown on the second graph). There was also a corresponding drop in the ratio of low to high frequency ranges during that time. This would seem to indicate a small rise in parasympathetic activity.

Figure 3.12 shows the heart rate variability and derived respiration spectra for two segments of the meditation protocol. Figure (a) is the first eyes closed portion, and figure (b) is a three minute section of meditation. Both show the main variability peak (shown by the solid line) below 0.15 Hz, at around 0.1 Hz. The derived respiration signal (shown by the dashed line), appears at close to 0.3 Hz, which should not be the case since respiration is usually very slow during meditation.

Figure 3.12b shows a smaller heart rate variability peak appearing in the high frequency range at close to 0.3 Hz. This corresponds to the rise in high frequency area shown by the time frequency analysis in figure 3.11 described above. It also lines up with the derived respiration peak for that time. This data would indicate that the subject increased his breathing rate from 6 breaths per minute at rest to 16 to 18 breaths per
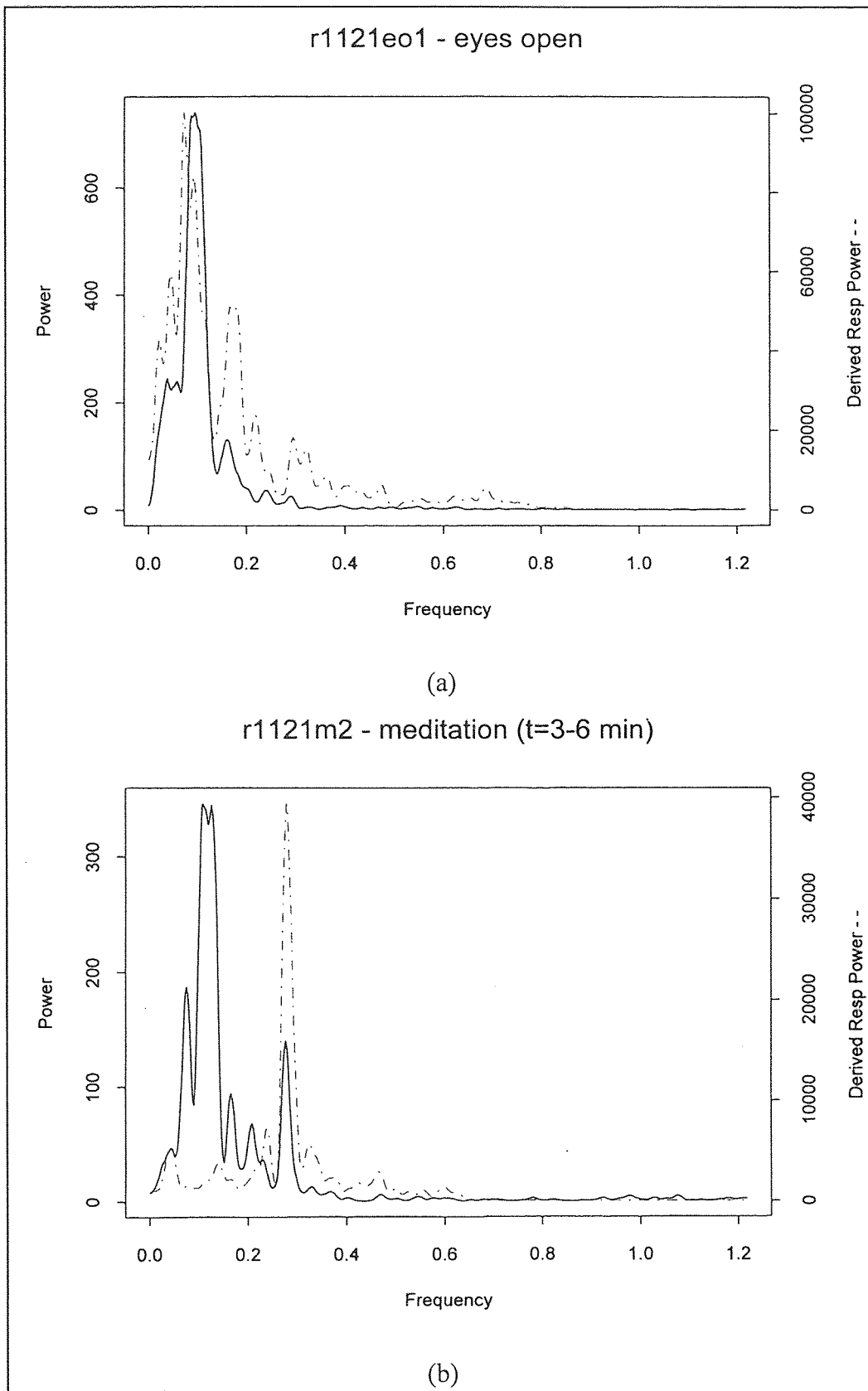
Figure 3.12 Heart rate variability during meditation. (a) eyes closed (b) meditation

minute during meditation. Because of the nature of meditation this is difficult to believe. A more plausible explanation is that some fault may lie in calculating the derived respiration signal from the ECG.

If a rise in parasympathetic activity was occurring, it should show in the low frequency range (where the heart rate variability peak corresponding to respiration is), not the high frequency range. The graph of the low frequency range does not change, which could mean either parasympathetic activity did not change, or parasympathetic activity did change while sympathetic activity changed in the opposite direction. More testing is necessary to explore these questions. Certainly a larger pool of subjects is needed to account for the individual differences that will appear between subjects. Directly measuring the subject's respiration in some way may help to improve the derived respiration signal.

Figure 3.13 shows the skin temperature during the meditation. Transitions in the protocol are marked with initialed vertical lines: e.o. for eyes open, e.c. for eyes closed, and m. for meditation. There is a distinct time delay of about a minute between a change in the protocol and the response of the skin temperature. Skin temperature rose more than $7°C$ during meditation, which is a very drastic change. This shows the very relaxing nature of meditation on the body, and since the cutaneous blood flow is mediated by the sympathetic nervous system only, it is reasonable to conclude that the increase in skin temperature reflected an overall decrease in sympathetic tone.
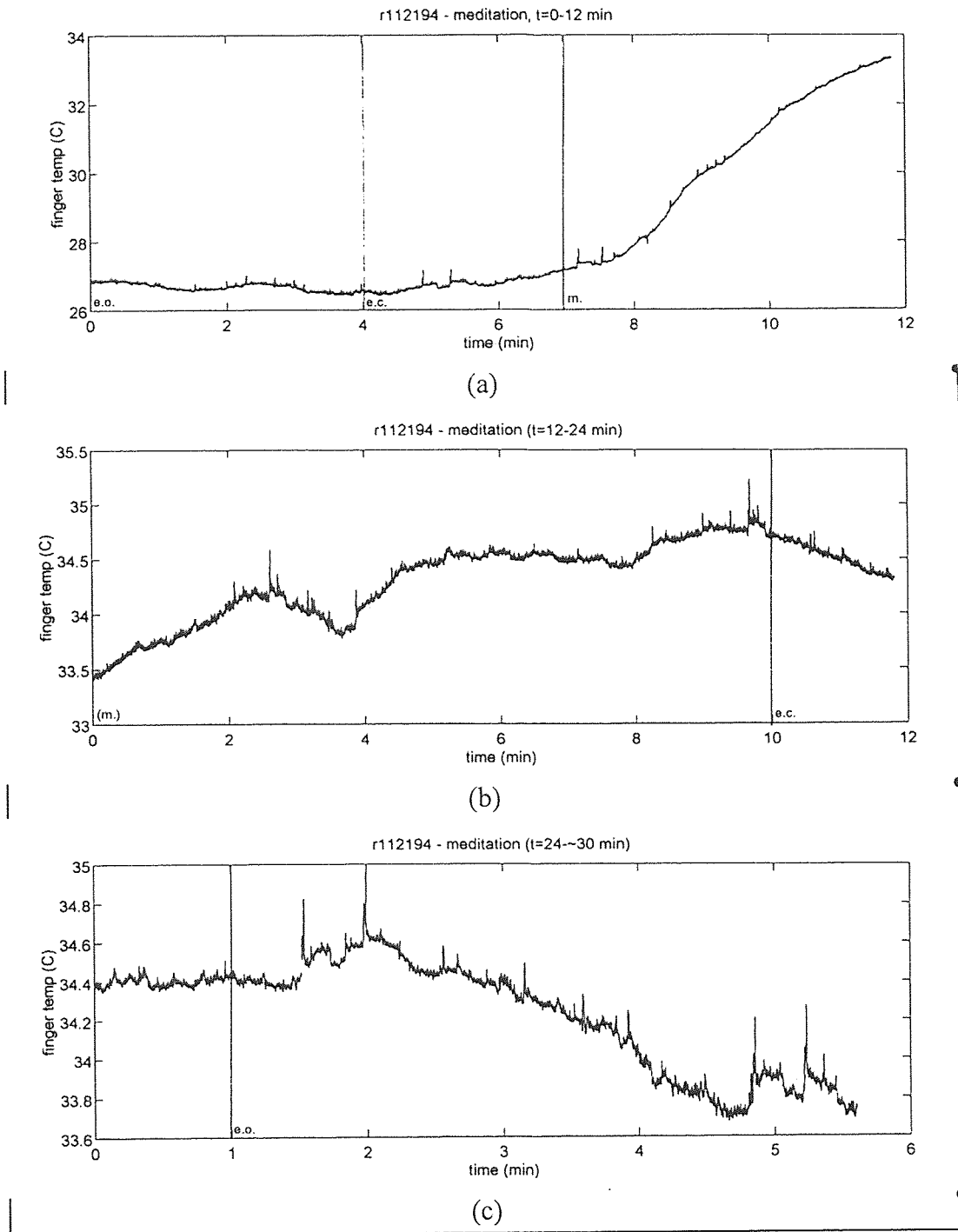
Figure 3.13 Skin temperature changes during meditation

CHAPTER 4

CONCLUSIONS

The noninvasive measurement of stress and relaxation responses can provide useful information about the state of health of an individual. The physiological responses of the heart, circulation, and the nervous system provide valuable clues to the state a person is in. The reaction to stress and relaxation involves a complex interplay between the mind, the body and the external environment. It has been demonstrated that even the thought that an unpleasant event will happen is enough to cause a powerful response from the autonomic nervous system before the event even occurs.

Extracting physiological data under controlled conditions has proven to be an intricate process, as there are many variables to be controlled, including the psychological contribution to the physiological state. The work for this thesis has laid the foundation for many future experiments that can more fully explore the physiological underpinnings of the stress and relaxation responses.

4.1 The Psychological Component of Stress and Relaxation

One of the major conclusions of these experiments is the importance of the conscious mind in inducing a stress or relaxation response. The act of meditation itself is a conscious control of the relaxation response, as the meditator consciously initiates a session with the chosen phrase, initiating a set of responses that cause the person to relax completely. At the other end of the spectrum, anticipation of an event, especially if it is

perceived by the person as unpleasant or threatening, can cause the stress response: the sympathetic response of a quickening heart rate and decrease in skin temperature.

An experimenter wishing to measure the physiological components of stress must be aware of the psychological component. This must be at least controlled for, though if the experiment is designed well it can be taken advantage of to produce the response that is to be measured. The mental anticipation of an unpleasant event is one way to accomplish this.

4.2 Skin Temperature as a Measure of Sympathetic Activity

Peripheral blood flow is extremely sensitive to changes in sympathetic tone. The measurement of skin temperature has shown that skin temperature will decrease when a person is experiencing stress, corresponding to an increase in sympathetic tone. Skin temperature will increase when a person is relaxed, indicating a decrease in sympathetic tone. Most times changes in sympathetic tone are accompanied by changes in parasympathetic tone in the opposite direction. This measure has one major drawback, which is the time delay between the instant of an event and the change in skin temperature caused by the thermal inertiance of the skin. Skin temperature can only be used to record average changes in sympathetic function over long periods of time, rather than the much quicker changes that often happen with a mass sympathetic discharge.

Since the temperature of the skin changes due to changes in peripheral circulation, measurement of blood flow directly would be a better method to measure how the sympathetic nervous system is acting on the peripheral blood vessels. One way to

measure blood flow noninvasively is by venous occlusion plethysmography. Instruments are available that use plethysmography to measure blood flow in the fingertip. There are many other methods as well, including Doppler flowmeters, and it would be worthwhile to investigate which ones would be best suited to measuring rapid changes in blood flow.

4.3 Time Frequency Analysis of Heart Rate Variability Using the Wigner Distribution

Time frequency analysis is a powerful tool for measuring rapid changes in frequency over time. The difficulty arose in extracting useful and relevant information from a complicated signal representation. Using the Wigner distribution, general trends in vagal tone and the sympathetic-parasympathetic mixture could be seen. However, specific rapid changes in frequency were often hidden due to small amplitude frequency components other than the respiratory peak and the low frequency peak as well as by cross terms produced by the Wigner distribution itself. The first problem arises from the sensitivity of the Wigner to the small components that are already in the signal. The second is a characteristic of the Wigner distribution itself. A worthwhile endeavor for future studies would be to use a distribution that produces less cross terms so that the true frequency components could be seen.

One result that could be clearly seen is the rapid change in comfort level when subjects breathe at frequencies different that their natural one. This effect appeared very dramatically and points to one of the pitfalls in using paced breathing in these tests. The purpose of the paced breathing was to forcibly place the respiration peak above 0.15 Hz so that the effects of stress on the low frequency peak could be determined. However,

when this is uncomfortable for the subject, this discomfort causes a marked decrease in sympathetic tone and itself becomes a stressor, and can effectively block the autonomic effects of another external stress. Future studies similar to the present one should control for this effect. One possible way is to screen subjects before the experiment by taking between 5 and 10 minutes of data to measure the subject's normal resting respiration rate. Only those subjects that normally breathe at frequencies above 0.15 Hz would be used in the study, and the pacing frequency during the stress protocol could be set at the subject's natural breathing frequency to minimize the stress caused by discomfort.

4.4 Future Work

This pilot study has shown that there is a wealth of information to be drawn from the study of stress, and it has great potential benefits to patients and caregivers alike, as well as the general population. There is still a lot to discover before this can happen. The following paragraphs will detail a couple of directions this research can proceed.

The study has shown that individuals can react very differently to an experimental procedure based on their physical and psychological condition. Refinement of the experimental protocol to truly take advantage of the psychological component of stress and to measure its effects on the body is one possibility. Such an experiment would need a large number of participants to wash out the heterogeneous effects of the individuals in the group. Another possibility is to compare different homogeneous groups that differ by one important characteristic, such as athletic versus sedentary persons or meditators versus non-meditators.

There is still a wealth of information contained in the time frequency analysis of heart rate variability. Use of a distribution other than the Wigner distribution may give a clearer picture of the rapid changes in frequency over time with less noise. Calculations of slope, means, areas, and other mathematical properties may reveal information hidden in the distribution.

The application of time frequency analysis to EEG signals is also another route to follow. The calculation of rapid changes in the EEG frequency over time, together with the measurement of EEG frequency coherence over time may also give interesting insights into the mental state of an individual.

Finally, intersubject coherence was mentioned toward the beginning of this thesis. It would be a worthwhile project in itself to measure the EEG coherence between two or more individual meditators. Some researchers have investigated a possible field effect connected with EEG and meditation [21], [25], [26], and meditators themselves report deeper and more relaxing meditations when they meditate in groups compared to when they meditate alone. It would also be interesting if a higher intersubject EEG coherence might lead to entrainment of other physiological parameters, such as heart rate or respiration rate.

APPENDIX A

FIGURES OF ORIGINAL DATA

The following graphs show raw data for two subjects who participated in the final stress protocol. Each subject had slightly different times for each event, but both performed the same sequence of events. The following chart summarizes the figures that appear in this appendix.

Table A.1 Summary of Appendix A figures.

Figures	Subject	Protocol	Event	Time on Graph (minutes)
A.1 - A.5	m120994	pacing	baseline rest paced 12 bpm paced 6 bpm pre-stress rest	0 - 4 4 - 8 8 - 12 12 - 17
A.6 - A.10	m120994	stress	paced 12 bpm only anticipation stress paced 12 bpm only recovery	0 - 2 2 - 8.5 8.5 - 10.5 10.5 - 13.5 13.5 - 19
A.11 - A.15	q121194	pacing	baseline rest paced 12 bpm paced 6 bpm pre-stress rest	0 - 4 4 - 8 8 - 12 12 - 16.5
A.16 - A.20	q121194	stress	paced 12 bpm only anticipation stress paced 12 bpm only recovery	0 - 2 2 - 5 5 - 8 8 - 11 11 - 17

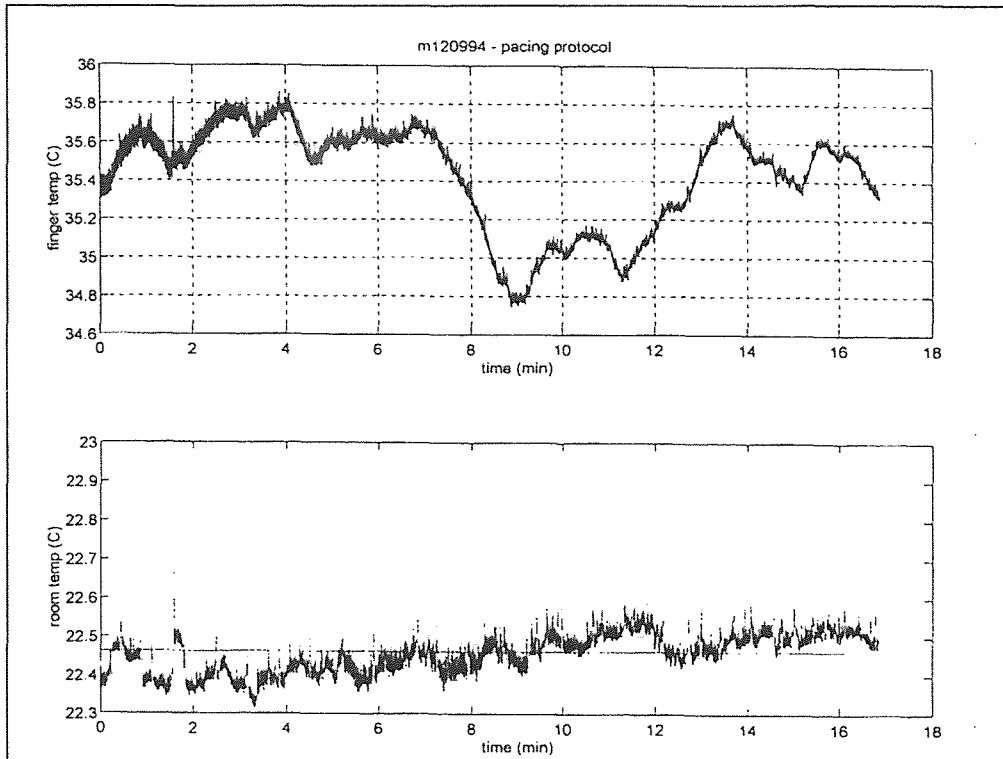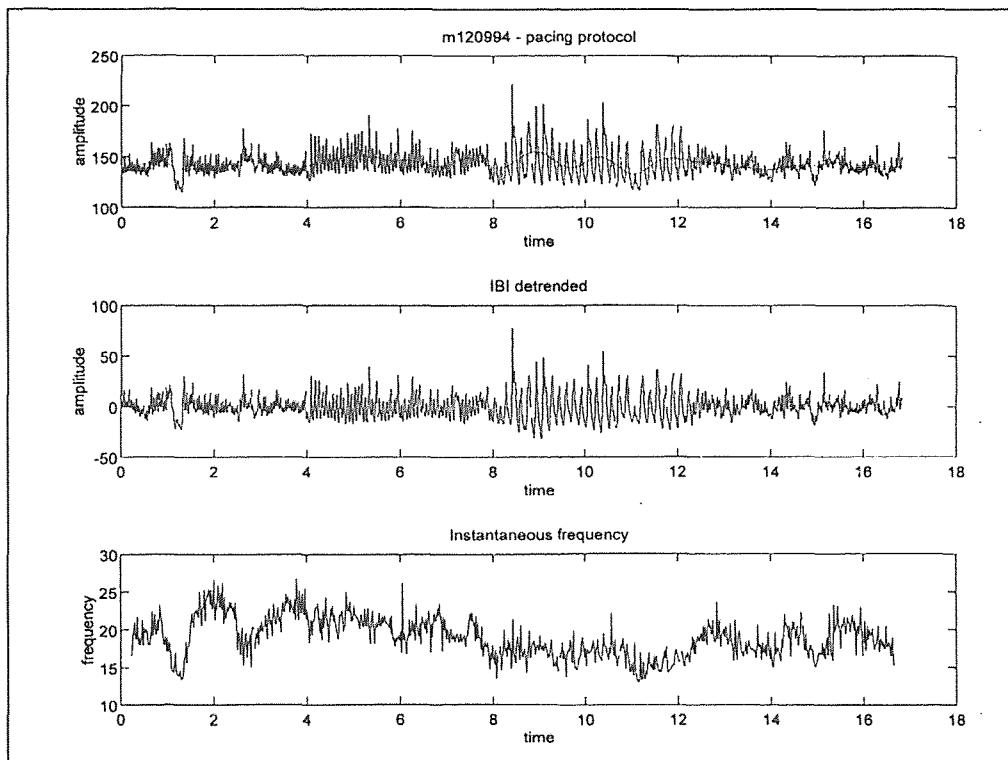**Figure A.1** Pacing protocol: skin temperature and room temperature.

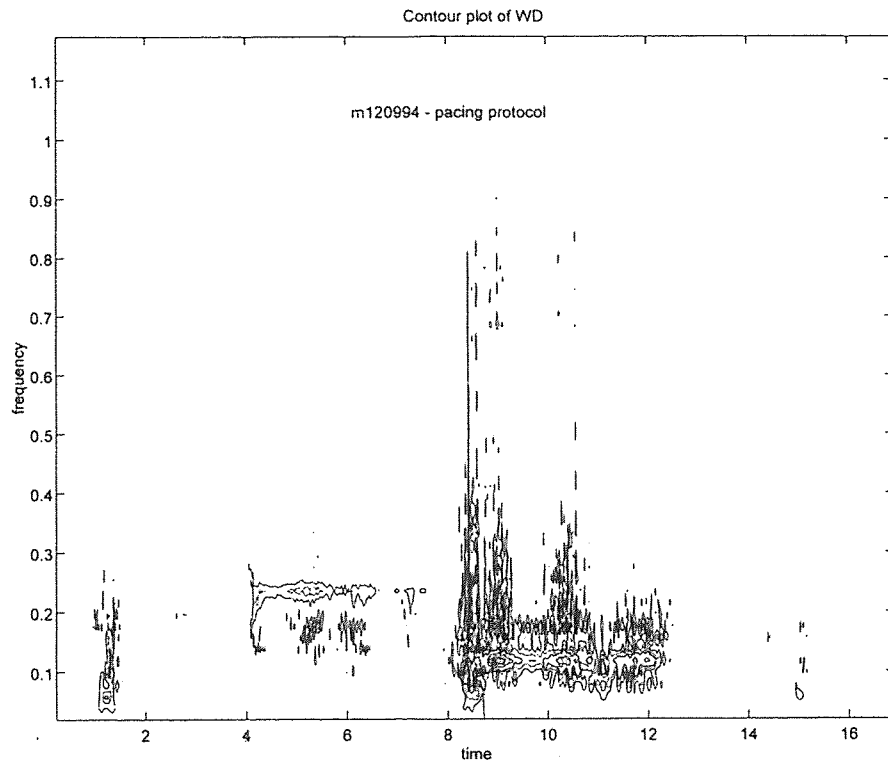**Figure A.2** Interbeat interval and instantaneous frequency.

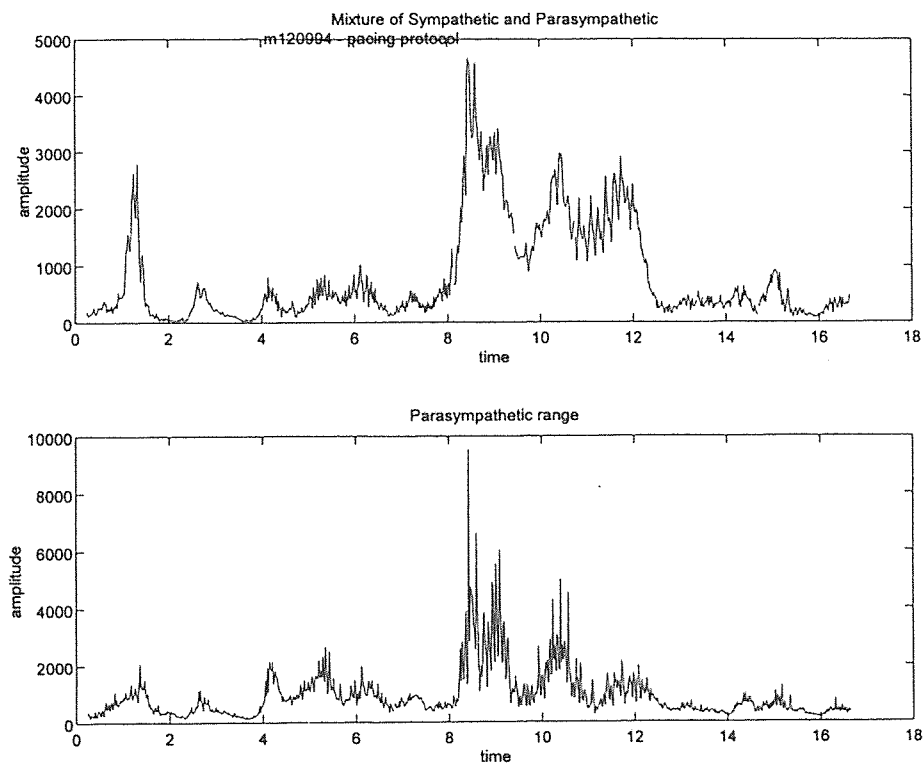**Figure A.3** Wigner distribution of heart rate variability.

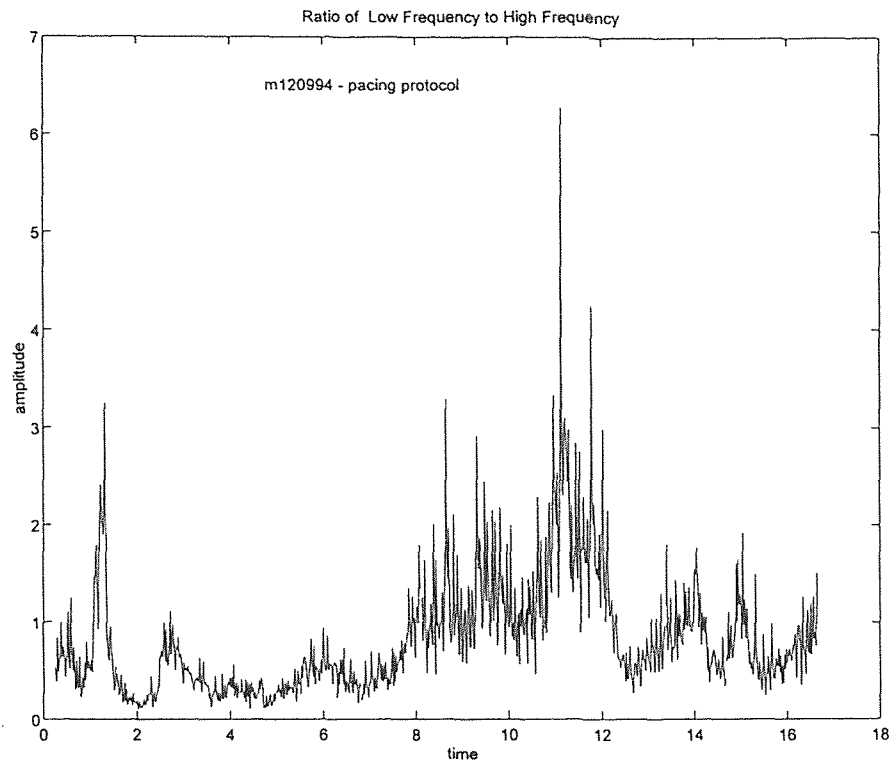**Figure A.4** Low frequency and high frequency areas.

Figure A.5 Ratio of low to high frequency ranges.

Figure A.6 Stress protocol: skin temperature and room temperature.

Figure A.7 Interbeat intervals and instantaneous frequency.

Figure A.8 Wigner distribution of heart rate variability.

Figure A.9 Low frequency and high frequency areas.

Figure A.10 Ratio of low to high frequency ranges.

Figure A.11 Pacing protocol: skin temperature and room temperature.

Figure A.12 Interbeat interval and instantaneous frequency.

Figure A.13 Wigner distribution of heart rate variability.
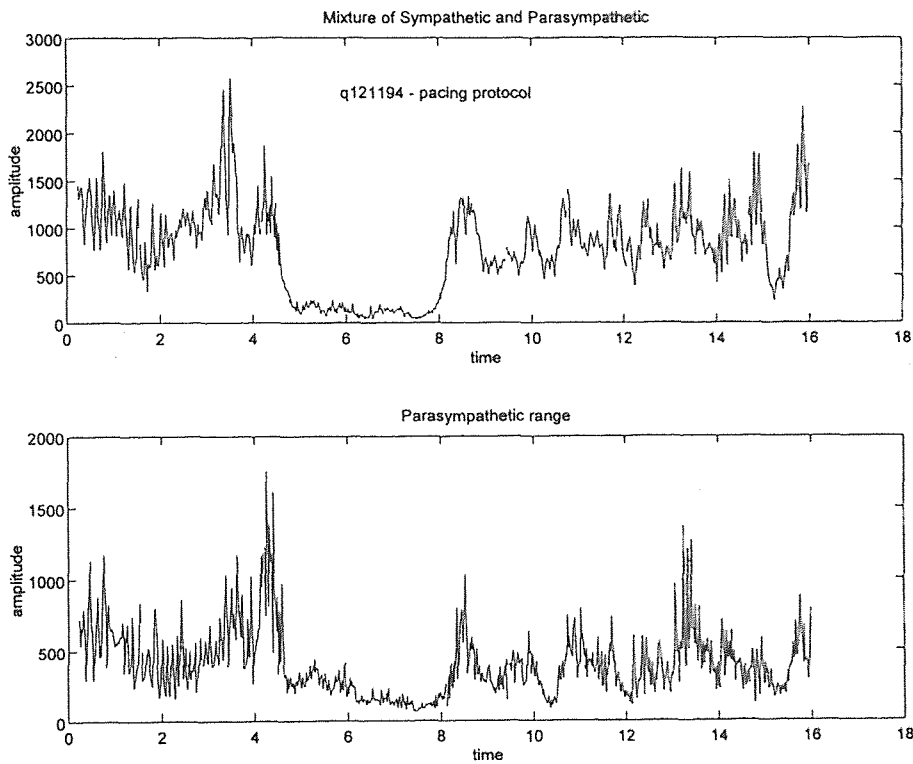
Figure A.14 Low frequency and high frequency areas.
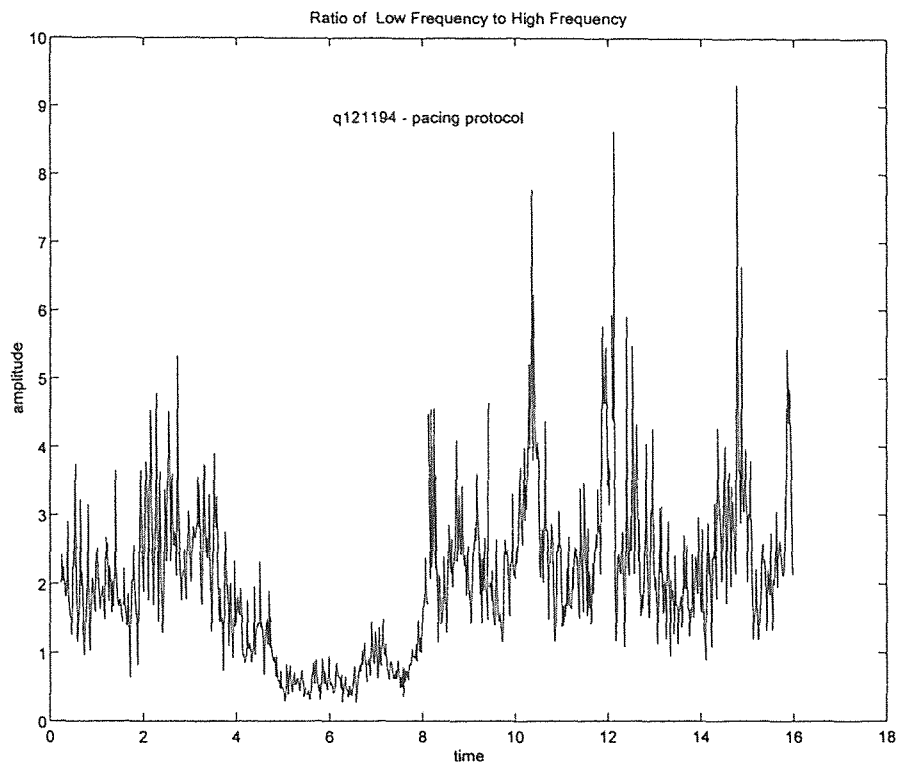
Figure A.15 Ratio of low to high frequency ranges.
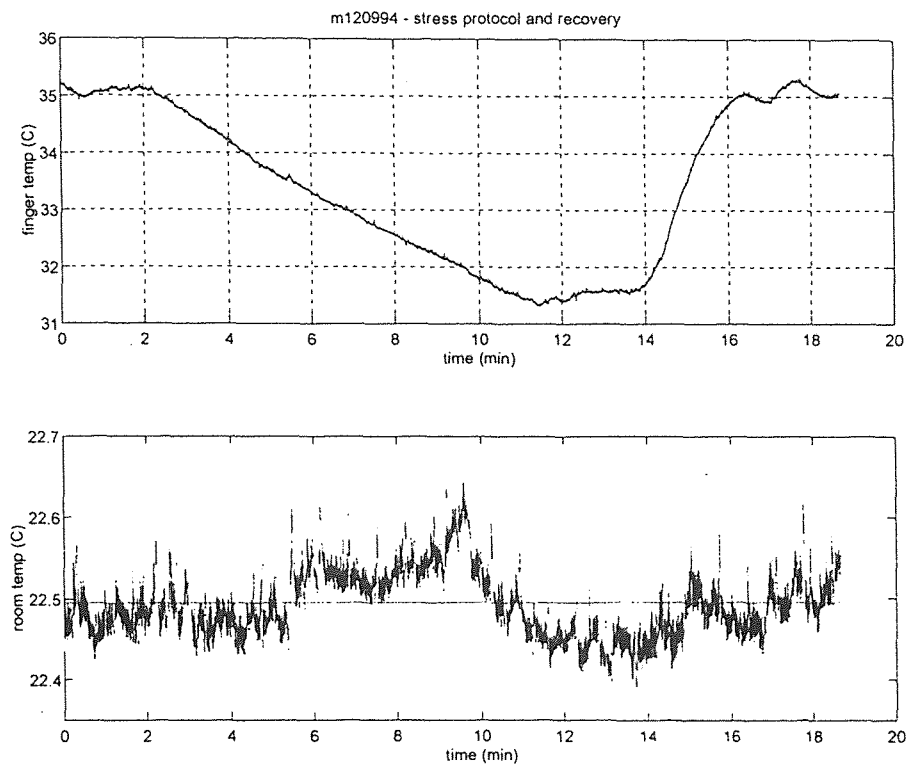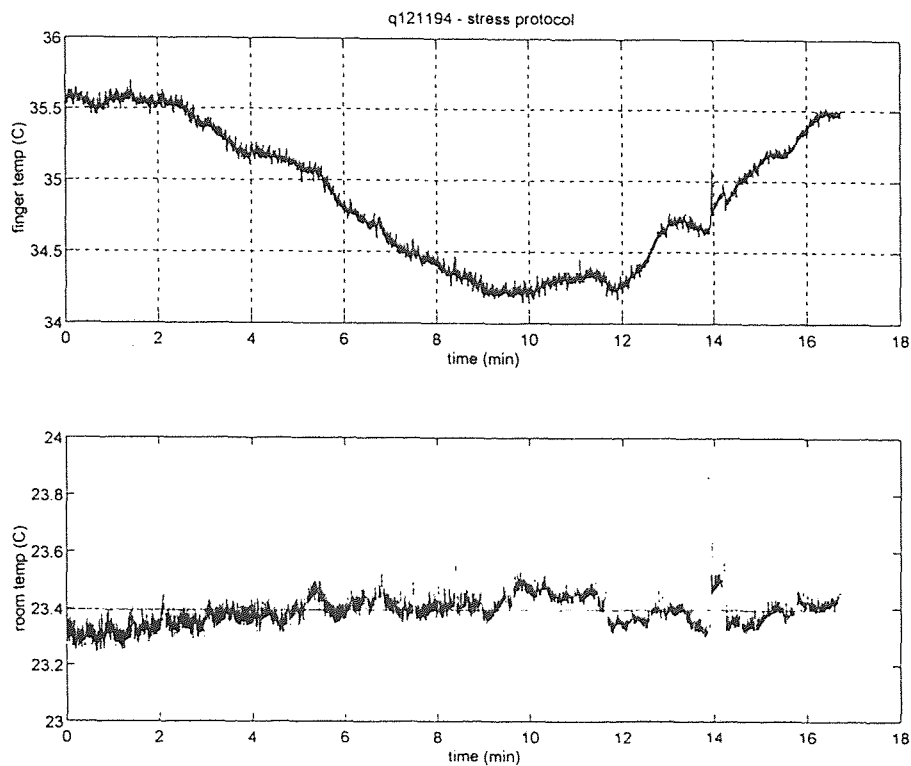

Figure A.16 Stress protocol: skin temperature and room temperature.
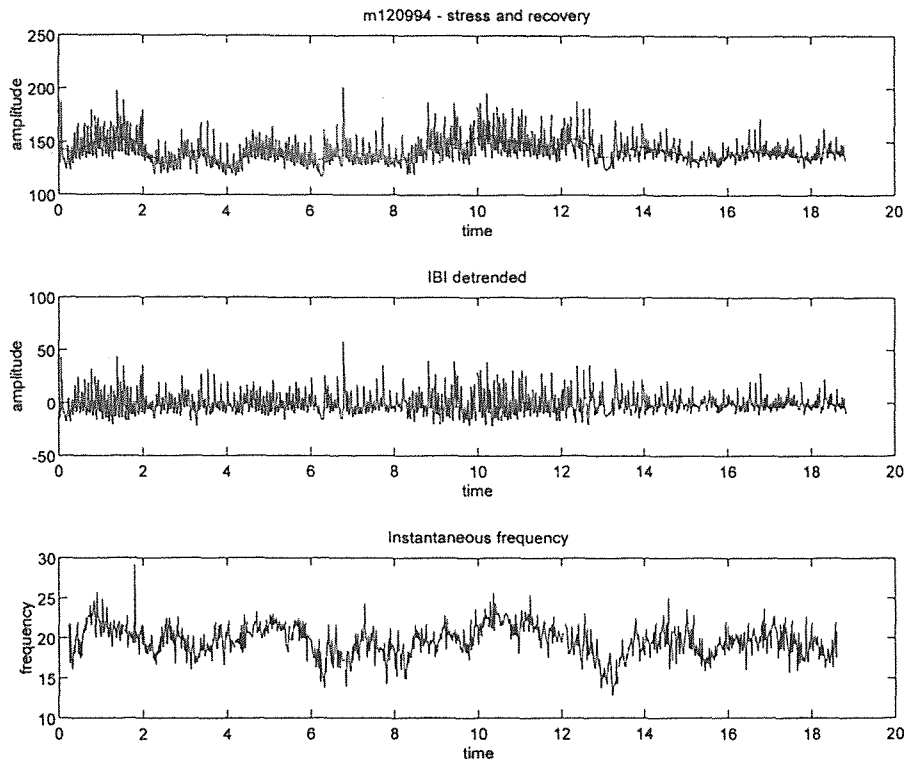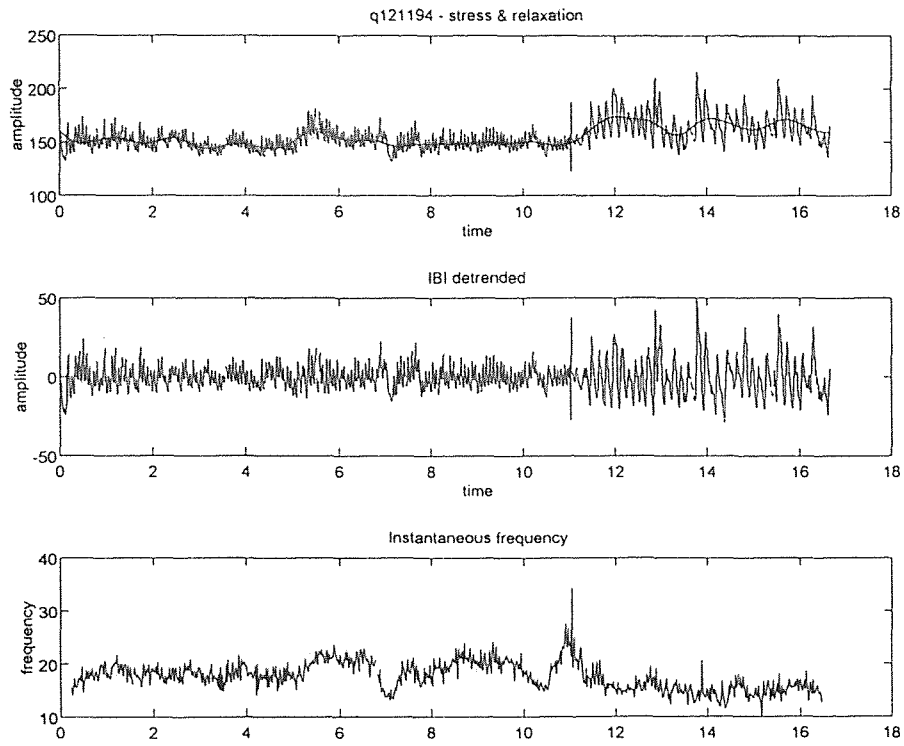
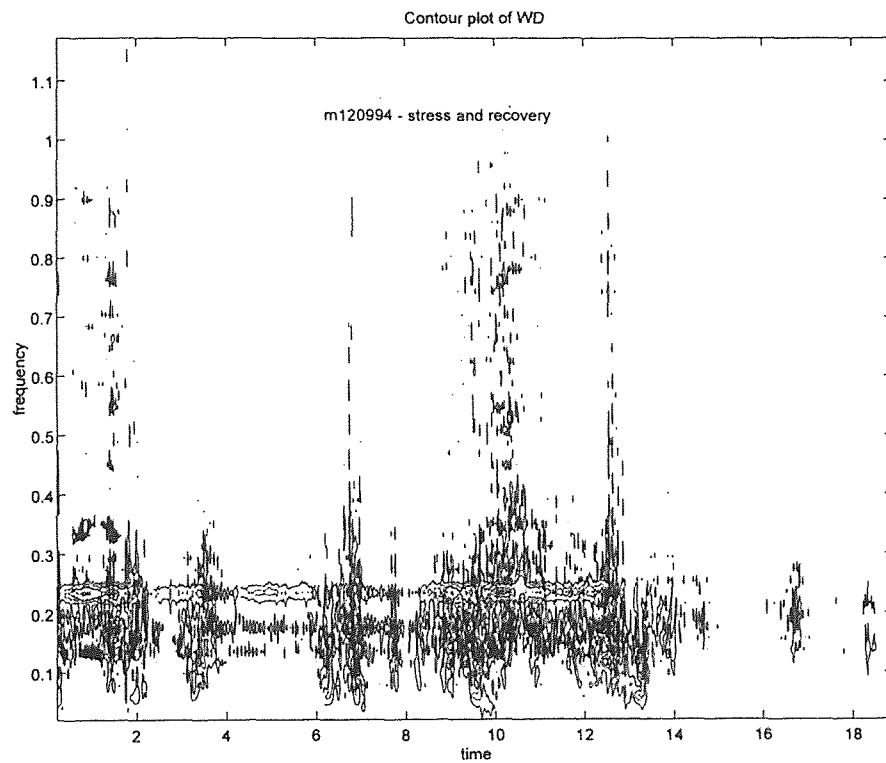**Figure A.17** Interbeat intervals and instantaneous frequency.
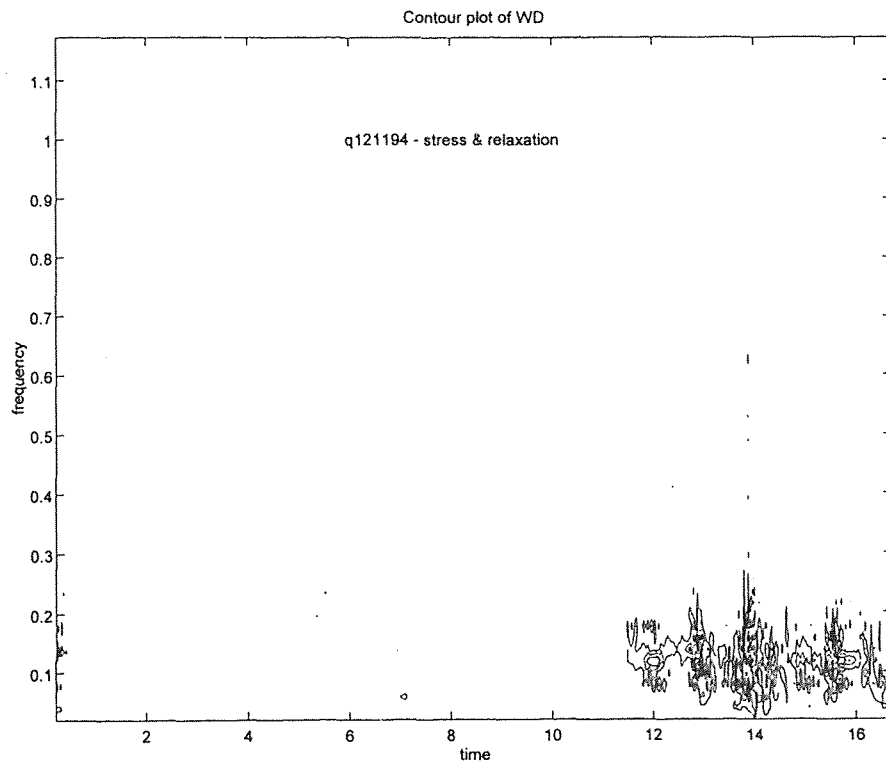
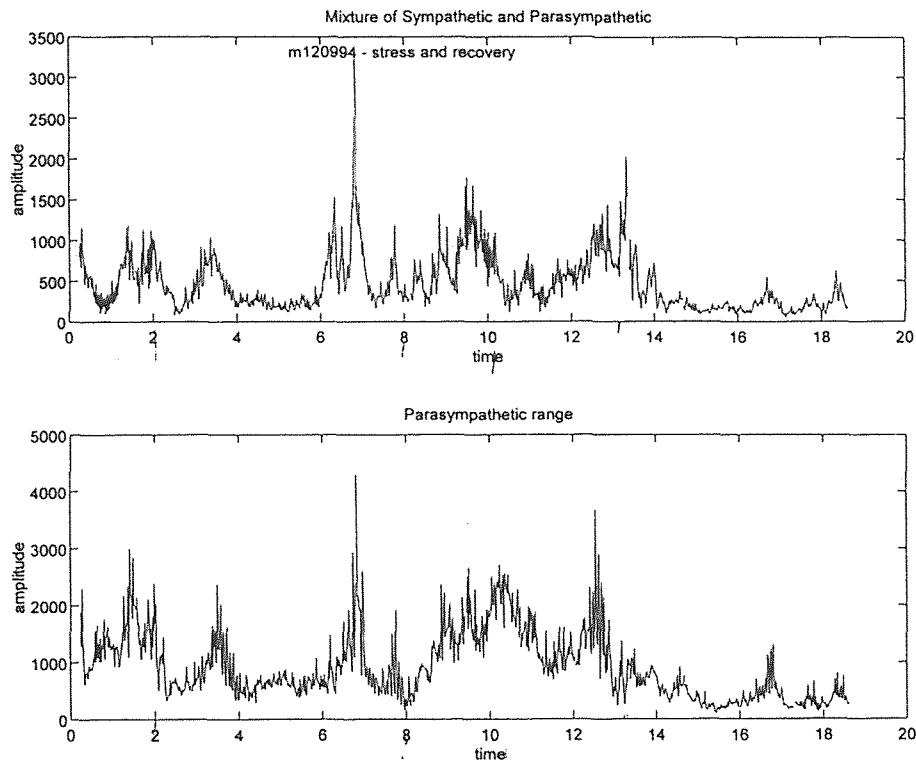**Figure A.18** Wigner distribution of heart rate variability.
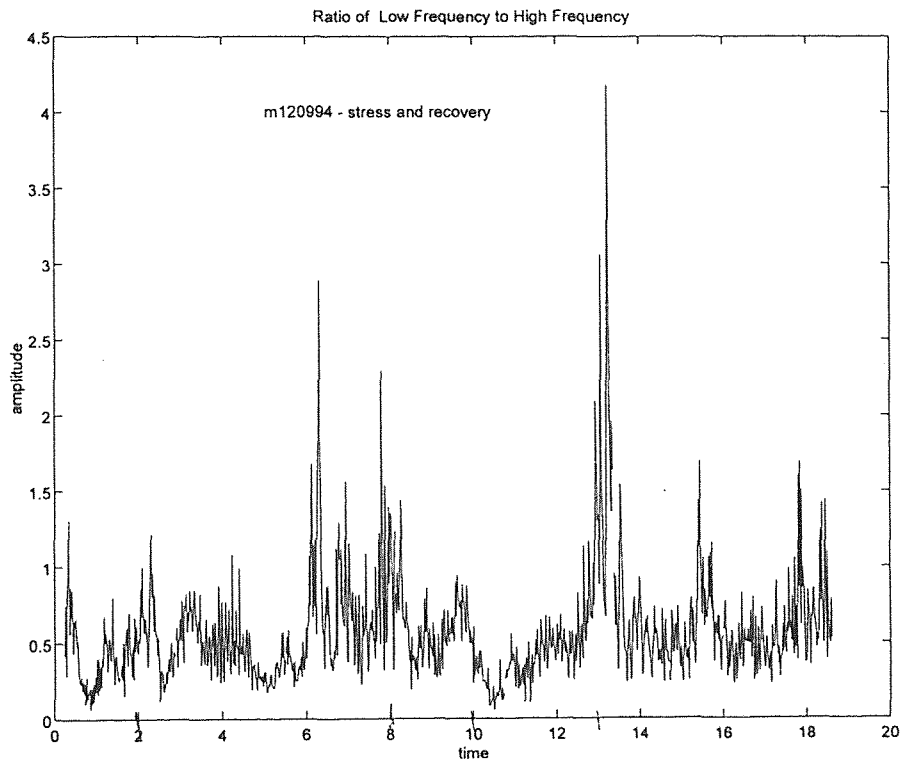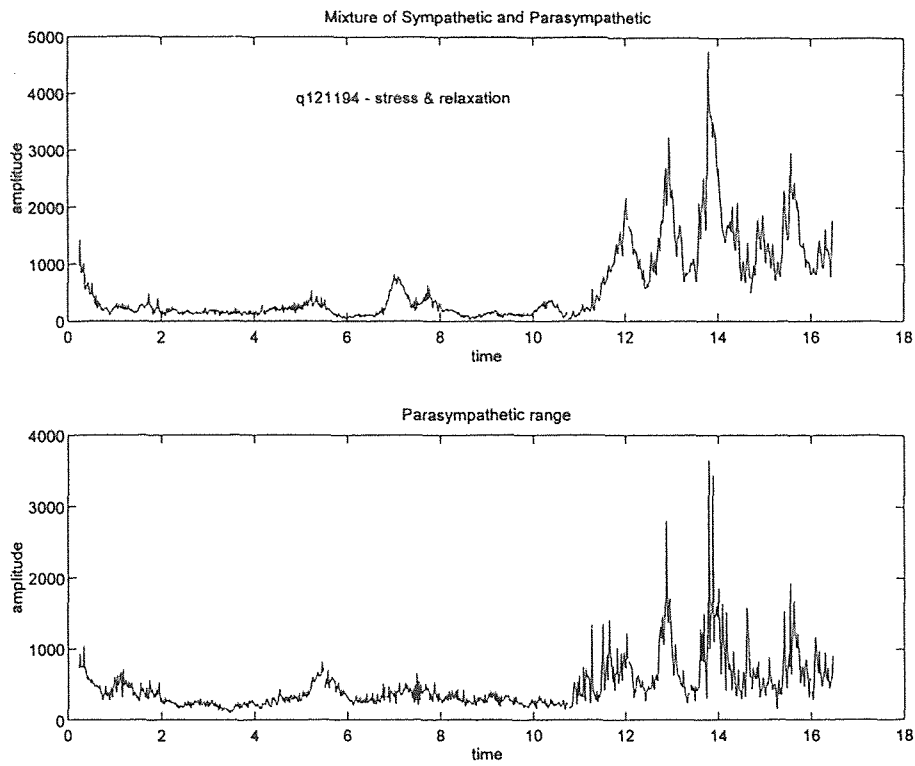
Figure A.19 Low frequency and high frequency areas.
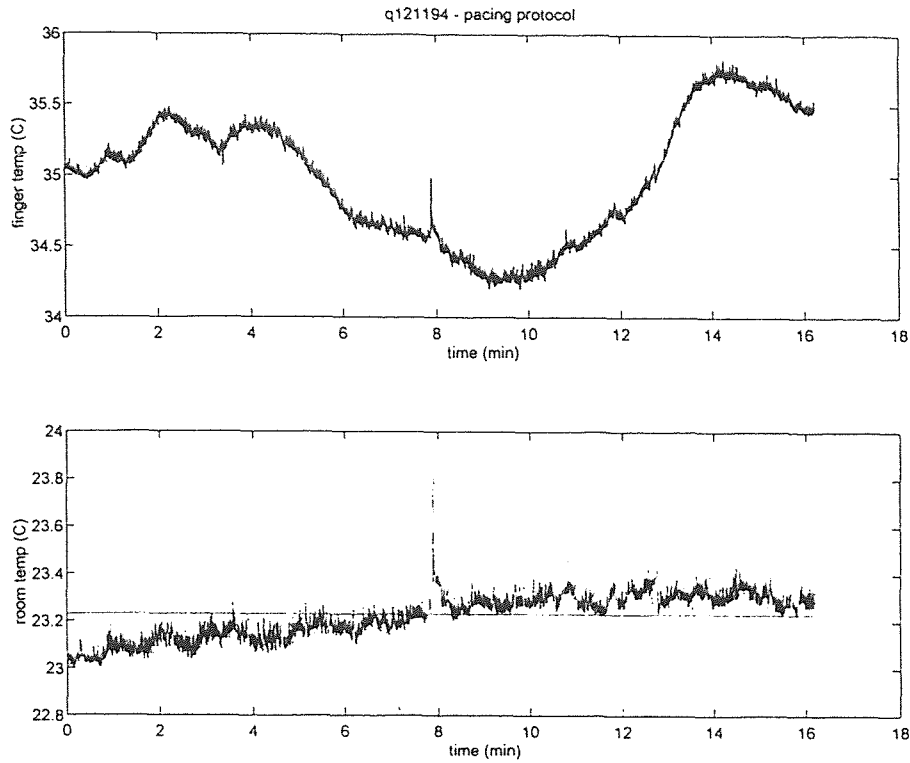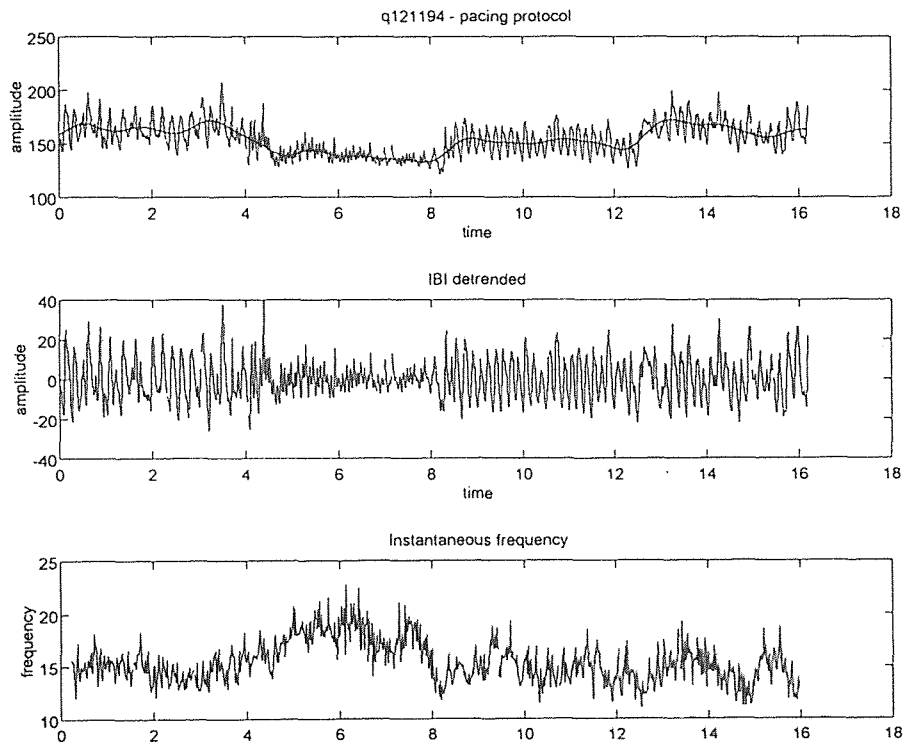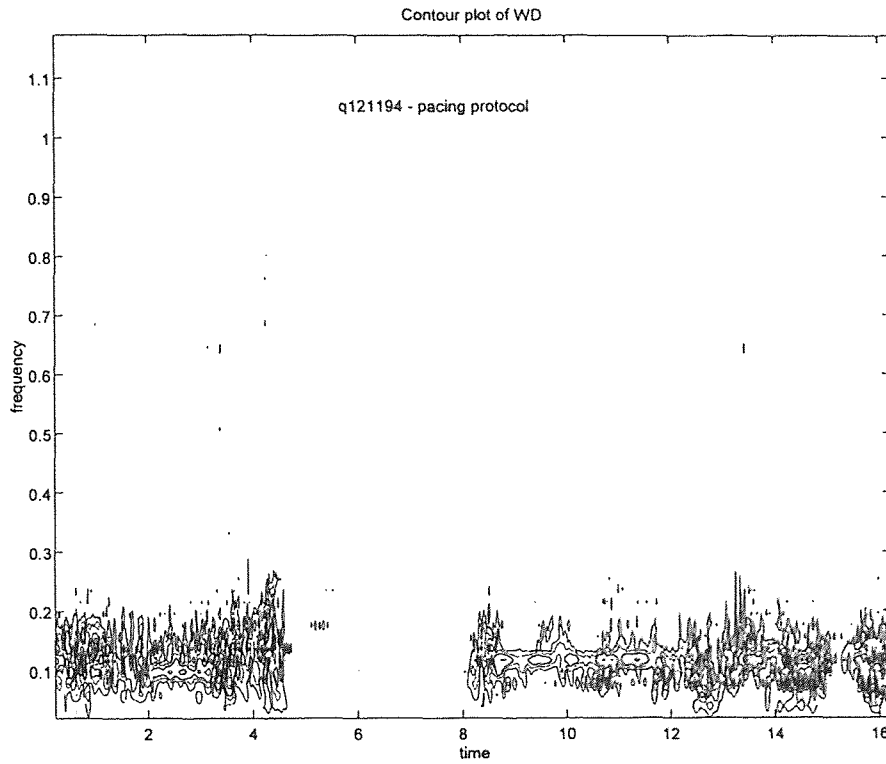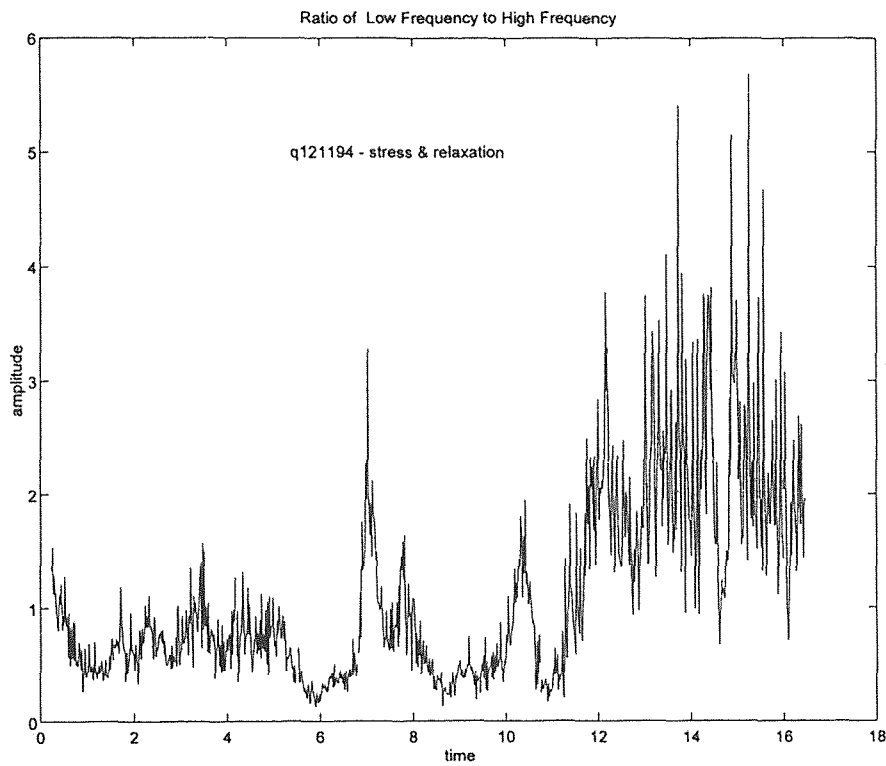

Figure A.20 Ratio of low to high frequency ranges.

THERMISTOR AMPLIFIER SCHEMATIC DIAGRAM
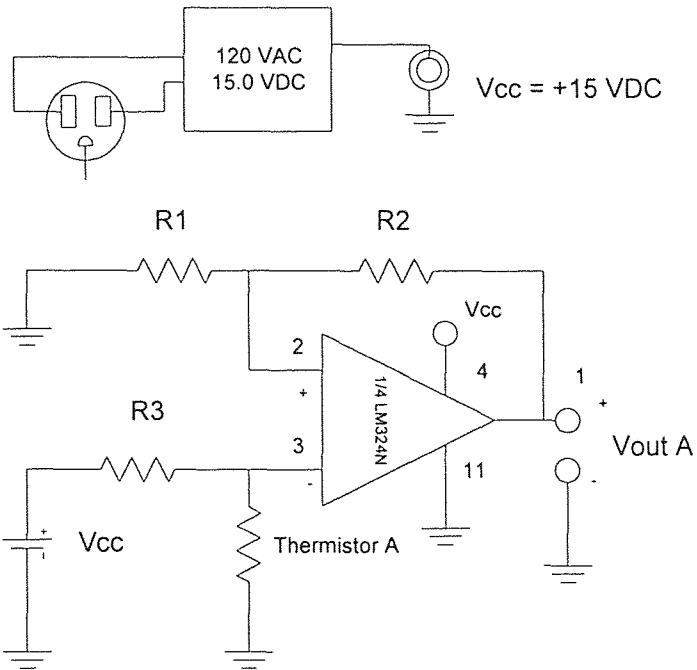
Resistors ±1.0%	
R1	200 kΩ
R2	2.2 MΩ
R3	2.2 MΩ
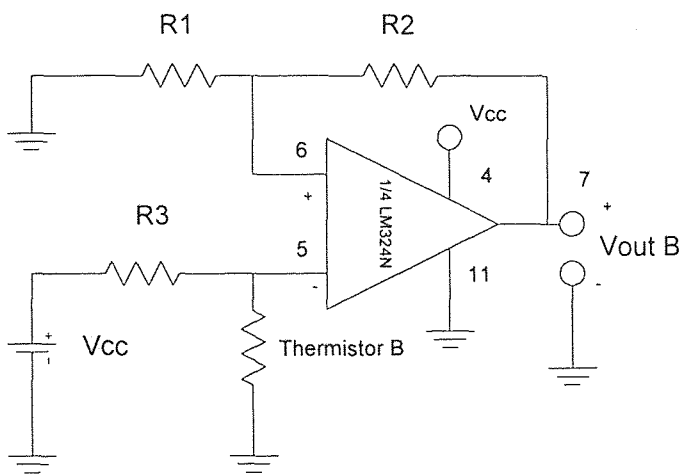
APPENDIX C

COMPUTER PROGRAMS

COSPAR is a MATLAB program to calculate the Coherence Spectral Array.

```
function cospar(x,y,Fs)
% COSPAR(x,y,Fs) Coherence Spectral Array. This routine calculates
% coherence for two signals and creates a cospar matrix
% using the methods of Levine (1976). The matrix is displayed
% in a mesh and contour plot with COHMESH.


x=x(:);
y=y(:); %column vectors
n=max(size(x));
%Fs=200;


% parameters for SPECTRUM
% 256 point windows shifted by 19 points
m=256;
noverlap=237;
threshhold=0.95;  % Coherence threshhold

% filter data to remove low frequency components
[b,a]=ellip(7,0.05,50,1.5/(Fs/2),'high');
x=filtfilt(b,a,x);
y=filtfilt(b,a,y);

% filter 60 Hz interference from the signal
[b,a]=butter(9,45/(Fs/2));
x=filtfilt(b,a,x);
y=filtfilt(b,a,y);

% calculate coherence for 5 second intervals and compile in a matrix
k=fix(n/(5*Fs));
index=1:(5*Fs);
Coh=zeros(m/2,k);

for i=1:k
```

```
  P=spectr2(x(index),y(index),m,noverlap);
  Coh(:,i)=P(:,5);
  index=index+(5*Fs);
  disp(k-i)
end


% leave only coherence peaks above threshhold
for j=1:m/2;
for l=1:k;
   if Coh(j,l)<threshhold
     Coh(j,l)=threshhold;
   end
  end
end


% plot the results
cohmesh(Coh,Fs);
Title=input('enter graph title: ','s');
subplot(211),title(Title);
```

COHMESH creates the output plots for COSPAR

```
function cohmesh(C,Fs)
%  COHMESH Graph results of COSPAR.
%  COHMESH(C,Fs) generates a mesh plot and a contour plot of the
%  coherence spectral array calculated by COSPAR.

[m,n]=size(C);
t=((5*n)*(0:n-1)/n)/60;
f=(0:m-1)/m*Fs/2;
Co=C(1:m/2,:);


% mesh plot
subplot(211),mesh(f(1:m/2),t,Co');
view([15,55]);
ylabel('time (min)');
xlabel('frequency (Hz)');
zlabel('coherence');
colormap('gray');
brighten(-1);

%contour plot
```

```
subplot(212),contour(f(1:m/2),t,Co',5);
ylabel('time (min)');
xlabel('frequency (Hz)');

grid
end
```

SPECTR2 is a modified form of the SPECTRUM program included in MATLAB's Signal Processing Toolbox.

```
function P = spectr2(x,y,m,noverlap)
%SPECTR2 Slightly modified SPECTRUM for use with COSPAR
%
%SPECTRUM Power spectrum estimate of one or two data sequences.
%       P = SPECTRUM(X,Y,M) performs FFT analysis of the two sequences
%       X and Y using the Welch method of power spectrum estimation.
%       The X and Y sequences of N points are divided into K sections of
%       M points each (M must be a power of two). Using an M-point FFT,
%       successive sections are Hanning windowed, FFT'd and accumulated.
%       SPECTRUM returns the M/2 by 8 array
%          P = [Pxx Pyy Pxy Txy Cxy Pxxc Pyyc Pxyc]
%       where
%         Pxx  = X-vector power spectral density
%         Pyy  = Y-vector power spectral density
%         Pxy  = Cross spectral density
%         Txy  = Complex transfer function from X to Y
%              (Use ABS and ANGLE for magnitude and phase)
%         Cxy  = Coherence function between X and Y
%         Pxxc,Pyyc,Pxyc = Confidence range (95 percent).
%
%       See SPECPLOT to plot these results.
%       P = SPECTRUM(X,Y,M,NOVERLAP) specifies that the M-point sections
%       should overlap NOVERLAP points.
%       Pxx = SPECTRUM(X,M) and SPECTRUM(X,M,NOVERLAP) return the single
%       sequence power spectrum and confidence range.
%
%       See also ETFE, SPA, and ARX in the Identification Toolbox.

%       J.N. Little 7-9-86
%       Revised 4-25-88 CRD, 12-20-88 LS, 8-31-89 JNL, 8-11-92 LS
%       Copyright (c) 1986-92 by the MathWorks, Inc.

%       The units on the power spectra Pxx and Pyy are such that, using
%       Parseval's theorem:
```

```
%
%         SUM(Pxx)/LENGTH(Pxx) = SUM(X.^2)/LENGTH(X) = COV(X)
%
%       The RMS value of the signal is the square root of this.
%       If the input signal is in Volts as a function of time, then
%       the units on Pxx are Volts^2*seconds = Volt^2/Hz.
%       To normalize Pxx so that a unit sine wave corresponds to
%       one unit of Pxx, use Pn = 2*SQRT(Pxx/LENGTH(Pxx))
%
%       Here are the covariance, RMS, and spectral amplitude values of
%       some common functions:
%       Function  Cov=SUM(Pxx)/LENGTH(Pxx)  RMS       Pxx
%       a*sin(w*t)      a^2/2         a/sqrt(2)  a^2*LENGTH(Pxx)/4
%Normal: a*rand(t)      a^2           a          a^2
%Uniform: a*rand(t)     a^2/12        a/sqrt(12) a^2/12
%
%       For example, a pure sine wave with amplitude A has an RMS value
%       of A/sqrt(2), so A = SQRT(2*SUM(Pxx)/LENGTH(Pxx)).
%
%       See Page 556, A.V. Oppenheim and R.W. Schafer, Digital Signal
%       Processing, Prentice-Hall, 1975.

if (nargin == 2), m = y; noverlap = 0; end
if (nargin == 3)
        if (max(size(y)) == 1)
                noverlap = m;
                m = y;
                nargin = 2;
        else
                noverlap = 0;
        end
end

x = x(:);               % Make sure x and y are column vectors
y = y(:);
n = max(size(x));       % Number of data points
k = fix((n-noverlap)/(m-noverlap));   % Number of windows
                        % (k = fix(n/m) for noverlap=0)
index = 1:m;
w = kaiser(m,9);        % Window specification; change this if you want:
                        % (Try HAMMING, BLACKMAN, BARTLETT, or your own)
                        %
                        % Kaiser was chosen here based on Harris (1978)
                        % for discriminating closely spaced frequency
                        % components. -CK
```

```
                              %
KMU = k*norm(w)^2;          % Normalizing scale factor


if (nargin == 2)          % Single sequence case.
        Pxx = zeros(m,1); Pxx2 = zeros(m,1);
        for i=1:k
                xw = w.*detrend(x(index));
                index = index + (m - noverlap);
                Xx = abs(fft(xw)).^2;
                Pxx = Pxx + Xx;
                Pxx2 = Pxx2 + abs(Xx).^2;
        end
        % Select first half
        select = [1:m/2];
        Pxx = Pxx(select);
        Pxx2 = Pxx2(select);
        cPxx = zeros(m/2,1);
        if k > 1
                c = (k.*Pxx2-abs(Pxx).^2)./(k-1);
                c = max(c,zeros(m/2,1));
                cPxx = sqrt(c);
        end
        pp = 0.95; % 95 percent confidence.
        f = sqrt(2)*erfinv(pp);  % Equal-tails.
        P = [Pxx f.*cPxx]/KMU;
        return
end

Pxx = zeros(m,1); % Dual sequence case.
Pyy = Pxx; Pxy = Pxx; Pxx2 = Pxx; Pyy2 = Pxx; Pxy2 = Pxx;

for i=1:k
        xw = w.*detrend(x(index));
        yw = w.*detrend(y(index));
        index = index + (m - noverlap);
        Xx = fft(xw);
        Yy = fft(yw);
        Yy2 = abs(Yy).^2;
        Xx2 = abs(Xx).^2;
        Xy  = Yy .* conj(Xx);
        Pxx = Pxx + Xx2;
        Pyy = Pyy + Yy2;
        Pxy = Pxy + Xy;
        Pxx2 = Pxx2 + abs(Xx2).^2;
```

```
        Pyy2 = Pyy2 + abs(Yy2).^2;
        Pxy2 = Pxy2 + Xy .* conj(Xy);
end

% Select first half
select = [1:m/2];

Pxx = Pxx(select);
Pyy = Pyy(select);
Pxy = Pxy(select);
Pxx2 = Pxx2(select);
Pyy2 = Pyy2(select);
Pxy2 = Pxy2(select);

cPxx = zeros(m/2,1);
cPyy = cPxx;
cPxy = cPxx;
if k > 1
   c = max((k.*Pxx2-abs(Pxx).^2)./(k-1),zeros(m/2,1));
   cPxx = sqrt(c);
   c = max((k.*Pyy2-abs(Pyy).^2)./(k-1),zeros(m/2,1));
   cPyy = sqrt(c);
   c = max((k.*Pxy2-abs(Pxy).^2)./(k-1),zeros(m/2,1));
   cPxy = sqrt(c);
end

Txy = Pxy./Pxx;
Cxy = (abs(Pxy).^2)./(Pxx.*Pyy);

pp = 0.95; % 95 percent confidence.
f = sqrt(2)*erfinv(pp);  % Equal-tails.

P = [ [Pxx Pyy Pxy]./KMU ...
      Txy Cxy ...
      f.*[cPxx cPyy cPxy]./KMU ];


POWSPEC calculates the four channel EEG power spectrum.

function powspec(data,Fs)
% POWSPEC(data,Fs) - A routine to calculate the average power
% spectral density in a signal in 1 Hz bands fom 3 Hz to 28 Hz.
% The variable 'data' is a four channel matrix of EEG signals, and
% Fs is the sampling frequency.
%
```

```
% Power is calculated by taking 5 second intervals and finding
% the area under the spectrum for each 1 Hz band of interest for
% each channel. These areas are averaged within each band and graphed,
% together with a dashed line representing a +1 standard deviation.
%

[m,n]=size(data);
k=fix(m/(5*Fs));
index=1:(5*Fs);
f=(Fs/2)*(1:1024)/1024;
freqband=3:28;% Frequency band of interest
f=freqband-2;% frequency count vector
minimum(f)=floor(freqband*1024/(Fs/2));% Low point of 1 Hz band
maximum(f)=ceil((freqband+1)*1024/(Fs/2));% High point of 1 Hz band
area=zeros(k,max(f));

% Calculating the areas
for channel=1:4
        for interval=1:k
                xw=detrend(data(index,channel));
                Xx=abs(fft(xw,2048)).^2;
                for fr=1:26
                        area(interval,fr)=sum(Xx(minimum(fr):maximum(fr)));
                end
                index=index+(5*Fs);
        end
        avgarea=mean(area);
        stdarea=std(area);

        %plotting the graphs...
        subplot(2,2,channel);
        semilogy(freqband,avgarea,'r');
        hold on
        semilogy(freqband,avgarea,'ro');
        semilogy(freqband,avgarea+stdarea,'b:');
        hold off
        xlabel('frequency (Hz)'),ylabel('relative power');
        if channel==1
                title('F3')
        elseif channel==2
                title('F4')
        elseif channel==3
                title('C3')
        else
                title('C4')
```

```
        end
        index=1:(5*Fs);
end
```

THERM is a program that converts the ASCII data from streamer into temperature in degrees Celcius.

```
function therm(therma,thermb)
% THERM(therma,thermb)
% Therm is a calibration program that coverts das-1601 thermistor
% data into temperature in degrees Celcius. The contants used
% were calculated from a linear least squares fit to manually
% obtained calibration data.
%


pPa=[-23.7 1340.7];
pPb=[-20.7 1217.6];

%[b,a]=butter(5,10/200);
%therma=filtfilt(b,a,therma);
%thermb=filtfilt(b,a,thermb);
therma=decimate(therma,10,'fir');
thermb=decimate(thermb,10,'fir');
time=(0:(max(size(therma))-1))/1200;

thermA=(therma-pPa(2))/pPa(1);
thermB=(thermb-pPb(2))/pPb(1);
meanroomtemp=mean(thermA);
mrt=meanroomtemp*ones(size(thermA));
Title=input('Enter graph title: ','s');

subplot(211)
plot(time,thermB,'b')
xlabel('time (min)');
ylabel('finger temp (C)');
title(Title);

subplot(212)
plot(time,thermA)
hold on;
plot(time,mrt,'m:')
hold off;
xlabel('time (min)');
```

ylabel('room temp (C)');

%plot((thermB-thermA))

SYMPAR1 is the latest version of SYMPAR used to calculate the Wigner distribution on the IIBI signal.

```
function sympar1(rawdata,top)
% SYMPAR1(iibi,gtitle)
%
% Program calculates the Vagal tone and Sympo-vagal ratio.
% It is an implementation of time-frequency analysis
% using the Wigner distribution.
%
% iibi is the interpolated interbeat interval calculated
% by pslwsu, either in Matlab or in S-plus. Gtitle is the
% title of the output graphs.

% Written by Sanjay Fernando.
%
% last revision: 12/16/94 by Christopher King
%

rawdata=rawdata(:);
order=5;
freq=0.03;
sample=20;
nfreq=freq/sample;
[b,a]=butter(order,nfreq);
dtrend=filtfilt(b,a,rawdata);
dtrendata=rawdata-dtrend;
[row,col]=size(dtrendata);
I=1:row;
I=I(:);
A=(I/sample)/60;

% This  part is for testing Janse Kaiser Wigner calculation
% algorithm with no window
fs=1000;
m=512;                  % The size of the fft we will be computing.
skip=25;        % Number of points we skip to get the next segment.
p=60;         % The number of freq vals we will be plotting
k=fix((row-m)/skip);    % the number of spectra we compute
w=ones(size(1:m));      % window specification. Can be changed.
```

```
w=w(:);
x=hilbert(dtrendata);   % Forms the analytic funcion of x
L=m/2;
l=-(L-1):(L-1);
n=L;
Z=zeros([p,k]);
for i=1:k
        % Here I think 0 lag is at the Lth point, hence the first
        % time location is at LT=128*.001 or .128 sec; hmmm.
        g=x(n+l).*conj(x(n-l));
        g(2*L)=0;
        y=w.*g; % Apply window to g or kernal.

        Y=2/m*abs(fft(y,m)); % evidently because it's analytic
                            % we only need 2/N
        Z(:,i)=Y(1:p);
        n=n+skip;
end


LFC = input('Please enter the low frequency range in index numbers. ');
symvag=sum(Z(LFC,1:k));
HFC=input('Please enter the high frequency range in index numbers. ');
vagal=sum(Z(HFC,1:k));
symtopar=symvag./vagal;



% This section is for determining the instantaneous frequency
% from the Wigner distribution.



[r,c]=size(Z);   %Determines the size of the matrix created by wgjka4.m.
for i=1:c;       %Repeation based on number of columns.
  W=Z(:,i);       %W is assigned the values of the column.
  Y=(1:r)';       %Y represents the frequencies.
  M=W.*Y;
  S=sum(M);
  F=sum(W);       %Sum of the Wigner Distribution values.
  E(i)=S/F;
end


% Plotting commands
```

```
J=[12.8+(1:k)*1.25]/60;

subplot(3,1,1);
plot(A,rawdata,'r',A,dtrend,'g');
title(top);
xlabel('time')
ylabel('amplitude')

subplot(3,1,2);
plot(A,dtrendata);
title('IBI detrended');
xlabel('time');
ylabel('amplitude');

subplot(3,1,3);
plot(J,E);
xlabel('time');
ylabel('frequency');
title('Instantaneous frequency');


faxis=(1:p)*(.0391/2);
figure

mesh(J,faxis,Z);
xlabel('time');
ylabel('frequency');
title(top);

figure
contour(J,faxis,Z);
gtext(top);
xlabel('time');
ylabel('frequency');
title('Contour plot of WD');

figure

subplot(2,1,1);
plot(J,symvag);
gtext(top);
title(' Mixture of Sympathetic and Parasympathetic');
xlabel('time');
ylabel('amplitude');
```

```
subplot(2,1,2);
plot(J,vagal);
title('Parasympathetic range');
xlabel('time');
ylabel('amplitude');

figure
plot(J,symtopar);
gtext(top);
title('Ratio of Low Frequency to High Frequency')
xlabel('time');
ylabel('amplitude');
```

STITCH is a short program to speed up splicing two matricies of lengths *m* rows and *n* rows to make one of length *m+n* rows.

```
function data=stitch(A,B)
%
% data=STITCH(a,b) connects two matricies together sequentially,
% a then b. The output data is the rowa + rowb by col matrix
% containing a and b. The columns of a and b must be the same.
%
[r1,c]=size(A);
[r2,c]=size(B);
data=zeros([r1+r2,c]);
data(1:r1,:)=A;
data(r1+1:r1+r2,:)=B;
return
```

APPENDIX D

DATA ANALYSIS PROCEDURES

D.1 EEG COHERENCE AND AVERAGE POWER SPECTRUM ANALYSIS

1. Unpack the .dat files to .asc files using kunpack2.

2. Before starting MATLAB, connect to `ambition\users`. (From now on, we'll designate this as `e:\`).

3. Run MATLAB. Type `whitebg` to set the graph background to white.

4. Load the `.asc` files into MATLAB. Change to the directory the files are in and type:

    ```
    load x092294a.asc
    ```

    After you've loded all of them in, you can type `whos` to see the files, which are now matrix variables. Note that the `.asc` extension is absent.

5. Change to the directory with the eeg functions.

    ```
    cd e:\chris\mfiles\eeg
    ```

    the following files should be present:
    ```
    cospar.m
    cohmesh.m
    powspec.m
    powspec2.m
    stitch.m
    spectr2.m
    ```

6. If the file was unpacked in pieces, it needs to be spliced back together for the coherence calculations. Type:

    ```
    data=stitch(x092294a,x092294b);
    ```

    This stitches the first two sections together. To add subsequent sections, type:

    ```
    data=stitch(data,x092294c);
    ```

92

7. To calculate coherence (for example, between the F3 and F4 electrodes), type:

```
cospar(data(:,col1),data(:,col2),Fs);
```

Here, `col1` and `col2` are the columns that the eeg data is in, usually 5 and 6.
`Fs` is the sampling frequency, usually 200.
The program will take around 10 minutes to run for a 10 minute file. At the end, it
   will prompt for the graph title. Type one in and press return.

8. The average power spectrum estimation of the EEG signal is calculated and averaged
   over time in 1 Hz bands from 3 Hz to 28 Hz. Therefore, it is important that the data be
   split into sections corresponding to distinct events in the protocol. For example,
   suppose that the subject sat with eyes closed from t=2 minutes to t=4 minutes. For 2
   channels of EEG, type:

```
powspec2(data(24000:48000,5:6));
```

Here, row (or sample) 24000 corresponds to t=2 minutes(120 sec. * 200
   samples/sec.), and 48000 to t=4 minutes(240 s * 200 samples/s). the column
   designation 5:6 indicates both eeg channels.
If there are 4 channels of EEG, use `powspec` with the same input arguements.
Alternatively, you can assign each section of data a variable name and use those
   variable names in place of data above.

D.2 TIME FREQUENCY ANALYSIS OF IBI USING symparl.m

This program is a MATLAB m-file. Upon starting MATLAB, type `whitebg` for a white
graph background.

1. The data needed is the interpolated inter-beat interval. There are two ways to get this:

   • In MATLAB: run `pslwsu`. When the program has finished, type `whos`. In the
     list of variables you should see one called `iibi`. This is the one you want.

   • In S-Plus: after you have created the `.fin` file, you must convert it to an ascii file
     in order to load it into MATLAB. Type:

   ```
   write(x092294a.fin$ibi,file="x092294a.ibi",ncol=1)
   ```

   Now load the .ibi file (which is an ascii file) into MATLAB:

   ```
   load x092294a.ibi
   ```

If you now type `whos`, the file should show up as the variable `x092294a`.

2. Run the program

    ```
    symparl(data,'graphtitle')
    ```

    Here, `data` is either `iibi` or `x092294a`, and `graphtitle` is the title you choose. It must, however, be in single quotes as shown.

3. The program will ask for frequency index ranges for the calculation of the area under the high and low freqiency peaks..
    for the low frequency range:
    .05-.15 Hz use 2:8 (rest, pace 12 & 18, excercise, recovery)
    .05..10 Hz use 2:6 (pace 8)

    for the high frequency range:
    .15-.4 Hz use 8:20 (rest, pace 12 & 18)
   .10-.4 Hz use 6:20 (pace 8)
    .15-.8 Hz use 8:40 (excercise and recovery)

4. The program creates five output graphs. If you want to print them you can do so manually.

5. On three graphs you will see a cross-hair. Place it where you want your graph title to go and click the left mouse button.

EQUIPMENT SETUP

The diagram below shows the laboratory setup for the stress experiments. The subject is facing toward the bottom of the page. During the antcipation portion of the experiment, the experimenter moves from the position shown in front of the data acquisition computer to behind the equipment where the audio cassette player is.
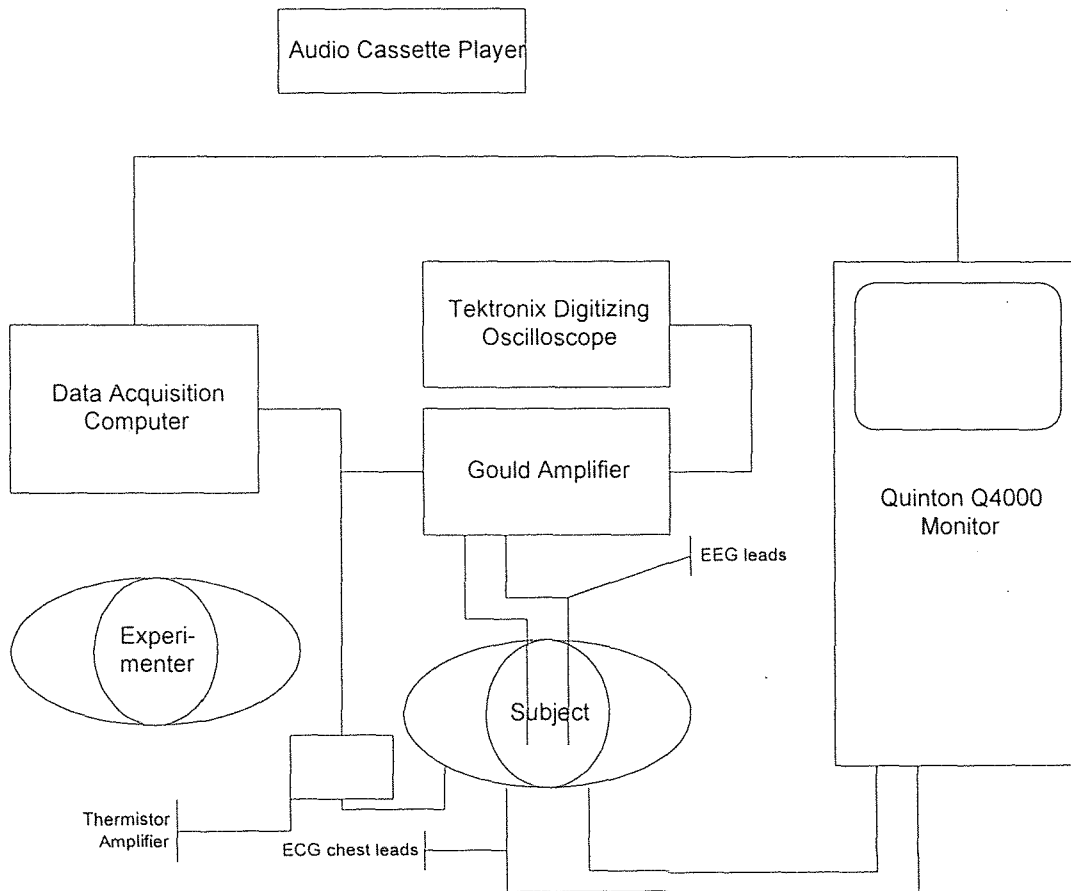
REFERENCES

1. Bloomfield, H. H., M. P. Cain, and D. T. Jaffe. 1975. *TM: Discovering Inner Energy and Overcoming Stress.* New York, Delacorte Press.

2. Blumberg, H., and B. G. Wallin. 1987. "Direct Evidence of Neurally Mediated Vasodialation in Hairy Skin of the Human Foot." *J. Physiol.* 382:105-21.

3. Brown, R. G. 1983. *Introduction to Random Signal Analysis and Kalman Filtering.* New York, John Wiley & Sons.

4. Clark, J. W. 1992. "The Origin of Biopotentials". *Medical Instrumentation: Application and Design.* J. G. Webster, ed. Boston, Houghton Mifflin Company.

5. Cooke, J. P., M. A. Creager, P. J. Osmundson, and J. T. Shepherd. 1990. "Sex Differences in Control of Cutaneous Blood Flow." *Circulation.* 82(5):1607-15.

6. Dillbeck, M. C., and D. W. Orme-Johnson. 1987. "Physiological Differences Between Meditation and Rest." *American Psychologist.* Sept. 1987:879-81.

7. Dillbeck, M. C., D. W. Orme-Johnson, and R. K. Wallace. 1981. "Frontal EEG Coherence, H-Reflex Recovery, Concept Learning, and the TM-Sidhi Program." *Intern. J. Neuroscience.* 15:151-57.

8. Fernando, S., and S. Reisman. 1994 "Biomedical Applications of Time-Frequency Analysis." *Proceedings of the IEEE-SP International Symposium on Time-Frequency and Time-Scale Analysis.* 576-9.

9. Gaylord, C., D. Orme-Johnson, and F. Travis. 1989. "The Effects of the Transcendental Meditation Technique and Progressive Muscle Relaxation on EEG coherence, Stress Reactivity, and Mental Health in Black Adults." *Intern. J. Neuroscience.* 46:77-86.

10. Goff, W. R. 1974. "Human Averaged Evoked Potentials: Procedures for Stimulating and Recording." *Methods in Physiological Psychology; Vol. I: Bioelectric Recording Techniques; Part B: Electroencephalography and Human Brain Potentials.* New York, Academic Press.

11. Guyton, A. C. 1991. *Textbook of Medical Physiology, Eighth Edition.* Philadelphia, Harcourt Brace Jovanovich.

12. Halperin, J. H., R. A. Cohen, and J. D. Coffman. 1983. "Digital Vasodilation During Mental Stress in Patients with Raynaud's Disease." *Cardiovascular Research.* 17:671-77.

13. Harris, F. J. 1978. "On the Use of Windows for Harmonic Analysis with the Discrete Fourier Transform." *Proceedings of the IEEE.* 66:51-83.

14. Harris, R. W. and T. J. Ledwidge. 1974. *Introduction to Noise Analysis.* London, Pion Limited.

15. Hoffman, J. W., H. Benson, P. J. Arns, G. L. Stainbrook, L. Landsberg, J. B. Young, and A. Gill. 1982. "Reduced Sympathetic Nervous System Responsivity Associated with the Relaxation Response." *Science.* 215:190-2.

16. Jacobs, G. D., and J. F. Lubar. 1989. "Spectral Analysis of the Central Nervous System Effects of the Relaxation Response Elicited by Autogenic Training." *Behavioral Medicine.* Fall 1989:125-32.

17. Jevning, R., R. K. Wallace, and M. Beidebach. 1992. "The physiology of Meditation: A Review. A Wakeful Hypometabolic Integrated Response." *Neuroscience and Behavioral Reviews.* 16:415-24.

18. Kamath, M. D. and E. L. Fallen. 1993. "Power Spectral Analysis of Heart Rate Variability: A Noninvasive Signature of Cardiac Autonomic Function." *Critical Reviews in Biomedical Engineering.* 21(3):245-311.

19. Levine, P. 1976. "The Coherence Spectral Array (COSPAR) and its Application to the Study of Spatial Ordering in the EEG." *Proceedings of the San Diego Biomedical Symposium.* San Francisco, Academic Press, 15:237-47.

20. Oberle, J., M. Elam, T. Karlsson, and B. G. Wallin. 1988. "Temperatire-dependent Interaction Between Vasoconstrictor and Vasodilator Mechanisms in Human Skin." *Acta Physiol. Scand.* 132:459-69.

21. Orme-Johnson, D., M. C. Dillbeck, and R. K. Wallace. 1982. "Intersubject EEG Coherence: Is Consciousness A Field?" *Intern. J. Neuroscience.* 16:203-9.

22. Shin, S. J., W. N. Tapp, S. S. Reisman, and B. H. Natelson. 1989. "Assesment of Autonomic Regulation of Heart Rate Variability by the Method of Complex Demodulation." *IEEE Transactions on Biomedical Engineering.* 36(2):274-282.

23. Tansey, M. A. 1991. "Wechsler (WISC-R) Changes Following Treatment of Learning Disabilities Via EEG Biofeedback Training in a Private Practice Setting." *Australian J. Psychology.* 43(3):147-53.

24. Tansey, M. A. 1993. "Ten Year Stability of EEG Biofeedback Results for a Hyperactive Boy Who Failed Fourth Grade Perceptually Impaired Class." *Biofeedback and Self Regulation.* 18(1):33-44.

25. Tourenne, C. J. 1985. "A Model of the Electric Field of the Brain at EEG and Microwave Frequencies." *J. Theor. Biol..* 116:495-507.

26. Travis, F. T., and D. W. Orme-Johnson. 1989. "Field Model of Consciousness: EEG Coherence as Indicators of Field Effects." *Intern. J. Neuroscience.* 49:203-11.

27. Wallace, R. K., P. J. Mills, D. W. Orme-Johnson, M. C. Dillbeck, and E. Jacobe. 1983. "Modification of the Paired H Reflex through the Transcendental Meditation and TM-Sidhi Program." *Experimental Neurology.* 79:77-86.

28. Welch, P. D. 1967. "The Use of Fast Fourier Transform for the Estimation of Power Spectra: A Method Based on Time Averaging Over Short, Modified Periodograms." *IEEE Transactions on Audio and Electroacoustics.* AU-15(2):70-3.

29. West, M. A. 1980. "Meditation and the EEG." *Psychological Medicine.* 10:369-375.

30. Zhao, L. 1994. "Derivation of Respiration from Electrocardiogram During Heart Rate Variability Studies." Masters Thesis, New Jresey Institute of Technology, Newark, NJ.